

h

FLUORESCENT PROBES FOR DETECTION OF
ALDEHYDE COMPOUNDS



A Thesis Submitted in Partial Fulfillment of the Requirements
for the Degree of Master of Science in Chemistry
Department of Chemistry
FACULTY OF SCIENCE
Chulalongkorn University
Academic Year 2018
Copyright of Chulalongkorn University

ฟลูออเรสเซนซ์โพรบสำหรับการตรวจวัดสารประกอบแอลดีไฮด์



วิทยานิพนธ์นี้เป็นส่วนหนึ่งของการศึกษาตามหลักสูตรปริญญาวิทยาศาสตรมหาบัณฑิต
สาขาวิชาเคมี ภาควิชาเคมี
คณะวิทยาศาสตร์ จุฬาลงกรณ์มหาวิทยาลัย
ปีการศึกษา 2561
ลิขสิทธิ์ของจุฬาลงกรณ์มหาวิทยาลัย

ปริญญานิพนธ์ ปริญญาโท : ฟลูออเรสเซนต์โพรบสำหรับการตรวจวัดสารประกอบแอลดีไฮด์ .
 (FLUORESCENT PROBES FOR DETECTION OF
 ALDEHYDE COMPOUNDS) อ.ที่ปรึกษาวิทยานิพนธ์หลัก : ผศ. ดร.บุญยรัตน์ ธรรมพัฒน์กิจ

สารประกอบแอลดีไฮด์สายยาวเช่น เฮกซานาล เฮปทานาล, ออกทานาล และโนนทานาลถูกใช้เป็นตัวชี้วัดทางชีวภาพของโรคมะเร็งปอดและตัวชี้วัดคุณภาพของผลิตภัณฑ์ไขมันและน้ำมัน จากส่วนประกอบของแอลดีไฮด์สายยาว ซึ่งส่วนหางสายไฮโดรคาร์บอนที่ไม่ชอบน้ำและส่วนหัวของหมู่ฟังก์ชันแอลดีไฮด์ที่ชอบน้ำเป็นข้อดีที่ผู้วิจัยคาดหวังว่าจะสามารถทำหน้าที่เป็นสารลดแรงตึงผิวที่ชักนำให้เข้ากันได้พอดีในการฟอร์มตัวด้วยตัวมันเองให้เกิดไมเซลล์ที่สมบูรณ์ ในงานวิจัยนี้ ได้ประสบความสำเร็จในการเตรียมโพรบระดับนาโนไมเซลล์ที่ใช้สำหรับตรวจวัดสารประกอบแอลดีไฮด์สายยาวได้อย่างจำเพาะเจาะจงโดยใช้คอนเซ็ปต์ว่า สารประกอบแอลดีไฮด์สายยาวหลังจากเกิดปฏิกิริยากับ Naph-NH_2 แล้วจะถูกชักนำให้ฟอร์มไมเซลล์ที่สมบูรณ์จากการแตกตัวกันเองด้วยไฮโดรโฟบิกสายยาว ทำให้เกิดการจัดเรียงตัวของไมเซลล์แบบสมบูรณ์ ส่งผลทำให้ไมเซลล์มีความสามารถในการกักเก็บโมเลกุลสีข้อมได้อย่างมีประสิทธิภาพแล้วทำให้เกิดการเพิ่มขึ้นของสัญญาณฟลูออเรสเซนต์ของโมเลกุลสีข้อมในไมเซลล์ระดับนาโน สิ่งที่สำคัญคือ การเพิ่มขึ้นของสัญญาณฟลูออเรสเซนต์ของ $\text{Naph-NH}_2/\text{CTAB}/\text{S}2$ ที่ความยาวคลื่น 542 นาโนเมตร จะแปรผันตรงกับความเข้มข้นของแอลดีไฮด์สายยาวในระบบฟอสเฟตบัฟเฟอร์ พีเอช 7.4 เวลาการทำปฏิกิริยา 20 นาที ซึ่งให้ขีดจำกัดการตรวจวัดสำหรับ เฮกซานาล, เฮปทานาล, ออกทานาล และโนนทานาล เท่ากับ 74.38, 80.38, 80.98 และ 60.09 ไมโครโมลาร์ ตามลำดับ นอกจากนี้วัสดุเซ็นเซอร์ $\text{Naph-NH}_2/\text{CTAB}/\text{S}2$ ยังสามารถตรวจวัดเฮปทานาลในตัวอย่างเลือดซึ่งมีร้อยละการคืนกลับอยู่ในช่วง 94.01-102.4 เปอร์เซ็นต์ และได้นำวัสดุเซ็นเซอร์นี้ไปตรวจวัดสารประกอบแอลดีไฮด์สายยาวภายในเซลล์มะเร็ง A549 พบว่าเห็นการเรืองแสงสีเขียวของ $\text{Naph-NH}_2/\text{CTAB}/\text{S}2$ ในเซลล์ แสดงว่าวัสดุเซ็นเซอร์นี้สามารถเข้าไปในนิวเคลียสและไซโตพลาสซึมได้ นอกจากนี้เพื่อเพิ่มประสิทธิภาพของความไวของวัสดุเซ็นเซอร์ในการตรวจวัดแอลดีไฮด์สายยาว ได้ใช้ Gel 1 ซึ่งเป็นเจลเลเตอร์ที่มีองค์ประกอบของน้ำตาลกลูโคสและสายไฮโดรคาร์บอนของกรดไขมันลอริกในการรวมกันกับ $\text{Naph-NH}_2/\text{CTAB}/\text{S}2$ สร้างไฮโดรเจลในการตรวจวัดแอลดีไฮด์สายยาว พบว่าวัสดุเซ็นเซอร์ในไฮโดรเจลนี้สามารถเพิ่มความไวในการตรวจวัดได้ 10 เท่า และมีขีดจำกัดการตรวจวัด เท่ากับ 7.45, 7.59, 13.61 และ 21.69 ไมโครโมลาร์ตามลำดับ ดังนั้น $\text{Naph-NH}_2/\text{CTAB}/\text{S}2$ จึงเป็นวัสดุเซ็นเซอร์ที่มีประสิทธิภาพที่ให้ความจำเพาะเจาะจงและความไวสูงต่อการตรวจวัดแอลดีไฮด์สายยาวและง่ายต่อการนำไปใช้ประโยชน์ในตัวอย่างจริงได้

จุฬาลงกรณ์มหาวิทยาลัย

CHULALONGKORN UNIVERSITY

ภาควิชา	ภาควิชาเคมี	ลายมือชื่อนิสิต
สาขาวิชา	เคมี
ปีการศึกษา	2561	ลายมือชื่อ อ.ที่ปรึกษาวิทยานิพนธ์หลัก

5972010323 : MASTER OF SCIENCE

long-chain aldehydes/ nanomicelle/ fluorescence

Piyanan Pranee : FLUORESCENT PROBES FOR DETECTION OF ALDEHYDE COMPOUNDS. ADVISOR: Asst. Prof. Boosayarat Tomapatanaget, Ph.D.

Long-chain aldehyde compounds such as hexanal, heptanal, octanal and nonanal are regarded as potential biomarkers of many lung cancer disease and served as the important quality indicators of fat and oil products. As advantage of the hydrophobic tails of hydrocarbon chain and hydrophilic head of aldehyde, we expected that long-chained aldehydes might act as the induced-fit surfactants to form the completely self-assembling organized nanomicelle. In this research, the nanomicellar probes for specific long-chain aldehyde compounds have been achieved in the challenge concept such that among aldehydes especially long-chain aldehyde compounds, would react with Naph-NH₂ to form complete micelle-like particles via hydrophobic self-packing aspect resulting in a highly efficient encapsulation and a consequent fluorescent enhancement of dye-doped nanomicelle. Importantly, the fluorescent enhancement of Naph-NH₂/CTAB/S2 at 542 nm corresponds to the amount of long-chain aldehyde added. The reaction time of probes was completed in 20 min in PBS buffer pH 7.4 with the limit of detection (LOD) of 74.38, 80.38, 80.98 and 64.09 μ M for hexanal, heptanal, octanal, and nonanal, respectively. Moreover, Naph-NH₂/CTAB/S2 was able to detect heptanal in blood samples with percent recovery in a range of 94-102. This sensor material was further studied on long-chain aldehyde detection in A549 cancer cells. The observation of green fluorescent in cell revealed that Naph-NH₂/CTAB/S2 was internalized to the nucleus and cytoplasm. To improve the sensitivity of this sensing platform, the gelator (Gel 1) containing sucrose and long-chain hydrocarbon of lauric acid was utilized to cooperate with Naph-NH₂/CTAB/S2 micellar material for long-chain aldehyde sensing aspect. Surprisingly, it showed approximately 10-fold improvement of sensitivity with LOD of 7.45, 7.59, 13.61 and 21.69 μ M, respectively. Consequently, this Naph-NH₂/CTAB/S2 highlights the promising selectivity and sensitivity for determination of long-chain aldehyde detection and a benefit for easy checking in real samples.

Department:	Department of Chemistry	Student's Signature
	
Field of Study:	Chemistry	Advisor's Signature
	
Academic Year:	2018	

ACKNOWLEDGEMENTS

I would like to express my very great appreciation to Assistant Professor Dr. Boosayarat Tomapatanaget, my research advisor, for her patient guidance, honest kindness, enthusiastic encouragement and constructive recommendation throughout my master's degree. Secondary, I would like to offer my special thanks to Associate Professor Dr. Khanitha Pudhom, Miss Naunpun Sangphech, Miss Titiporn Sansureerungsikul for her valuable suggestions for cell culture and cell imaging by using confocal fluorescence microscopy.

Moreover, I would also like to thank Associated Professor Dr. Vudhichai Parasuk, Assist. Prof. Dr. Fuangfa Unob, Dr. Numpon Insin and Dr. Gamolwan Tumcharern for their comments and supervision as thesis examination committee. Special thanks to Professor Dr. Thawatchai Tuntulani and Dr. Pannee Leeladee for their worthy comments and advices every group meeting event.

I would like to extend my thanks to Mr. Jaturong Kongwutthivech for his synthesis of Gel 1 gelator, his valuable laboratory techniques and generous supports. I would also like to thank Ms. Chiraporn Chaicham for her valuable suggestions of laboratory skills. Also, I like to thank all the Supramolecular Chemistry Research Unit (SCRU) members, who have shared their precious time throughout the entire graduate degree.

Furthermore, I would like to acknowledge Science Achievement Scholarship of Thailand (SAST) and Center of Excellence on Petrochemical and Material Technology (PETROMAT), Thailand

Eventually, I wish to thank my family for their endless amounts of love, important moral support and always being there for me throughout my life.

Piyanan Pranee

TABLE OF CONTENTS

	Page
ABSTRACT (THAI)	iii
ABSTRACT (ENGLISH)	iv
ACKNOWLEDGEMENTS	v
TABLE OF CONTENTS	vi
LIST OF TABLES	x
LIST OF FIGURES	xii
LIST OF ABBREVIATION AND SYMBOLS	xix
CHAPTER I	1
1.1 Introduction	1
1.1.1 Supramolecular chemistry	1
1.1.2 Molecular recognition	1
1.1.3 Fluorescence	2
1.1.4 Micelle	4
1.1.5 Gel	7
1.2 Literature reviews	8
1.2.1 Amine-functionalized sensor for aldehyde detection	8
1.2.2 Hydrazine-functionalized sensor for aldehyde detection	11
1.2.3 Micelle for sensing application	13
1.2.4 Gel material for sensing application	15
1.3 Objectives	22
CHAPTER II	23
2.1 General procedures	23
2.1.1 Analytical instruments	23
2.1.2 Materials	23
2.2 Synthesis	24

2.2.1 Synthesis of Phenazine-2,3-diamine[52].....	24
2.2.2 Synthesis of hydrazine-functionalized sensor (Naph-NH ₂)	24
2.2.2.1 Synthesis of 6-Bromo-2-phenyl-1H-benzo[de]isoquinoline-1,3(2H)- dione (1)	25
2.2.2.2 Synthesis of 6-hydrazinyl-2-phenyl-1H-phenalene-1,3(2H)-dione (Naph- NH ₂).....	26
2.2.3 Synthesis of 6-Methoxy-2-phenyl-1H-benzo[de]isoquinoline-1,3(2H)- dione (Naph-OMe)	27
2.2.4 Synthesis of 6,6'-Disulfanediybis(hexan-1-ol) (S2)	28
2.3 Qualitative discrimination of aldehydes using amine-functionalized and hydrazine-functionalized sensor	29
2.3.1 Screening studied of amine-functionalized and hydrazine-functionalized sensor with heptanal	29
2.3.2 Fluorescence studies of 6-hydrazinyl-2-phenyl-1H-phenalene-1,3(2H)- dione (Naph-NH ₂) with aldehydes	29
2.3.3 Optimization of micellar system for 6-hydrazinyl-2-phenyl-1H- phenalene-1,3(2H)-dione (Naph-NH ₂)	31
2.3.3.1 Optimization of surfactant for 6-hydrazinyl-2-phenyl-1H-phenalene- 1,3(2H)-dione (Naph-NH ₂)	31
2.3.3.2 Critical micelle concentration (CMC) studies of CTAB	32
2.3.3.3 Optimization of co-surfactant in CTAB micellar system for encapsulation of Naph-NH ₂	33
2.3.3.4 Critical micelle concentration (CMC) studies of S2	34
2.3.3.5 Optimization of S2 concentration in CTAB micellar system for encapsulation of Naph-NH ₂	35
2.3.3.6 Optimization of Naph-NH ₂ concentration in CTAB/S2 micellar system	36
2.3.4 pH studies of Naph-NH ₂ in micellar system for heptanal detection	37
2.3.5 The role of hydrazine functional group of Naph-NH ₂ on Naph- NH ₂ /CTAB/S2 micellar sensor	38
2.3.6 The kinetic profile of Naph-NH ₂ /CTAB/S2 micellar sensor	39

2.3.7 Determination for long-chain aldehyde detection by using Naph-NH ₂ /CTAB/S2 micellar sensor.	39
2.3.8 Selectivity of Naph-NH ₂ /CTAB/S2 nanomicellar sensor for long-chain aldehyde sensing.....	40
2.3.9 The Naph-NH ₂ /CTAB/S2 micellar sensor for long-chain aldehyde detection in blood sample.....	42
2.3.10 Cellular uptake of Naph-NH ₂ /CTAB/S2 micellar sensor.....	43
2.4 Naph-NH ₂ /CTAB/S2@Gel 1 for long-chain aldehyde detection.....	44
2.4.1 Optimization of Gel 1.....	44
2.4.2 Optical property of Naph-NH ₂ /CTAB/S2@Gel 1.....	44
2.4.3 Kinetic study of Naph-NH ₂ /CTAB/S2@Gel 1.....	45
2.4.4 Determination of long-chain aldehydes by using Naph-NH ₂ /CTAB/S2@Gel 1.....	45
2.4.5 Selectivity of Naph-NH ₂ /CTAB/S2@Gel 1 sensor for long-chain aldehyde sensing.....	46
CHAPTER III.....	47
3.1 Conceptual design of fluorescent micellar probe for long-chain aldehydes sensing.....	47
3.2 Synthesis.....	49
3.2.1 Synthesis and characterization of phenazine-2,3-diamine [60].....	49
3.2.2 Synthesis and characterization of 6-Bromo-2-phenyl-1H-benzo[de]isoquinoline-1,3(2H)-dione (1).....	50
3.2.3 Synthesis and characterization of 6-hydrazinyl-2-phenyl-1H-phenalene-1,3(2H)-dione (Naph-NH ₂).....	51
3.2.4 Synthesis and characterization of 6-Methoxy-2-phenyl-1H-benzo[de]isoquinoline-1,3(2H)-dione (Naph-OMe).....	52
3.2.5 Synthesis and characterization of 6,6'-Disulfanediybis(hexan-1-ol) (S2).....	54
3.3 Amine-functionalized fluorescence sensor.....	55
3.4 Hydrazine-functionalized fluorescence sensor.....	56
3.5 Optimization of micellar system for long-chain aldehyde detection.....	60

3.6 The effect on pH of Naph-NH ₂ /CTAB/S2 micellar sensor for long-chain aldehyde detection	68
3.7 Characterization of Naph-NH ₂ /CTAB/S2 micellar sensor for long-chain aldehyde detection	69
3.8 The optical studies of Naph-NH ₂ /CTAB/S2 micellar sensor	72
3.9 The kinetic profiles of Naph-NH ₂ /CTAB/S2 micellar sensor	73
3.10 The effect of hydrazine functional group on Naph-NH ₂ /CTAB/S2 micellar sensor	74
3.11 Determination of long-chain aldehydes using Naph-NH ₂ /CTAB/S2 sensor ..	75
3.12 Selectivity of Naph-NH ₂ /CTAB/S2 micellar sensor	80
3.13 Determination of long-chain aldehydes in real blood sample	81
3.14 Biological application in lung cancer cell (A549)	82
3.15 Naph-NH ₂ /CTAB/S2 based gel (Naph-NH ₂ /CTAB/S2@gel) for long-chain aldehyde detection	84
3.15.1 Optimization conditions of Gel 1 for gelation.....	86
3.15.2 Characterization of Naph-NH ₂ /CTAB/S2@Gel 1.....	89
3.15.3 Optical property of Naph-NH ₂ /CTAB/S2@Gel 1.....	91
3.15.4 Kinetic studies of Naph-NH ₂ /CTAB/S2@Gel 1for long-chain detection	93
3.15.5 Determination of long-chain aldehydes using Naph-NH ₂ /CTAB/S2@Gel 1.....	94
3.15.6 The selectivity of Naph-NH ₂ /CTAB/S2@Gel 1 toward long-chain aldehyde.....	97
CHAPTER IV	98
REFERENCES	100
APPENDIX.....	106
VITA.....	117

LIST OF TABLES

Table 2.1 amine-functionalized and hydrazine-functionalized sensor with heptanal .	29
Table 2.2 The amounts of representative aldehyde compounds	30
Table 2.3 The amounts of surfactants for optimized micellar sensor	31
Table 2.4 The critical micelle concentration (CMC) studies of Naph-NH₂ in CTAB micellar system (2.5% DMSO/PBS buffer pH 7.4).....	32
Table 2.5 The co-surfactants coupled with CTAB for encapsulation of Naph-NH₂ ..	33
Table 2.6 The critical micelle concentration (CMC) studies of Naph-OMe in S2 micellar system (2.5% DMSO/PBS buffer pH 7.4).....	34
Table 2.7 The optimization of S2 concentration for encapsulation Naph-NH₂ in CTAB/S2 micellar system. (2.5% DMSO/PBS buffer pH 7.4)	35
Table 2.8 The various concentration of Naph-NH₂ for heptanal sensing in CTAB/S2 micellar system. (2.5% DMSO/PBS buffer pH 7.4).....	36
Table 2.8 (continue)	37
Table 2.9 The types of buffer at various pH	38
Table 2.10 The various aldehyde at concentration of 0.05 M.....	39
Table 2.11 The various organic compounds actually found in breath of cancer patient.	41
Table 2.12 The Naph-NH₂/CTAB/S2 micellar sensor for long-chain aldehyde detection in blood sample by using standard addition method.	43
Table 3.1 Size distribution of Naph-NH₂/S2/CTAB micellar sensor by DLS.....	70
Table 3.2 Zeta potential measurement of Naph-NH₂/S2/CTAB micellar sensor	71
Table 3.3 limit of detection (LOD) and limit of quantification (LOQ) for long-chain aldehyde detection by using Naph-NH₂/CTAB/S2 incomplete micellar sensor	79
Table 3.4 Percent recovery of Naph-NH₂/CTAB/S2 for long-chain aldehyde detection.	79
Table 3.5 Percent recovery of Naph-NH₂/CTAB/S2 for long-chain aldehyde detection.	82
Table 3.6 The self-assembled studies of Gel 1 chelator in 100% DMSO	87

Table 3.7 The self-assembled studies of Gel 1 chelator in 0.01 M PBS buffer pH 7.4	87
Table 3.8 The self-assembled organized studies of 0.98 wt % Gel 1 gelator in various ratio of mixed solvent	88
Table 3.9 The self-assembled organized studies of 1.94 wt % Gel 1 in various ratio of mixed solvent	88
Table 3.10 limit of detection (LOD) and limit of quantification (LOQ) for long-chain aldehyde detection of Naph-NH₂/CTAB/S2@Gel 1 in 60% DMSO/PBS buffer pH 7.4	96
Table 3.11 Percent recovery for long-chain aldehyde detection by Naph- NH₂/CTAB/S2@Gel 1	96



LIST OF FIGURES

Figure 1.1 The schematic presentation of chemical sensory composition.	2
Figure 1.2 The schematic Jablonski diagrams	3
Figure 1.3 The on-off PET process of fluorescence sensor	4
Figure 1.4 The schematic presentation of micelle and reverse micelle.	5
Figure 1.5 The plots of surfactant concentration versus a physical property, such as viscosity, conductance, surface tension, osmotic pressure, or molar conductivity [31].	6
Figure 1.6 Schematic representation of the gelation process for supramolecular gel organization.....	8
Figure 1.7 The conceptual of 1 and 2 for salicylaldehyde sensing with the micrographs under UV-light and UV-lamp [40].	9
Figure 1.8 The detection principle based on a reaction between FI-NH₂ and formaldehyde [41].....	10
Figure 1.9 (a) The proposed reaction mechanism of formaldehyde detection, (b) The fluorescence spectra of BOD-NH₂ after introduction of formaldehyde (FA) ranging from 0-500 μ M, (c) The fluorescence responses of BOD-NH₂ towards reactive chemical species, amino acids and other relevant biological species (1 blank, 2 FA, 3 FA+ 250 μ M NaHSO ₃ , 4 FA + 500 μ M NaHSO ₃ , 5 acetaldehyde, 6 methylglyoxal, 7 glyoxal, 8 benzaldehyde, 9 pyridoxal, 10, 4-nitro-benzaldehyde, 11 sodium pyruvate, 12 alanine, 13 glycine, 14 serine, 15 arginine, 16 cysteine, 17 glutathione, 18 glucose, 19 hydrogen peroxide, 20 hydrogen sulfide, 21 methane acid, 22 dehydroascorbate) [42].....	11
Figure 1.10 Fluorescence response mechanism for formaldehyde detection in lysosome [43].....	12
Figure 1.11 Fluorescence responsive mechanism for biomolecule carbonyl detection [44].....	13
Figure 1.12 Fluorescence responsive mechanism for hydrogen sulfide (a), fluorescence spectra of azo-fluorescent dye in micellar system (b) and schematic representation of the micellar effect including CTAB and SDS [45].....	14
Figure 1.13 a) Structure of fluorophore b) Picric acid (PA) and 2,6-bis(picrylamino)-3,5-dinitropyridine (PVX) c) Fluorescence spectra of fluorophore in water and in the	

micellar aqueous solution. SDS, DTAB, Triton X- 100) d) Representation of fluorophore distribution in SDS and in DTAB [33]	15
Figure 1.14 (a) Chemical structures of cetyltrimethylammonium bromide (CTAB), phenyl boronic acid (PBA), and the complexation of PBA and sugar, (b) Visual appearance of WLM gel with various concentration of glucose, (c) Mechanism of the formation of worm-like micelles (MLMs) at pH 9.4 and its deformation in the presence of glucose [46]	16
Figure 1.15 Representation of the assembly mechanism and energy transfer process of S1 and Eu ³⁺ ions [47]	17
Figure 1.16 Proposed detection mechanism of TNP based on G-P gel [48].....	18
Figure 1.17 Construction and mechanism operating in fluorescent dye encapsulated MCM-enzyme-hydrogel hybrid sensory system [49]	19
Figure 1.18 The chemical structure of 1 and 2 gelator, The SEM micrographs of gel 1 (a) and gel 2 (b) [50]	20
Figure 1.19 The chemical structure and TEM images of maltose-based gelators [51]	21
Figure 2.1 Synthesis pathway of phenazine-2,3-diamine	24
Figure 2.2 Synthesis pathway of hydrazine-functionalized sensor (Naph-NH ₂)	24
Figure 2.3 Synthesis pathway of 6-Methoxy-2-phenyl-1H-benzo[de]isoquinoline-1,3(2H)-dione (Naph-OMe).....	27
Figure 2.4 Synthesis pathway of 6,6'-Disulfanediybis(hexan-1-ol) (S2).....	28
Figure 2.5	111
Figure 3.1 Conceptual design of fluorescent micellar probe for long-chain aldehydes sensing.....	47
Figure 3.2 Chemical structures of fluorescence sensors for aldehyde sensing	48
Figure 3.3 The ¹ H-NMR spectrum of phenazine-2,3-diamine in <i>d</i> ₆ -DMSO at 400 MHz	49
Figure 3.4 The ¹ H-NMR spectrum of 6-Bromo-2-phenyl-1H-benzo[de]isoquinoline-1,3(2H)-dione (1) in <i>d</i> ₆ -DMSO at 400 MHz.....	51
Figure 3.5 The ¹ H-NMR spectrum of 6-hydrazinyl-2-phenyl-1H-phenalene-1,3(2H)-dione (Naph-NH ₂) in <i>d</i> ₆ -DMSO at 400 MHz.....	52

- Figure 3.6** The $^1\text{H-NMR}$ spectrum of 6-Methoxy-2-phenyl-1H-benzo[de]isoquinoline-1,3(2H)-dione (**Naph-OMe**) in d_6 -DMSO at 400 MHz53
- Figure 3.7** The $^1\text{H-NMR}$ spectrum of 6'-Disulfanediylbis(hexan-1-ol) (**S2**) in d_6 -DMSO at 400 MHz.....54
- Figure 3.8** Fluorescence spectra of 0.5 mM 1,2-phenylenediamine after introduction of 0.25 mM heptanal in 100% DMF. ($\lambda_{\text{ex}} = 428$ nm, PMT 800)55
- Figure 3.9** Fluorescence spectra (a) and the fluorescence response (b) of 0.5 mM phenazine-2,3-diamine after introduction of 0.25 mM heptanal in DMF. (10-450 min), ($\lambda_{\text{ex}} = 350$ nm, PMT 800).....56
- Figure 3.10** Fluorescence spectra of 0.5 mM 4-hydrazinobenzoic acid upon introduction of 0.25 mM heptanal in DMF (a) and in 2.5% DMF/PBS buffer pH 7.4 (b). (20 min, $\lambda_{\text{ex}} = 430$ nm).....57
- Figure 3.11** Chemical structures of representative aldehydes including; (a) formaldehyde (b) heptanal (c) benzaldehyde (d) 3-hydroxybenzaldehyde (e) 4-nitrobenzaldehyde58
- Figure 3.12** Relative fluorescence intensity (I/I_0) of 5.0×10^{-5} M **Naph-NH₂** after introduction of various aldehydes (0.25 mM) in 100% DMSO. ($\lambda_{\text{ex}} = 445$ nm)59
- Figure 3.13** Fluorescence spectra of 5.0×10^{-5} M **Naph-NH₂** in 100% DMSO (black line) and 2.5% DMSO/PBS buffer pH 7.4 (red line). ($\lambda_{\text{ex}} = 445$ nm)59
- Figure 3.14** Relative fluorescence intensity (I/I_0) at 542 nm of 5.0×10^{-5} M **Naph-NH₂** upon introduction of various aldehydes (0.25 mM) in 2.5% DMSO/PBS buffer pH 7.4.60
- Figure 3.15** Chemical structures of surfactants including (a) Cetrimonium bromide (CTAB), (b) Sodium dodecyl sulfate (SDS) and (c) Triton X-10061
- Figure 3.16** Fluorescence spectra of 5.0×10^{-5} M **Naph-NH₂** in PBS buffer (0.01 M, pH 7.4) and in 6.67 mM of three different micellar systems. (2.5% DMSO/PBS buffer pH 7.4, $\lambda_{\text{ex}} = 445$ nm)61
- Figure 3.17** Fluorescence spectra (a) and fluorescent intensity (b) at 542 nm of 5.0×10^{-5} M **Naph-NH₂** in CTAB micellar system at a concentration range from 0.0 mM to 3.0 mM. (c) Relative fluorescence intensity of **Naph-NH₂/CTAB** micelle at 542 nm (I/I_0) upon introduction of various aldehydes (2.5% DMSO/PBS buffer pH 7.4, $\lambda_{\text{ex}} = 445$ nm).63
- Figure 3.18** Fluorescence response at 542 nm of **Naph-NH₂/CTAB** micellar system with various co-surfactant including ethanol, butanol, hexanol, octanol, 6-mercaptop-1-

hexanol, **S2**, ethylenediamine, ethanolamine and cysteamine. (2.5% DMSO/PBS buffer pH 7.4, $\lambda_{\text{ex}} = 445 \text{ nm}$). 65

Figure 3.19 Fluorescence spectra (a) and fluorescent curve (b) at 458 nm of $5.0 \times 10^{-5} \text{ M}$ **Naph-OMe** in **S2** micellar system at a concentration range from 0.2 mM to 2.0 mM ($\lambda_{\text{ex}} = 385 \text{ nm}$). (c) Relative fluorescence intensity at 542 nm (I/I_0) of **Naph-NH₂/CTAB** micelle with various **S2** concentration toward 0.25 mM heptanal. (d) Relative fluorescence intensity of **Naph-NH₂/CTAB/S2** micelle at 542 nm (I/I_0) after introduction of various aldehydes (2.5% DMSO/PBS buffer pH 7.4, $\lambda_{\text{ex}} = 445 \text{ nm}$).. 66

Figure 3.20 The studies of **Naph-NH₂** concentration of **CTAB/S2** micellar system in 2.5% DMSO/PBS buffer pH 7.4. ($\lambda_{\text{ex}} = 445 \text{ nm}$) 67

Figure 3.21 Determination of pH effect on **Naph-NH₂/CTAB/S2** toward 0.25 mM heptanal with various pH in the range of 5.0- 9.0. (2.5% DMSO/ buffer solution, $\lambda_{\text{ex}} = 445 \text{ nm}$) 68

Figure 3.22 TEM photographs of **Naph-NH₂/CTAB/S2** micelles (a), **Naph-NH₂/CTAB/S2** micelle after introduction of 0.25 mM heptanal (b) and 0.50 mM heptanal (c)..... 69

Figure 3.23 DLS of **Naph-NH₂/S2/CTAB** micelles before (black line) and after introduction of 0.25 mM (red line) and 0.50 mM (blue line) heptanal, respectively., in 2.5% DMSO/ 0.01 M PBS buffer pH 7.4 70

Figure 3.24 UV-visible (a) and fluorescence (b) spectra of **Naph-NH₂/ PBS buffer** (black line), **Naph-NH₂/CTAB/S2** before (red line) and after (blue line) introduction of 0.25 mM heptanal in 2.5% DMSO/PBS buffer pH 7.4 ($\lambda_{\text{ex}} = 445 \text{ nm}$)..... 72

Figure 3.25 The kinetic profiles of **Naph-NH₂/PBS buffer** (black line) and **Naph-NH₂/CTAB/S2** in the absence (red line) and in the presence (blue line) of 0.25 mM heptanal. (2.5% DMSO/PBS buffer pH 7.4, $\lambda_{\text{ex}} = 445 \text{ nm}$)..... 74

Figure 3.26 Fluorescence spectra of **Naph-OMe/PBS buffer** and **Naph-OMe/CTAB/S2** micelle after introduction of 0.25 mM various aldehydes including formaldehyde, heptanal, benzaldehyde, 3-hydroxybenzaldehyde and 4-nitrobenzaldehyde. (2.5% DMSO/PBS buffer pH 7.4, $\lambda_{\text{ex}} = 385 \text{ nm}$)..... 75

Figure 3.27 Mechanism of condensation reaction between hydrazine and aldehyde [65]..... 76

Figure 3.28 (a) Fluorescence titration spectra and (b) relative fluorescence intensity (I/I_0) after introduction of various hexanal concentration. The inset showed the linear rang of hexanal detection from 0.03 to 0.67 mM (0.03-1.00 mM) in 2.5% DMSO/PBS buffer pH 7.4 ($\lambda_{\text{ex}} = 445 \text{ nm}$). 77

- Figure 3.29** (a) Fluorescence titration spectra and (b) relative fluorescence intensity (I/I_0) after introduction of various heptanal concentration. The inset showed the linear range of heptanal detection from 0.03 to 0.33 mM (0.03-0.67 mM) in 2.5% DMSO/PBS buffer pH 7.4 ($\lambda_{ex} = 445$ nm). 77
- Figure 3.30** (a) Fluorescence titration spectra and (b) relative fluorescence intensity (I/I_0) after introduction of various octanal concentration. The inset showed the linear range of octanal detection from 0.03 to 0.42 mM (0.03-1.00 mM) in 2.5% DMSO/PBS buffer pH 7.4 ($\lambda_{ex} = 445$ nm). 78
- Figure 3.31** (a) Fluorescence titration spectra and (b) relative fluorescence intensity (I/I_0) after introduction of various nonanal concentration. The inset showed the linear range of nonanal detection from 0.017 to 0.33 mM (0.017-0.667 mM) in 2.5% DMSO/PBS buffer ($\lambda_{ex} = 445$ nm). 78
- Figure 3.32** Fluorescence response at 542 nm **Naph-NH₂/CTAB/S2** micellar toward organic compounds which were found in breath of lung cancer patients. (2.5% DMSO/PBS buffer pH 7.4, $\lambda_{ex} = 445$ nm). 80
- Figure 3.33** (a) Fluorescence titration spectra and (b) relative fluorescence intensity (I/I_0) after spiked of various heptanal concentration in real blood sample. The inset showed the linear range of heptanal detection from 0.03 to 0.50 mM (0.03-1.17 mM) in 2.5% DMSO/PBS buffer pH 7.4 ($\lambda_{ex} = 445$ nm). 81
- Figure 3.34** Confocal images of A549 cancer cells (a) control, (b) incubation of **Naph-NH₂/CTAB/S2**, (c) **Naph-NH₂/CTAB/S2** and heptanal for 4 h using confocal fluorescence microscopy. 83
- Figure 3.35** The Chemical structure of **Gel 1** 84
- Figure 3.36** Schematic representation of the gelation mechanism of **Naph-NH₂/CTAB/S2@Gel 1** for long-chain aldehydes sensing 85
- Figure 3.37** SEM images of gelator (**Gel 1**) (a), **Naph-NH₂/CTAB/S2@Gel 1** (b), **Naph-NH₂/CTAB/S2@Gel 1** after introduction of 0.05 mM (c) and 0.3 mM heptanal (d). (1.94 wt % **Gel 1** in 60% DMSO/PBS buffer pH 7.4) 89
- Figure 3.38** FT-IR spectra of **Naph-NH₂** (black line), **Gel 1** (red line) and **Naph-NH₂/CTAB/S2@Gel 1** (blue line) 91
- Figure 3.39** Fluorescence spectra of **Naph-NH₂/CTAB/S2@Gel 1** (red line) and **Naph-NH₂/CTAB/S2** (black line) in the absence (dash line) and in the presence (solid line) of 0.05 mM heptanal ($\lambda_{ex} = 445$ nm). 92

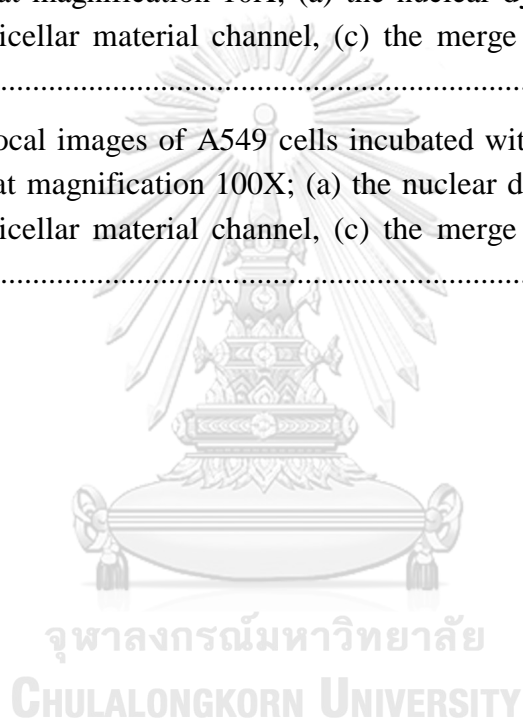
Figure 3.40 Fluorescence spectra of Naph-NH₂/CTAB/S2@Gel 1 (a) and Naph-NH₂/CTAB/S2 (b) ($\lambda_{\text{ex}} = 445$ nm). (1.94 wt % Gel 1 in 60% DMSO/PBS buffer pH 7.4)	93
Figure 3.41 The kinetic profiles of Naph-NH₂/CTAB/S2@Gel 1 in the absence (black line) and in the presence (red line) of 0.05 mM heptanal. (1.94 wt % Gel 1 in 60% DMSO/PBS buffer pH 7.4).....	93
Figure 3.42 Fluorescent titration curves of Naph-NH₂/CTAB/S2@Gel 1 toward hexanal (a), heptanal (b), octanal (c) and nonanal (d) under condition of 60% DMSO/PBS buffer pH 7.4 (1.94 wt % Gel 1 , $\lambda_{\text{ex}} = 445$ nm).	95
Figure 3.43 Fluorescence response at 542 nm Naph-NH₂/CTAB/S2@Gel micellar toward organic compounds which were found in breath of lung cancer patients. (60% DMSO/PBS buffer pH 7.4 (1.94 wt %, Gel 1 , $\lambda_{\text{ex}} = 445$ nm).	97
Figure A1 The ¹³ C-NMR spectrum of 1 in d ₆ -DMSO at 100 MHz.....	107
Figure A2 The ¹³ C-NMR spectrum of Naph-NH₂ in d ₆ -DMSO at 100 MHz.....	107
Figure A3 The ¹³ C-NMR spectrum of SL in d ₆ -DMSO at 100 MHz.....	108
Figure A4 The ¹³ C-NMR spectrum of S2 in d ₆ -CDCl ₃ at 100 MHz.....	108
Figure A5 The ¹³ C-NMR spectrum of Naph-OMe in d ₆ -CDCl ₃ at 100 MHz	109
Figure A6 The mass spectrum spectrum of 1 at m/z 352.52.....	109
Figure A7 The mass spectrum spectrum of Naph-NH₂ at m/z 303.50.....	110
Figure A8 The mass spectrum of Naph-OMe at m/z 325.51	110
Figure A9 The FT-IR spectrum (ATR) of compound 1 and Naph-NH₂	111
Figure A 10 Synthesis pathway of sucrose laurate monoester (Gel 1).....	111
Figure A11 The ¹ H-NMR spectrum of sucrose laurate monoester (Gel 1) in d ₆ -DMSO at 400 MHz	113
Figure A12 The studies of hydrophobic and hydrophilic properties of CTAB/S2 micellar system	113
Figure A13 Confocal images of A549 cells (control) at magnification 10X; (a) the nuclear dye channel, (b) the Naph-NH₂/CTAB/S2 micellar material channel, (c) the merge of three channels (d) the brightfield image	114
Figure A14 Confocal images of A549 cells (control) at magnification 100X; (a) the nuclear dye channel, (b) the Naph-NH₂/CTAB/S2 micellar material channel, (c) the merge of three channels (d) the brightfield image	114

Figure A15 Confocal images of A549 cells incubated with **Naph-NH₂/CTAB/S2** for 4 hr at magnification 10X; (a) the nuclear dye channel, (b) the **Naph-NH₂/CTAB/S2** micellar material channel, (c) the merge of three channels (d) the brightfield image 115

Figure A16 Confocal images of A549 cells incubated with **Naph-NH₂/CTAB/S2** for 4 hr at magnification 100X; (a) the nuclear dye channel, (b) the **Naph-NH₂/CTAB/S2** micellar material channel, (c) the merge of three channels (d) the brightfield image 115

Figure A17 Confocal images of A549 cells incubated with **Naph-NH₂/CTAB/S2** + heptanal for 4 hr at magnification 10X; (a) the nuclear dye channel, (b) the **Naph-NH₂/CTAB/S2** micellar material channel, (c) the merge of three channels (d) the brightfield image 116

Figure A18 Confocal images of A549 cells incubated with **Naph-NH₂/CTAB/S2** + heptanal for 4 hr at magnification 100X; (a) the nuclear dye channel, (b) the **Naph-NH₂/CTAB/S2** micellar material channel, (c) the merge of three channels (d) the brightfield image 116



LIST OF ABBREVIATION AND SYMBOLS

ACP or AP	Phosphatase enzyme
Anal. Calcd	Analysis calculated
^{13}C -NMR	Carbon-13 Nuclear Magnetic Resonance
δ	Chemical shift
J	Coupling constant
BODIPY	Boron-dipyrrromethene
$^{\circ}\text{C}$	Degree Celsius
CMs	Cylindrical micelle
$\text{Cu}(\text{acac})_2$	Copper acetate
CTAB	Cetyltrimethylammonium bromide
3D	Three dimension
DAPI	4,6-diamidino-2-phenylindole
DLS	Dynamic Light scattering
DMF	Dimethylformamide
DMSO	Dimethyl sulfoxide
λ_{ex}	Excitation wavelength
λ_{em}	Emission wavelength
equiv	Equivalence
EGME	Ethylene glycol monomethyl ether
FRET	Fluorescence resonance energy transfer
Fl-NH ₂	5-aminofluorescein
g	Gram
Glc	Glucose
h	Hour
HEPES	4-(2-hydroxyethyl)-1-piperazineethanesulfonic acid
HOMO	Highest occupied molecular orbital
HZ	Hertz
I/I_0	Relative fluorescent intensity
ITO	Indium tin oxide
LOD	Limit of detection

LOQ	Limit of quantification
LUMO	Lowest unoccupied molecular orbital
m/z	Mass per charge ratio
μL	Microliter
μM	Micromolar
min	Minute
Naph-NH ₂	6-hydrazinyl-2-phenyl-1H-phenalene-1,3(2H)-dione
Naph-OMe	6-Methoxy-2-phenyl-1H-benzo[de]isoquinoline-1,3(2H)-dione
NH ₂ -MCM41	Amine-modified silica nanoparticles
nm	Nanometer
NMR	Nuclear Magnetic Resonance
mM	Milimolar
min	Minute
¹ H-NMR	Proton Nuclear Magnetic Resonance
PA	Picric acid
PBA	Phenyl boronic acid
PBS	Phosphate buffered saline
PET	Photoinduced electron transfer
PMT	Photomultiplier tube
PVA	Polyvinyl alcohol
PYX	2,6-bis(picrylamino)-3,5-dinitropyridine
RT	Room temperature
S2	6,6'-Disulfanediylbis(hexan-1-ol)
SEM	Scanning Electron Microscopy
SL	Sucrose laurate monoester
SD	Standard deviation
SDS	Sodium dodecyl sulfate
SMA	Silica mesochannel array
s, d, t, m	Splitting pattern of ¹ H-NMR (singlet, doublet, triplet, multiplet)
T _{gel}	Sol-to-gel transition temperature

TEM	Transmission Electron Microscopy
TFA	Trifluoroacetic acid
TLC	Thin-layer chromatography
TNP	1,4,6-trinitrophenol
WLMs	Worm-like micelles
λ	Wavelength



CHAPTER I

INTRODUCTION AND LITERATURE REVIEWS

1.1 Introduction

1.1.1 Supramolecular chemistry

Jean-Marie Lehn [1] firstly created the word “Supramolecular chemistry” or “Host-guest chemistry” as the chemistry of the intermolecular bond, covering the structures and functions of the entities formed by the association of two or more chemical species. “Host” molecule was defined as a molecule that has binding site to self-assemble interact with “Guest” molecule through intermolecular interaction such as hydrogen bonding, pi-pi interaction, ion-dipole interaction and hydrophobic effects. Meanwhile, guest molecules can possibly be cation, anion or the sophisticated molecule such as hormones and enzyme.

The concepts in supramolecular chemistry were subdivided as the following; Molecular self-assembly, Molecular recognition and complexation, Template-directed synthesis, Mechanically-interlocked molecular architectures, Dynamic covalent chemistry, Biomimetics, Imprinting, Molecular machinery, Building blocks of supramolecular chemistry, Synthetic recognition motifs, Macrocycles, Structural units, Photo-/electro-chemically active units and Biologically-derived units [2-5].

Hence, supramolecular chemistry deals with the multidisciplinary field of chemistry research areas ranging from organic chemistry to inorganic chemistry; synthesis of host molecule with specific binding site, investigation the behavior of self-assemble complexation of host-guest molecule, and finally applying to materials in daily life. At the present, supramolecular approach has been extensively applied in many applications including smart sensory material technology, catalyst and biomedical therapeutic.

1.1.2 Molecular recognition

Molecular recognition is assigned as the recognition process of specific interaction between host and guest molecules through noncovalent bonding interaction [6, 7]. The perfect recognition processes are influenced by various factors such as an electronic

geometry as well as a polarity of host and guest. After introduction of guest as a target molecule, the responsive unit directly binds to it and subsequently causes one or more properties change which could be determined as the visual appearances such as absorbance, fluorescence emission and redox property [8-12]. Moreover, one of the molecular recognition is chemical recognition, which is composed of binding unit and signaling unit, as shown in Figure 1.1. In order to achieve molecular recognition, the binding site is designed to selectively interact with analytes, while the signaling unit is vital to produce a simultaneously response change after the complexation of host and guest. Hence, the molecular recognition plays an important role in sensory analysis method due to the beneficial properties including fast responsibility, easy operation, and simple low-cost techniques.

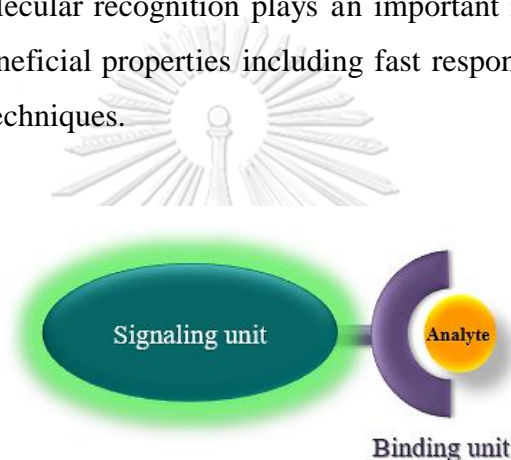


Figure 1.1 The schematic presentation of chemical sensory composition.

1.1.3 Fluorescence

Luminescence is an emission of light which occurred during the electronic transition from excited state to ground state. Luminescence is possibly generated by living organisms, chemical reactions, crystallization and mechanical action on solids. Conceptually, there are two types of luminescence, which are classified by their excited states and ground states; fluorescence and phosphorescence [13-15].

In case of fluorescence, photons incident on a sample and then electron jumps from ground state (S_0) to excited state (S_1). In order to return back to its ground state, electron needs to release an excess energy resulting in an emission of light with a longer wavelength [16, 17]. In term of phosphorescence, electron absorbs an energy from incident photons and then undergoes an intersystem crossing to triplet state (T_1). The

electronic transition of phosphorescence is forbidden because of the change of spin multiplicities. As a result of different electronic transition, the life time of phosphorescence is longer than fluorescence because direction of electron needs to be reversed before relaxing to the ground state [18, 19].

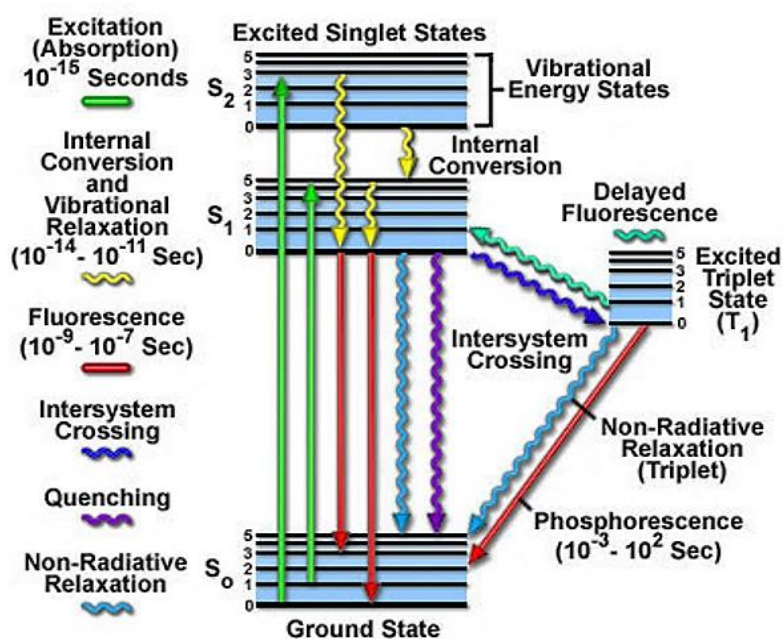


Figure 1.2 The schematic Jablonski diagrams

However, there are a few ways that energy may be dissipated since an electron is excited. The first one as known as vibrational relaxation, which was defined as a non-radiative process corresponding to the kinetic energy of vibrational mode and immediately occurred between the vibrational levels. Moreover, it is possible that the excited electron possibly transits from vibrational level in one electronic state to another vibrational level in another electronic state. This process is assigned as an internal conversion process and normally occurred at the same time as vibrational relaxation because of the overlap of vibrational state and electronic state [20].

Photoinduced electron transfer (PET)

Photoinduced electron transfer (PET) [21, 22] generally served as the transfer process of an electron from a donor to an acceptor. The electron of donor is irradiated by UV or visible light and then transfers to an acceptor. Furthermore, the fluorescent sensor containing fluorophore and responsive unit is able to perform the PET

phenomenon resulting in the weak emission because the electron from HOMO energy level of recognition site relaxes to HOMO of fluorophore causing the inhibition of electron transfer process of LUMO level of fluorophore.

In case of amine-derivative fluorescent sensor, amine functional group carries out as the interaction site and structurally contains the lone pair of nitrogen atom. Hence, the PET could occur from the amine to fluorophore affecting on the weak fluorescence (Figure 1.3). On the contrary, the PET process is suppressed since the amine group interacts with analytes such as aldehyde causing the change of HOMO-LUMO energy level. Based on the change of fluorescence via PET process, there are many researches in various areas deal with this process to investigate further applications.

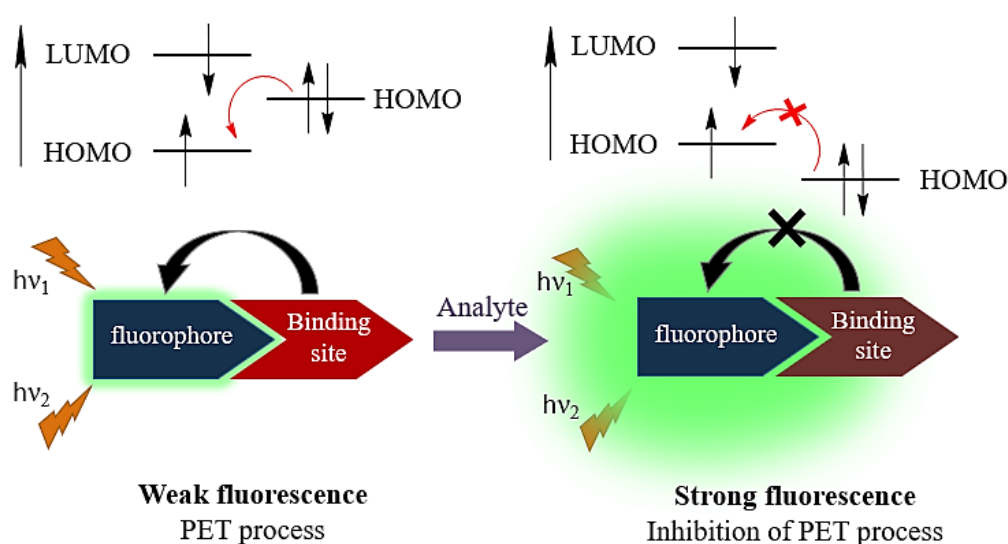


Figure 1.3 The on-off PET process of fluorescence sensor

1.1.4 Micelle

A micelle [23-27] is a supramolecular assembly of surfactants dispersed in liquid colloid. In general, surfactants structurally compose of hydrophilic head and hydrophobic tail. The hydrophilic head is possibly an anionic, a cationic, a zwitterionic, or a non-ionic group, while the tail is a nonpolar hydrocarbon chain. Moreover, surfactants are known as a surface-active molecule due to the combination of the hydrophobic and hydrophilic properties. In aqueous system, surfactant molecules self-

assembly aggregate to form micelles. The hydrophilic head groups expose to water, while hydrocarbon chains organize the hydrophobic core. This self-assembled construction is announced as a normal micelle (oil in water micelle). On the other hand, hydrocarbon chains expose to organic solvent, while the hydrophilic head groups organized water-like core, known as a reverse micelle (water in oil micelle) (Figure 1.4).

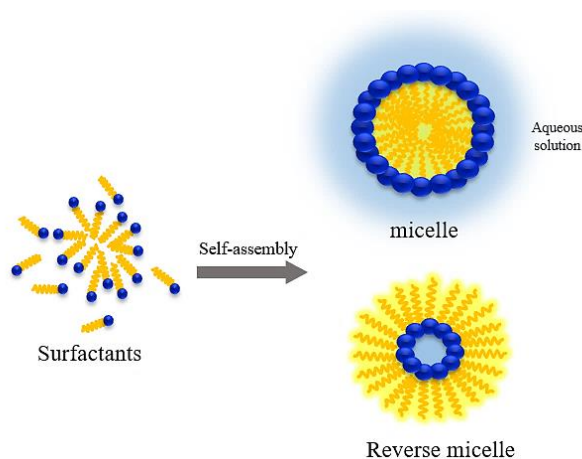


Figure 1.4 The schematic presentation of micelle and reverse micelle.

In general, the organization of self-assembled micelle is corresponding to the hydrophobic interaction of hydrocarbon chains and the polar repulsion of head groups. The formation of micelles in aqueous solution occurs as a result of the mass action model, phase separation model and the standard free energy (ΔG°_{mic}) [28].

$$\Delta G^{\circ}_{mic} = -RT \ln \chi_{CMC}$$

where, χ_{CMC} is the surfactant molar fraction at CMC.

The thermodynamic principle of micellar formation [25, 29, 30] is known as the hydrophobic effect; the driving force causes the spherical aggregation of surfactants dissolving in aqueous media which minimized the contact between hydrocarbon core and water. However, the shape and size of micelle is relatively corresponding to molecular geometry of its surfactants and conditions of solution including surfactant concentration, temperature, pressure and ionic strength. A characteristic of surfactant concentration at which micelles firstly appear in a solution is known as critical micelle concentration (CMC). Below the CMC value, increasing monomer concentration is corresponding to an increasing total surfactant concentration whereas there are no

micelles. Above the CMC, an increasing in the total surfactant concentration does not cause the concentration of monomer change because the surfactant self-assembly aggregates to form micelle. As a result of surfactant-to-micelle transition, the CMC could be determined by a plotting of the physical property [31] such as density, conductance, surface tension, osmotic pressure, or molar conductivity against its surfactant concentration, is illustrated by Preston's plot (Figure 1.5)

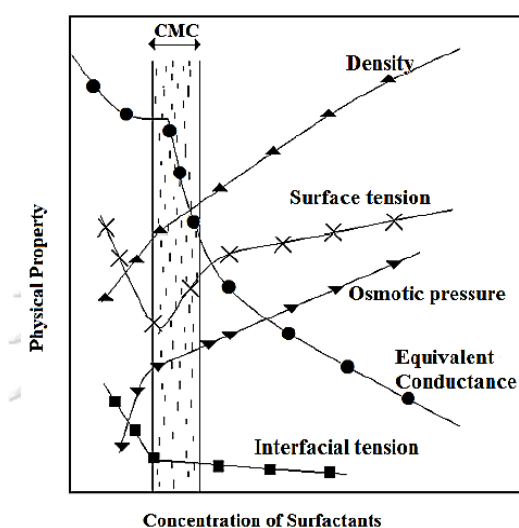


Figure 1.5 The plots of surfactant concentration versus a physical property, such as viscosity, conductance, surface tension, osmotic pressure, or molar conductivity [31].

Moreover, the hydrophobic core of nanomicelle acts as a nanocarrier for hydrophobic organic dye. Since the organic dye is encapsulated into micelle, the dye-surfactant interactions cause the photophysical changes; the characteristic spectra of absorption or emission shift in a wavelength, the new band sometimes appears and the original one disappears. The photophysical changes of dye are attributed to self-assembly of dye-surfactant complex, the aggregation of dye and the surrounding environmental change of dye. Furthermore, micelle possibly encourages a water-soluble and optical property of fluorescent sensor in aqueous environment. The enhancement of fluorescent emission suggests the encapsulation of fluorophore in micelle material that could protect the quenching or deactivation process by dissolved O_2 [32, 33].

In particular, the self-assembled micelle is at the forefront of nanotechnological revolution for various applications ranging from diagnostic imaging to drug-gene

delivery system. They have demonstrated a variety of favorable properties including a good biocompatibility, a good longevity, a good stability in *vitro* and *vivo*, the ability to effectively solubilize the poorly soluble drug or biomarker agents, and the capacity to encourage a permeability for accumulation in target organelles. According to the favorable properties of micelle, it is a fascinating nanomaterial to encapsulate fluorescence sensor for supporting the solubility, the optical property and the selectivity for sensing application in aqueous environment [34, 35].

1.1.5 Gel

Gel [36-39] could be described as a jelly-like material or an intermediate state of matter that lies between solid and liquid because it is more flexible than solid and not flowing as liquid. Moreover, a gelling system is able to immobilize or hold a solvent within its polymeric structure. Generally, gel consists of at least two parts. The first part is known as gelator which is built up a three-dimensional crosslink network to entrap the second part which is solvent or liquid part. After heating the mixture of gelator and solvent over sol-to-gel transition temperature (T_{gel}), the polymer can be liquified due to the collapse of their 3D network. Upon cooling process, the gelator gradually reforms their 3D crosslink network again. According to dispersed solvent of gelling system, it is classified into 2 types.

Hydrogels

Hydrogels or hydrophilic gels is a three-dimensional crosslinked network of water soluble homopolymers or copolymers. The structural polymer might possibly be made from natural polymers or synthetic polymers. The hydrogels are able to immobilize water into the gelling system because of chemical and physical interactions through covalent bond and hydrogen bond. In the presence of hydrophilic functional groups such as hydroxy, amide, carboxylic acid and amine groups on gelator, they effect on the hydrogel structure to encapsulate a large amount of water and maintain its structural integrity. Moreover, there are many advantage properties of hydrogel including biodegradation, biocompatibility and mechanical response. Consequently, it has been received considerable attention in a wide range of industrial and environmental

applications such as superabsorber impound water in agriculture and wound management systems in medication.

Organogels

Organogels is defined as a three-dimensional network of interconnected gelator molecule immobilized a liquid organic solvent as a continuous medium. There are many favorable features of these organogels including long-term use, thermoreversibility, high moisture and temperature resistance, and high capacity to incorporate polar and non-polar guest molecule.

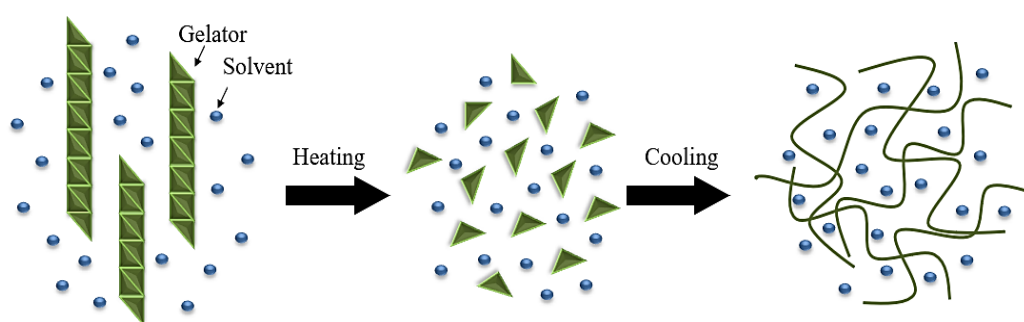


Figure 1.6 Schematic representation of the gelation process for supramolecular gel organization

1.2 Literature reviews

1.2.1 Amine-functionalized sensor for aldehyde detection

In 2015, Dilek O. and Bane L. [40] reported the fluorescent probe for selective targeting of aldehydes in organic solvent, as illustrated in Figure 1.7. There were two fluorescent probes including compound **1** and compound **2**, which were structurally BODIPY and rosamine derivative, respectively. The experimental results illustrated that **1** showed the yellow-bright solution under UV-light with the non-emissive fluorescence. Upon the introduction of salicylaldehyde as a target molecule, the green fluorescent emission at wavelength of 507 nm of **1** was dominantly enhanced under the excitation wavelength of 488 nm. Meanwhile, the solution of **2** showed the red color under UV-light and had a weak orange emission. In the presence of salicylaldehyde, the solution of **2** was obviously changed to pink with a combination of the strong orange fluorescence at 576 nm in quantum yield of 10-fold ($\lambda_{\text{ex}} = 548 \text{ nm}$). These optical

changes in both **1** and **2** could be suggested the blocked of photoinduced electron transfer (PET) process due to the conversion of amine group to imine, because its imine formation increased the energy level of LUMO to prevent the electron transfer.

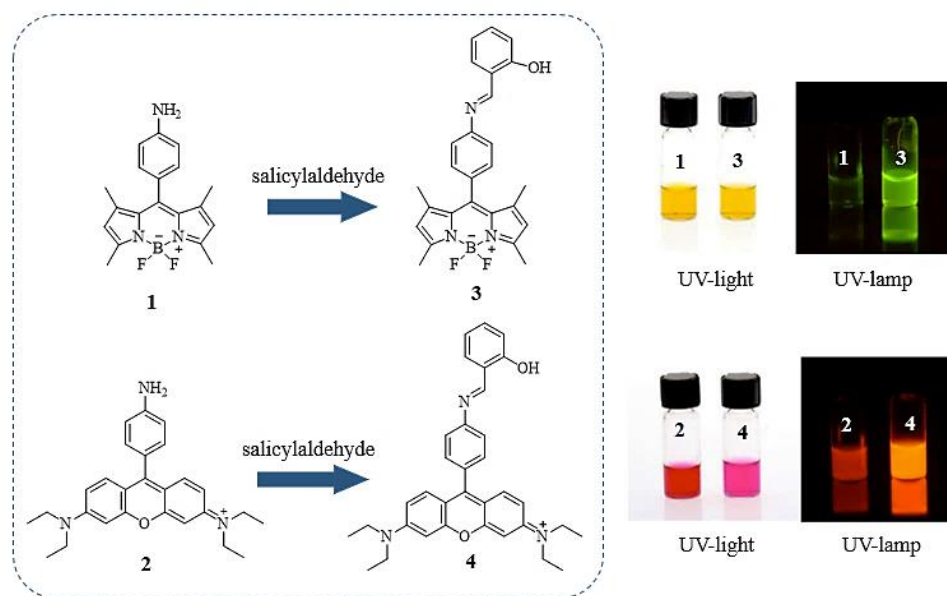


Figure 1.7 The conceptual of **1** and **2** for salicylaldehyde sensing with the micrographs under UV-light and UV-lamp [40].

In 2016, Aksornneam and coworkers [41] investigated 5-aminofluorescein (**FI-NH₂**) doped polyvinyl alcohol (PVA) film for monitoring formaldehyde by using fluorescence spectroscopy, as shown in Figure 1.8. The **FI-NH₂** was carried out as the fluorescent sensor which was consisted of xanthene and amine group as the fluorophore and interaction site, respectively. The reaction for aldehyde sensing was schiff base reaction between amine and formyl group. Subsequently, the imine formation directly affected on the florescent response. The results showed that the fluorescent emission at 520 nm was enhanced with the increment of formaldehyde concentration under the excitation wavelength of 444 nm. The optimal condition for formaldehyde sensing was assigned as 0.05 mM of **FI-NH₂** and 10 min for reaction time. The **FI-NH₂**/PVA sensing film had a good limit of detection ($3.820 \pm 0.079 \mu\text{g L}^{-1}$) and also served as a promising sensor-to-sensor reproducibility (up to 10 times). Furthermore, this developed **FI-NH₂**/PVA sensor was able to be applied for formaldehyde detection in real samples from vegetables, fruits and seafoods [41].

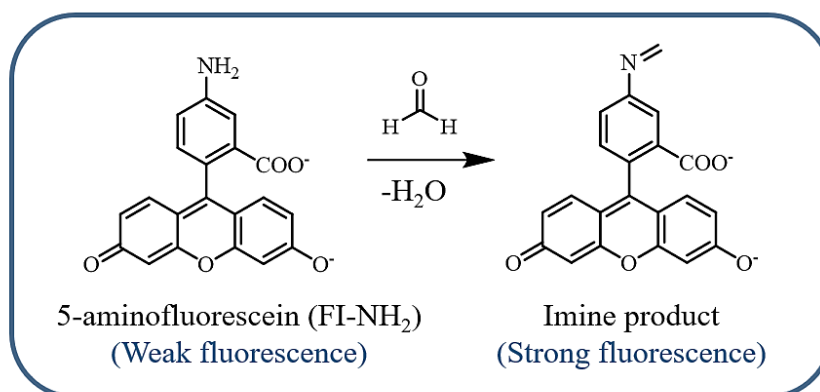


Figure 1.8 The detection principle based on a reaction between **FI-NH₂** and formaldehyde [41]

In 2018, Song and coworkers [42] constructed the reversible fluorescent probe for selective detection of formaldehyde in living cell and in vivo. This probe was BODIPY-derivative cooperated with amine group as the response unit. After the reaction of formaldehyde and amine derivative, an imine formation was obtained and then the C=N isomerization led to an energy decay of the excited state, resulting in fluorescence quenching. The maximum fluorescent wavelength of **BOD-NH₂** at 515 nm under the excitation of 495 nm in 10 mM HEPES buffer pH 7.4. The fluorescent of **BOD-NH₂** was gradually quenched upon increment of formaldehyde concentration ranging in 0-500 μM . The **BOD-NH₂** showed the good selectivity toward formaldehyde, as shown in Figure 1.9. Moreover, the **BOD-NH₂** probe has been successfully applied for detecting and imaging formaldehyde in both living cell and mice.

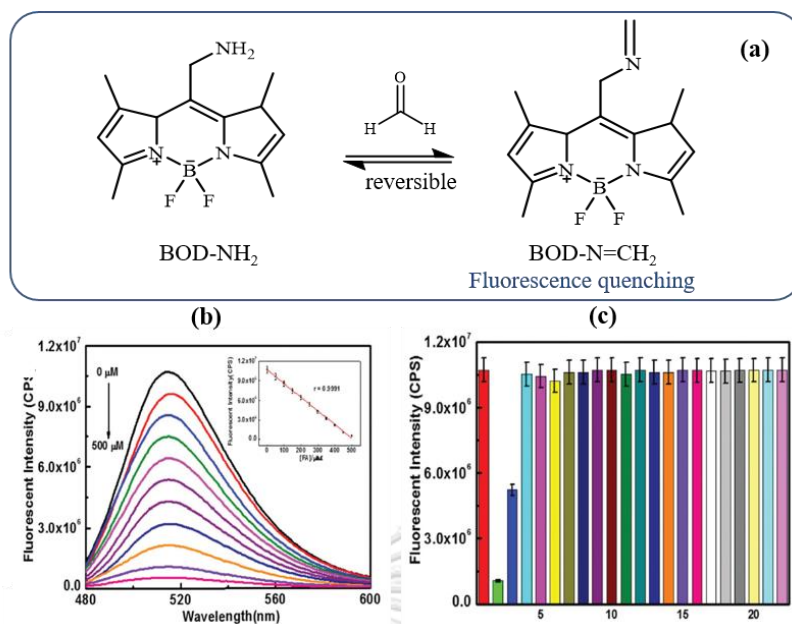


Figure 1.9 (a) The proposed reaction mechanism of formaldehyde detection, (b) The fluorescence spectra of **BOD-NH₂** after introduction of formaldehyde (FA) ranging from 0-500 μ M, (c) The fluorescence responses of **BOD-NH₂** towards reactive chemical species, amino acids and other relevant biological species (1 blank, 2 FA, 3 FA+ 250 μ M NaHSO₃, 4 FA + 500 μ M NaHSO₃, 5 acetaldehyde, 6 methylglyoxal, 7 glyoxal, 8 benzaldehyde, 9 pyridoxal, 10, 4-nitro-benzaldehyde, 11 sodium pyruvate, 12 alanine, 13 glycine, 14 serine, 15 arginine, 16 cysteine, 17 glutathione, 18 glucose, 19 hydrogen peroxide, 20 hydrogen sulfide, 21 methane acid, 22 dehydroascorbate) [42]

1.2.2 Hydrazine-functionalized sensor for aldehyde detection

In 2016, Tang and coworkers [43] studied a lysosome-targeted fluorescent probe for formaldehyde sensing. This probe composed of naphthalimide and hydrazine as the fluorophore and interaction site, respectively (Figure 1.10). In the presence of formaldehyde, the hydrazine reacted with formyl functional group to obtain hydrazone compound through condensation reaction. In this research, the fluorescent emission at 542 nm was largely enhanced (about 350-fold) after introduction of 200 μ M formaldehyde via inhibition of photoinduced electron transfer (PET) process. Furthermore, the fluorescent probe showed a specific detection toward formaldehyde

over other aldehydes and ketone due to its small-size structure. Interestingly, this probe provided the low cytotoxicity and high sensitivity for monitoring endogenous formaldehyde in living cells. Hence, the fluorescence sensor displayed its potential role for biological applications.

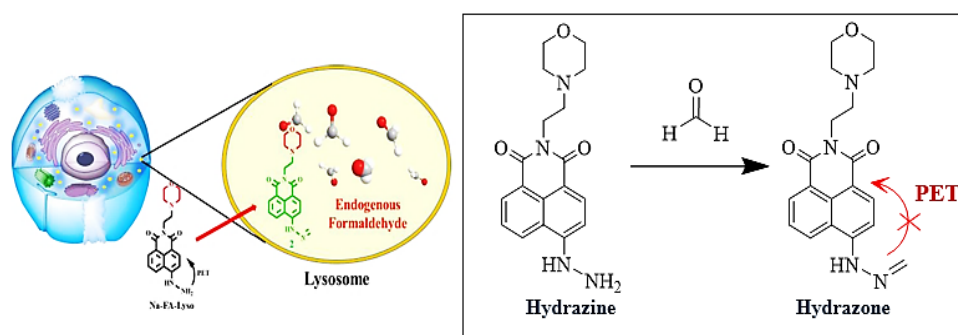


Figure 1.10 Fluorescence response mechanism for formaldehyde detection in lysosome [43]

Moreover, Kamalika and coworkers [44] successfully synthesized a hydrazine-functionalized benzocoumarin as a fluorescent probe for biomolecule carbonyl detection (Figure 1.11). In this approach, a hydrazine derivative of benzocoumarin (**BzCH**) displayed a characteristic of fluorophore in H-aggregates form. In general, H-aggregation is the facial stacking of molecule that often has non-fluorescent property. Upon introduction of carbonyl molecules, they reacted with the hydrazine to obtain hydrazone formation resulting in fluorescent enhancement with a combination of red-shift emission band. The increment of fluorescence was due to the deaggregation of fluorophore corresponding to sp^3 -hybridized carbon of hydrazone. Moreover, the fluorescence probe provided the large stoke shift, which could prevent the overlap between its absorption and emission spectra corresponding to inhibition of self-quenching. This sensor was capable of responding to carbonyl biomolecules in living cell following by the green fluorescence emission. Thus, this probe was an essential fluorescent sensor for carbonyl sensing in biological applications.

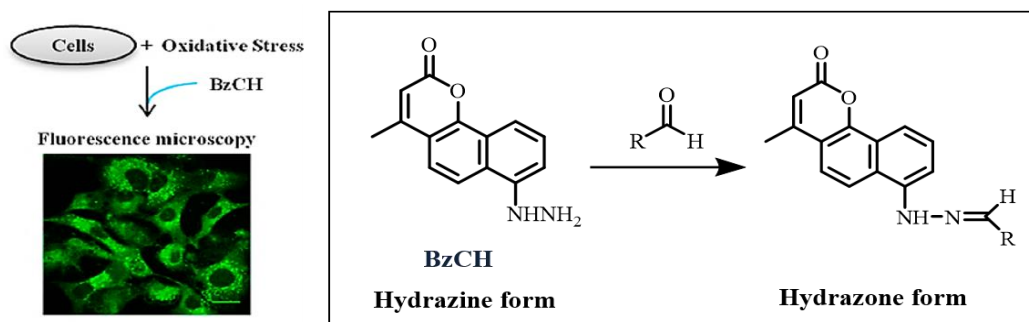


Figure 1.11 Fluorescence responsive mechanism for biomolecule carbonyl detection [44]

1.2.3 Micelle for sensing application

In 2013, Tian and coworkers [45] developed the fluorescent micellar probe for hydrogen sulfide sensing (Figure 1.12). The probe consists of naphthalimide and azo group as the fluorophore and responsive site, respectively. The cetyltrimethyl ammonium bromide (CTAB) and sodium dodecyl sulfate (SDS) was carried out as the surfactants for encapsulation of the azo-derivative fluorescent dye. In the presence of H_2S as a target molecule, azo group of probes was converted to amine via reduction reaction causing the fluorescence enhancement at 540 nm. In case of the micellar system for encapsulation of fluorescent probe, CTAB and SDS also affected on the sensing behavior in a different way, as shown in Figure 1.12c. These could be explained that H_2S normally exists in equilibrium between H^+ and HS^- in aqueous environment. Hence, the negative charge of SDS micelle reasonably repulsed to HS^- , meanwhile, the positive charge of CTAB was attractive to HS^- in order to react with azo-derivative dye. Furthermore, these micellar fluorescence sensors not only provided the high sensitivity and selectivity toward H_2S sensing in aqueous solution, but also were able to be applied for H_2S sensing in fetal brovine serum without any pretreatment of the sample.

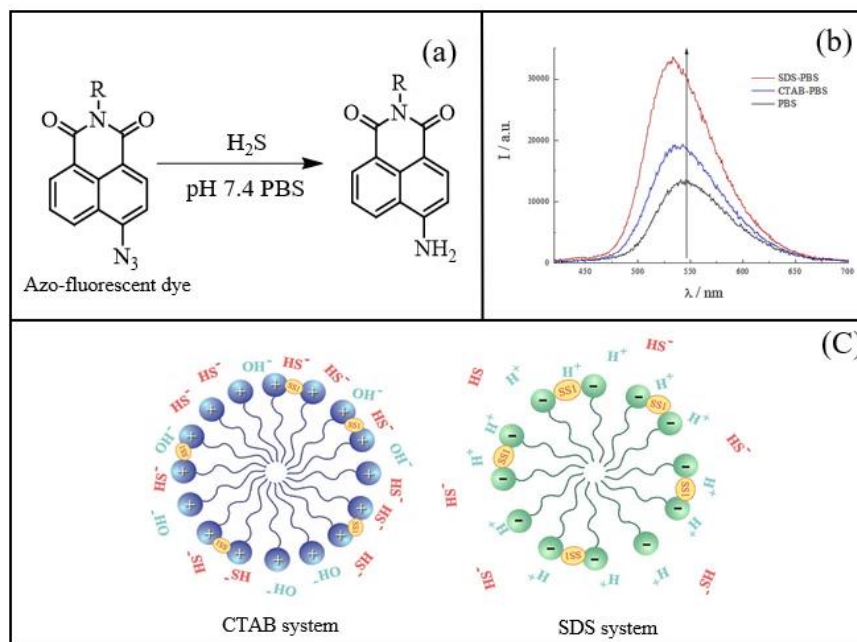


Figure 1.12 Fluorescence responsive mechanism for hydrogen sulfide (a), fluorescence spectra of azo-fluorescent dye in micellar system (b) and schematic representation of the micellar effect including CTAB and SDS [45]

In 2014, Ding and coworkers [33] prepared bispyrene-based fluorescent sensor for detection of picric acid (**PA**) and 2,6-bis(picrylamino)-3,5-dinitropyridine (**PYX**) in aqueous solution based on micellar system, as shown in Figure 1.13. In this study, bispyrene-based probe was encapsulated into both sodium dodecyl sulfate (SDS) micelle and dodecyltrimethylammonium bromide (DTAB). The fluorescent intensity of bispyrene-based probe in SDS micelle provided the maximum emission over other surfactants due to the electrostatic charge between negative charge of SDS and cation of fluorophore. Meanwhile, the electrostatic repulsion between fluorophore and positive charge of DTAB inhibited bispyrene-based probe to encapsulate fluorescent dye resulting in the weak emission intensity. According to the different emission behavior of fluorescent dye for sensing studied in various micellar systems, bispyrene-based probe in SDS and in DTAB was utilized for detection of **PA** and **PYX** sensing in an aqueous environment, respectively. These could be implied that the different sensing ability was caused by the difference of micellar system. Consequently, these

nanomicellar materials could take an important performance for **PA** and **PYX** sensing in aqueous environment.

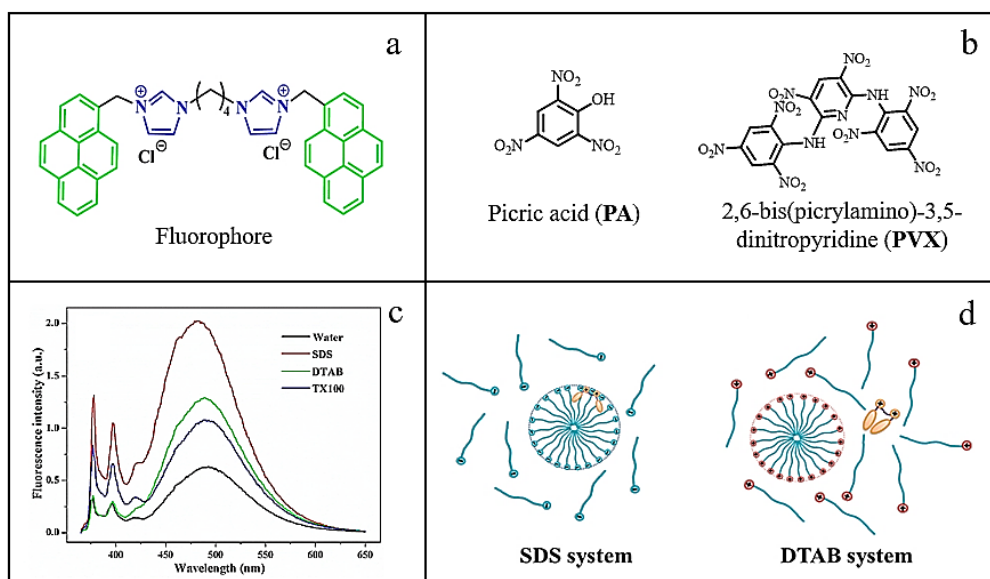


Figure 1.13 a) Structure of fluorophore b) Picric acid (**PA**) and 2,6-bis(picrylamino)-3,5-dinitropyridine (**PVX**) c) Fluorescence spectra of fluorophore in water and in the micellar aqueous solution. SDS, DTAB, Triton X-100) d) Representation of fluorophore distribution in SDS and in DTAB [33]

1.2.4 Gel material for sensing application

In 2018, Miki and coworkers [46] developed a glucose (**Glc**)-responsive gel formed by worm-like micelles (**WLMs**) for a self-regulating insulin delivery, as shown in Figure 1.14. The **WLMs** gel material was consisted of cetyltrimethylammonium bromide (**CTAB**) and phenyl boronic acid (**PBA**) under the aqueous condition at pH 9.4. In basic condition, the **PBA** typically existed in an ionized form because of its pK_a value of 8.8. Hence, the electrostatic interaction and cation - π interaction between the anion species of **PBA** and **CTAB** resulted in the self-assembly organization of gel. However, the viscous gel could not be established by using only **CTAB** surfactant without **PBA** due to the electrostatic repulsion on positive charge of **CTAB**. After the introduction of **Glc**, the gel-like property converted to the solution phase because the

PBA directly binded to **Glc** for **PBA/Glc** forming, which was too bulky or steric to locate inside the **WLN**s. Subsequently, the **PBA/Glc** transferred to aqueous solution inducing the enhancement of the electrostatic repulsion on head group of CTAB and destruction of CTAB-formed gel. As the mentioned above, CTAB surfactant partially played an important role to form soft-material gel which could be utilized for further developed material sensory.

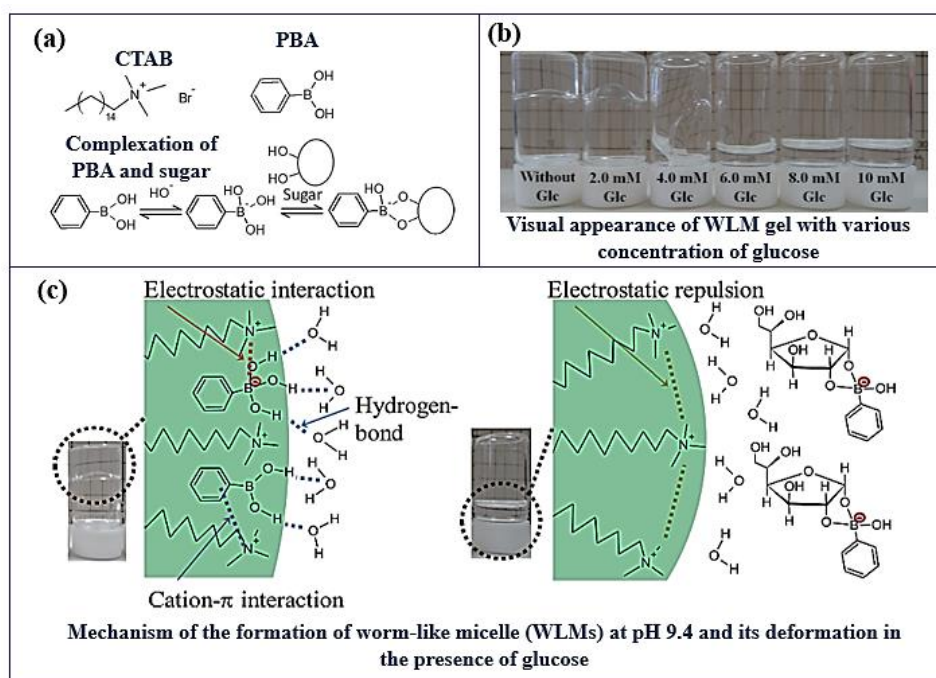


Figure 1.14 (a) Chemical structures of cetyltrimethylammonium bromide (CTAB), phenyl boronic acid (PBA), and the complexation of PBA and sugar, (b) Visual appearance of **WLM** gel with various concentration of glucose, (c) Mechanism of the formation of worm-like micelles (**MLMs**) at pH 9.4 and its deformation in the presence of glucose [46]

In 2015, Wang and coworkers [47] investigated sugar functionalized naphthalimide derivatives based on gel for Eu^{3+} optical sensing through energy transfer (ET) process (Figure 1.15). In this approach, **S1** was carried out as a fluorescence dye consisting of naphthalimide and hydrophilic sugar chain. Moreover, **S1** was also employed as a gelator for self-assembled organized organogel via a heating-cooling process. The green fluorescence emission of **S1** in gel was enhanced and showed red-

shift emission to 546 nm compared with the solution state, suggesting the aggregated-induced emission changed. In case of suspension-to-gel transformation, there were varieties of interactions inside **S1** gel including hydrogen bonding, π - π stacking, and hydrophobic interaction. Upon the introduction of Eu^{3+} into **S1** based on gel, its coordination of pyridine and carbonyl for lanthanide ions demonstrated a new red emission peak at 618 nm and a longer lifetime of luminescence response. Meanwhile, there was no significant change of **S1** in emission and lifetime response under solution system. These results could be described that the energy transfer process of **S1** based on gel occurred upon Eu^{3+} addition. Importantly, the gel system was capable for improvement the fluorescent efficiency and restriction of energy dissipation of **S1** sensor.

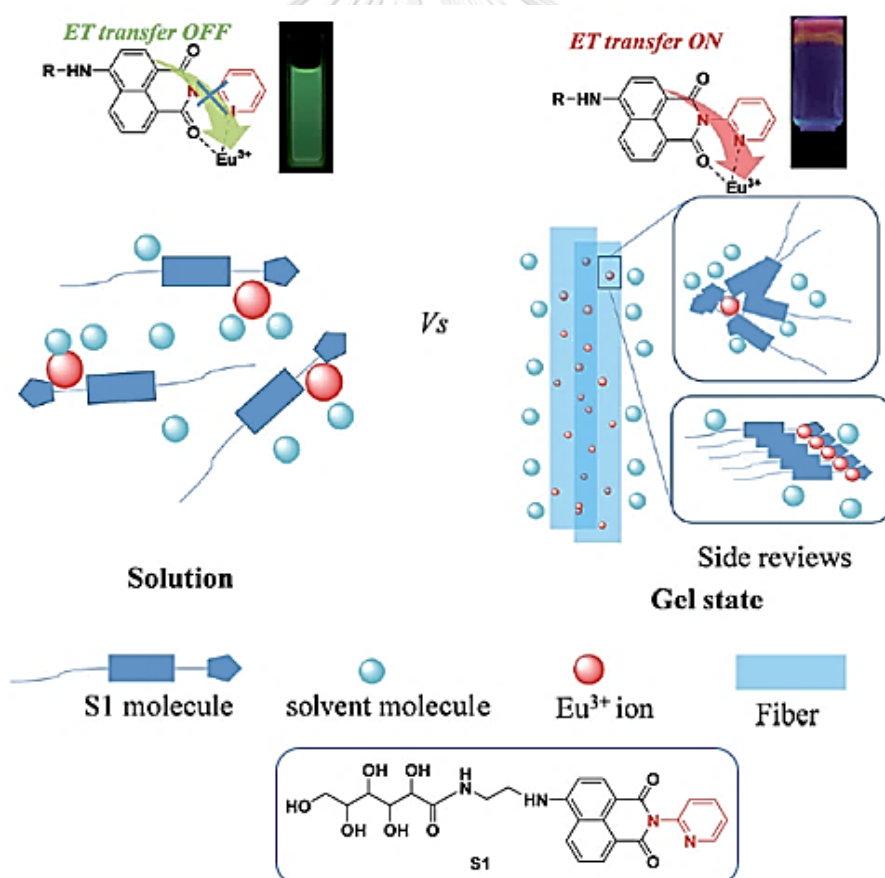


Figure 1.15 Representation of the assembly mechanism and energy transfer process of **S1** and Eu^{3+} ions [47]

In 2017, Cao and coworkers [48] reported naphthalimide-based supramolecular gel for visual detection of 1,4,6-trinitrophenol (**TNP**) by using fluorescent spectroscopy (Figure 1.16). In this research, the **G-P** molecule was served as both fluorescent sensor and gelator because of its electron-rich property and the intermolecular non-covalent interaction. In case of **G-P** gel-based sensor, the emission band displayed blue-shifted emission band from 501 nm to 485 nm. Hence, the gel-like system caused in the environmental surrounding change of **G-P** molecule. Owing to the conceptual design, the pyridine group of **G-P** was expected to interact with **TNP** via electron donor-acceptor interaction and subsequently affected on the photophysical property of gelling sensor. After the introduction of **TNP** as a target molecule, its blue fluorescence emission was prominently quenched because the intramolecular charge transfer (ICT) process of **G-P** was possibly suppressed. Furthermore, the **G-P** gelator was further applied as the test strips for portable sensing with a good selectivity over other nitro aromatic compounds. Hence, the **G-P** based gel has a potential to perform as the promising fluorescent probe for **TNP** sensing.

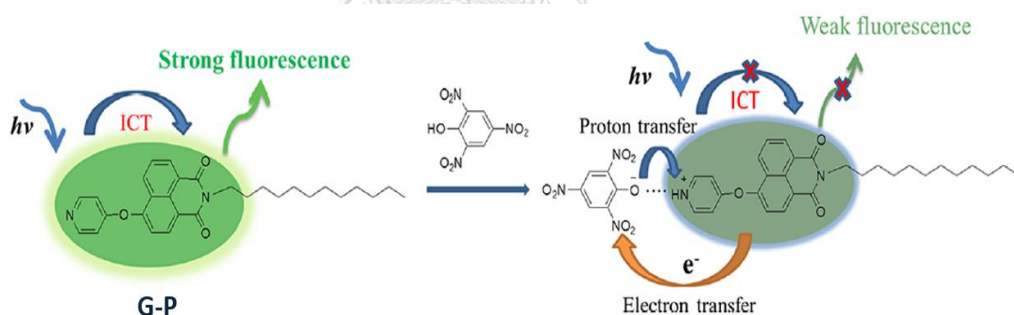


Figure 1.16 Proposed detection mechanism of **TNP** based on **G-P** gel [48]

In 2009, Wada and coworkers [49] successfully developed a fluorescence sensing system for determination of polyanions. The novel polyanion-selective sensor composed of a hybrid material of hydrogel, enzyme and **MCM41** silica nanoparticles. Firstly, the fluorescent probe (**P-coum 2**) was entrapped within amine-modified silica nanoparticles (**NH₂-MCM41**) in acidic aqueous solution (pH 5) through the electrostatic interaction between anionic species of **P-coum 2** and the cationic amines. Subsequently, they also constructed the fluorescent based **MCM41** material sensor for

polyanion by hybridization with supramolecular hydrogel. As a self-assembly organization of hydrogel, the combination between compound **1** and compound **4** was employed as a gelator through hydrogen bonding interaction. Furthermore, the phosphatase enzyme (**ACP** or **AP**) was entrapped in the hybrid material to interact with **P-coum 2**. In the presence of polyanion as a target molecule, the releasing of **P-coum 2** was efficiently induced because polyanion strongly bound to the positive charge of amine on **NH₂-MCM4** and subsequently **P-coum 2** was replaced. After that, **ACP** or **AP** enzyme hydrolyzed the phosphate group of **P-coum 2** and the fluorescence resonance energy transfer (FRET) was simultaneously occurred. The fluorescence emission was enhanced. Furthermore, this hybrid material provided a good selectivity toward polysulfate and polyphosphates such as Suc-8S, IP6, heparin and chondroitin sulfates. Hence, the hybrid material coupling of silica nanoparticles, hydrogel and enzyme was an alternative candidate material for further sensory applications.

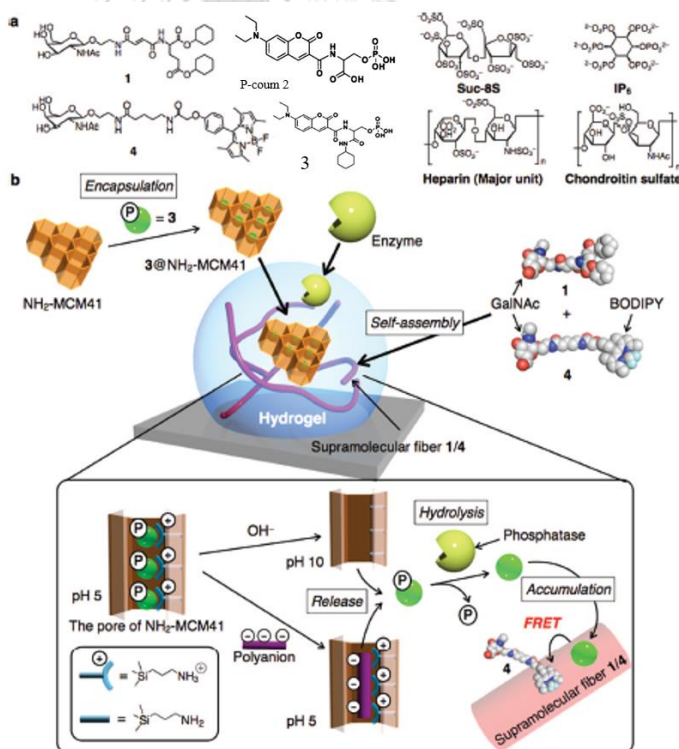


Figure 1.17 Construction and mechanism operating in fluorescent dye encapsulated MCM-enzyme-hydrogel hybrid sensory system [49]

Maria Emilia C. and coworkers [50] constructed di-lauroyl-L-tartaric acid hydrogel. The gelator containing long-chain hydrocarbon of lauric acid and lactose which is a disaccharide of galactose and glucose. According to the amphiphilic structure of hydrogelator, H-bonding of hydroxy groups on sugar moiety and vander waals interactions of non-polar tails performs as the driving force for gelation. At the room temperature at concentration of 0.1 w/v% in water, gelator **1** could form gel and does not flow after inversion of the flask at room temperature, whereas, the gelation of **2** did not occur and also precipitated. The morphology of gel **1** and gel **2** were studied by using SEM technique. The SEM micrographs of gel **1** has a dense 3D fiber network structure with an average diameter at 7.8 nm. Meanwhile, the gel **2** fibers have an external diameter of about 45 nm and also has a looser arrangement than gel **1**. These could be supposed that the physical properties of gel depend on the amount of carbon atom on flexible linker. Consequently, sugar-based gelator could impact on the self-assembly supramolecular hydrogelation.

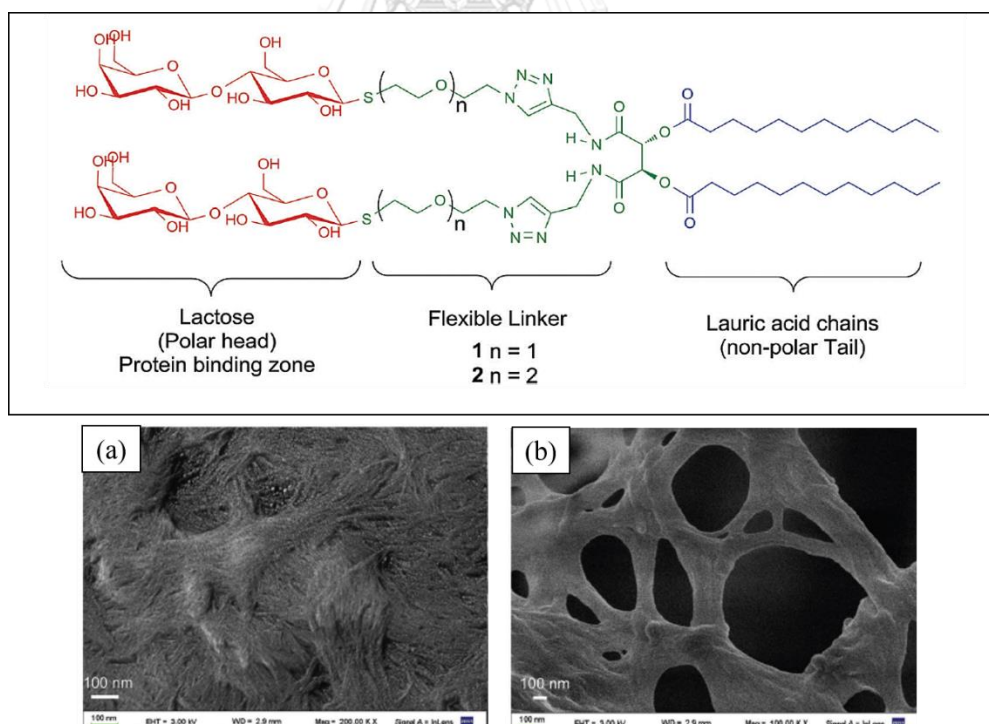


Figure 1.18 The chemical structure of **1** and **2** gelator, The SEM micrographs of gel **1** (a) and gel **2** (b) [50]

Maria J. Clemente and coworkers [51] investigated disaccharide-based gelator which has azobenzene as light-sensitive unit. The gelators were synthesized by the click reaction of a hydrophobic maltose and palmitic chain which has an azobenzene group on the hydrophobic tail at different position. All gelators could establish 3D network via π - π stacking of triazol ring, H-bonding of OH groups on maltose, and vander waals interaction of long-chain hydrocarbon. However, the gelation behaviors were different, for instance, the **Malt-Tz-Azo-C₁₆** and **Malt-Tz-C₁₀-Azo-OCH₃** could organize 3D gel in DMSO/water (1:1) at concentration at 1.5 wt% and 2.0 wt%, respectively. Meanwhile, **Malt-Tz-C₅-Azo-C₈** could not form gel. Moreover, the TEM results showed the different morphologies of the fiber network. Hence, the position of azobenzene ring played an essential role for gel organization.

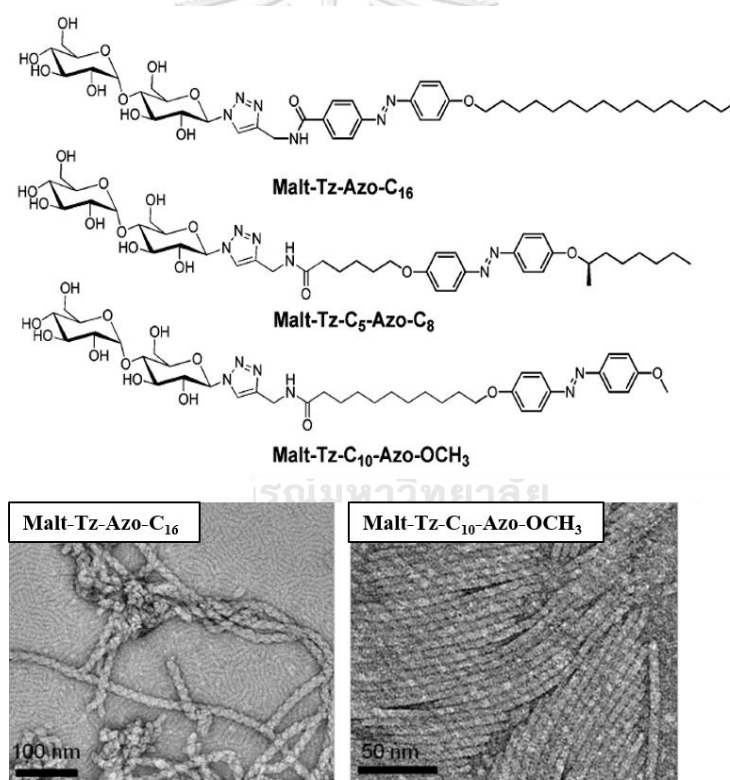


Figure 1.19 The chemical structure and TEM images of maltose-based gelators [51]

1.3 Objectives

- To synthesize fluorescent sensors for aldehyde detection
- To optimize the micellar system and study a sensing ability of nanomicelle for long-chain aldehyde detection by using UV-visible spectroscopy and fluorescence spectroscopy



CHAPTER II

EXPERIMENTAL

2.1 General procedures

2.1.1 Analytical instruments

Nuclear magnetic resonance (NMR) spectra were performed with a Varian Mercury Plus 400 spectrometer and Bruker Advance 400 spectrometer. The chemical shift (δ) was recorded in part per million (ppm) which had a residue proton solvent as an internal reference. Samples were dissolved in d_3 -CDCl₃ and d_6 -DMSO. Analysis of mass spectra was measured using MALDI-TOF mass spectrometer. UV-Visible absorption spectra were recorded in the range of 200-800 nm by using Varian Cary 50 UV-visible spectrophotometer. The resulting spectrum was presented as a graph of absorbance versus wavelength. All fluorescence spectra were measured by Cary Eclipse Varian fluorescence spectrophotometer which composed of Cary Eclipse a pulsed xenon lamp and photomultiplier tube as a light source and photomultiplier tube, respectively. All naked-eyed fluorescence photos were recorded by iPhone 8. Moreover, micelles were separated by using Eppendorf centrifuge 5804Rn and characterized by Transmission Electron Microscopy (TEM) and Scanning Electron Microscopy (SEM). Size distributions of nanomaterials were investigated by Dynamic Light Scattering (DLS) technique. The confocal laser scanning microscopy (CLSM) model Nikon Eclipse Ti with 405, 488 and 561 nm was carried out to study the cellular uptake of A549 cells.

2.1.2 Materials

All reagents were purchased from Aldrich, Merck, Fluka and TCI. They were used without further purification. All commercial grade solvents for synthesis were dried up with molecular sieve as a drying agent. Spectroscopic-grade dimethylsulfoxide (DMSO) in UV-visible and fluorescence measurement was obtained from Merck. Column chromatography was carried out on silica gel (Kieselgel 60, 0.063-0.200 mm, Merck). Thin-layer chromatography (TLC) was performed on silica gel plates (Kieselgel

60 F254, 1 mm, Merck). The lung cancer cells (A549) were obtained from the Institute of Biotechnology and Genetic Engineering, Chulalongkorn University.

2.2 Synthesis

2.2.1 Synthesis of Phenazine-2,3-diamine[52]

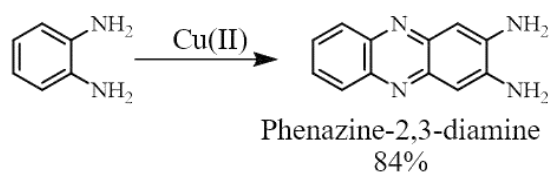


Figure 2.1 Synthesis pathway of phenazine-2,3-diamine

O-phenylenediamine (0.200 g, 1.85 mmol) and 10 mL of 0.1 M copper acetate (5.0 mmol) were mechanically stirred in water at room temperature for 4 h. After the reaction was completed, the resulting bluish colored solution was collected and then purified by extraction with dichloromethane to obtain phenazine-2,3-diamine. (84% yield)

¹H-NMR (400 MHz, *d*₆-DMSO): δ (in ppm) = 7.86 (s, 2 H, ArH), 7.53 (s, 2 H, ArH), 6.88 (s, 2H, ArH), 6.20 (s, 4 H)

2.2.2 Synthesis of hydrazine-functionalized sensor (Naph-NH₂)

The hydrazine-functionalized sensor (**Naph-NH₂**) was synthesized by using 4-bromo-1,8-naphthalic anhydride as a starting material. The pathway of synthesis was illustrated in Figure 2.2

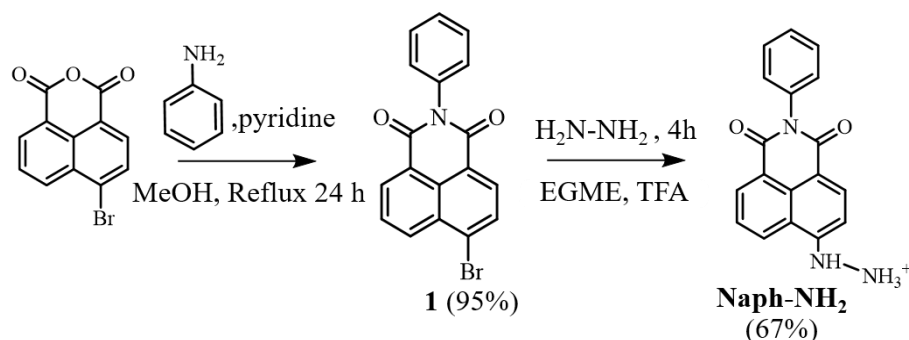
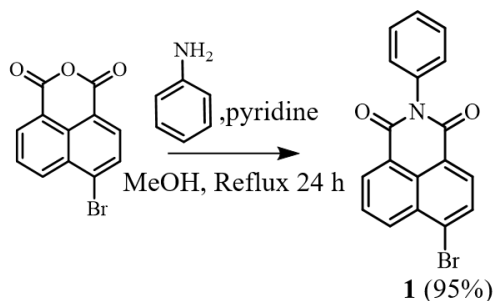


Figure 2.2 Synthesis pathway of hydrazine-functionalized sensor (**Naph-NH₂**)

2.2.2.1 Synthesis of 6-Bromo-2-phenyl-1H-benzo[de]isoquinoline-1,3(2H)-dione

(1)



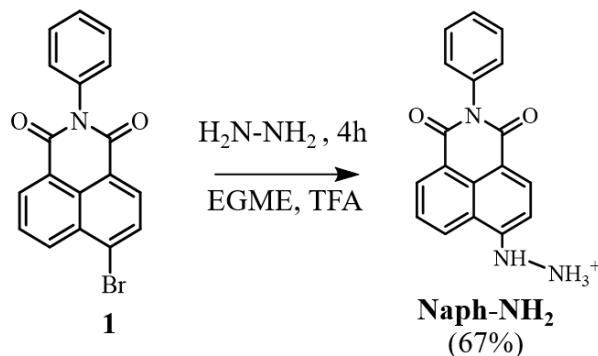
According to the hygroscopic property of aniline, it was distilled to obtain the colorless liquid before using. After that, 4-bromo-1,8-naphthalic anhydride (4.00 g, 14.44 mmol) was added into the methanolic solution of aniline (1.5 mL, 16.43 mmol) and stirred at room temperature for 5 min. The catalytic amount of pyridine was added to the mixture and it was refluxed overnight under nitrogen atmosphere. After the reaction was completed, methanol was removed by a rotary evaporator under reduced pressure. The crude product was recrystallized by methanol:hexane (1:1) to obtain a white colored compound (**1**) within 95% yield.

¹H-NMR (400 MHz, *d*₆-DMSO): δ (in ppm) = 8.56 (d, J = 6.8 Hz, 2 H, ArH), 8.31 (d, J = 6.6 Hz, 1 H, ArH), 8.22 (d, J = 6.5 Hz, 1 H, ArH), 8.00 (t, J = 7.3 Hz, 1 H), 7.64 (d, J = 7.4, 7.3 Hz, 2 H, ArH), 7.48 (t, J = 7.2, 7.3 Hz, 1 H, ArH), 7.37 (t, J = 6.8 Hz, 2 H, ArH).

¹³C-NMR (100 MHz, *d*₆-DMSO): 163.14, 163.08, 135.75, 132.69, 131.57, 131.36, 130.93, 129.92, 129.15, 129.01, 128.85, 128.81, 128.75, 128.26, 123.34, 122.57

MALDI-TOF mass: Anal. Calcd. m/z For $[\text{C}_{18}\text{H}_{11}\text{BrNO}_2]^+$ = 352.00 Found m/z = 352.52

2.2.2.2 Synthesis of 6-hydrazinyl-2-phenyl-1H-phenalene-1,3(2H)-dione (Naph-NH₂)



Compound **1** (0.200 g, 0.57 mmol) was dissolved in ethylene glycol monomethyl ether (EGME) and then added hydrazine monohydrate (0.70 mL, 14.40 mmol) was added into the mixture. The mixture was refluxed for 4 h under nitrogen atmosphere. After the reaction was completed, the crude product was obtained by cooling under non-aqueous condition. The trifluoroacetic acid (TFA) was used to adjust the product at pH 3-4. Finally, the sediment was recrystallized with hexane to afford **Naph-NH₂** as an orange solid. (67% yield)

¹H-NMR (400 MHz, *d*₆-DMSO): δ (in ppm) = 9.24 (s, 1 H, NH), 8.59 (d, *J* = 7.6 Hz, 2 H, ArH), 8.41 (d, *J* = 6.6 Hz, 2 H, ArH), 8.28 (d, *J* = 8.3 Hz, 2 H, ArH), 7.64 (s, 2 H, ArH), 7.21 (d, *J* = 8.6 Hz, 2 H, ArH), 5.53 (s, 2 H, NH₂).

¹³C-NMR (100 MHz, *d*₆-DMSO): 199.51, 160.62, 153.97, 134.79, 134.27, 133.22, 132.07, 131.89, 131.46, 130.74, 130.02, 129.73, 129.33, 128.72, 128.48, 127.62, 126.48, 124.59, 122.14, 119.73, 118.32, 106.71, 104.61, 31.12

MALDI-TOF mass: Anal. Calcd. *m/z* For [C₁₈H₁₄N₃O₂]⁺ = 304.11 Found *m/z* = 303.50

FT-IR (ATR-IR) cm⁻¹: 3336.1, 3288.9, 3225.9 (ν NH); 3054.8 (ν ArCH); 1625.8, 1570.7 (ν C=O); 1535.8, 1467.5, 1438.7 (ν ArC=C)

2.2.3 Synthesis of 6-Methoxy-2-phenyl-1H-benzo[de]isoquinoline-1,3(2H)-dione (Naph-OMe)

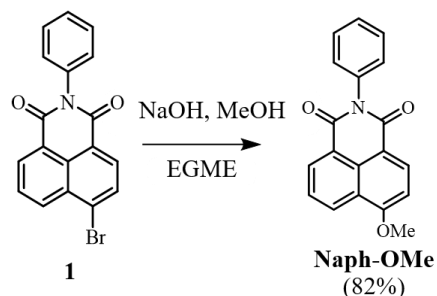


Figure 2.3 Synthesis pathway of 6-Methoxy-2-phenyl-1H-benzo[de]isoquinoline-1,3(2H)-dione (**Naph-OMe**)

The methanolic solution of NaOH (0.500 g, 12.5 mmol) was added to the mixture of compound **1** (0.200 g, 0.57 mmol) in ethylene glycol monomethyl ether (EGME). The reaction was refluxed overnight under nitrogen atmosphere. After cooling the mixture to the room temperature, the precipitated product was obtained by gradually adding a cold water. After that, the precipitate was filtered and also washed with cold ethanol to afford a yellow solid compound (**Naph-OMe**) in 82% yield.

¹H-NMR (400 MHz, *d*₆-CDCl₃): δ (in ppm) = 8.63 (dd, *J* = 16.4, 7.8 Hz, 3H, ArH), 7.74 (t, *J* = 7.8 Hz, 1H, ArH), 7.54 (d, *J* = 7.6 Hz, 2 H, ArH), 7.48 (d, *J* = 7.2 Hz, 1 H, ArH), 7.32 (d, *J* = 7.2 Hz, 2 H, ArH), 7.09 (d, *J* = 8.3 Hz, 1 H ArH), 4.16 (s, 3 H, CH₃).

¹³C-NMR (100 MHz, *d*₆-DMSO): 136.63, 133.76, 131.55, 129.62, 129.26, 128.86, 128.52, 126.88, 106.75, 57.15, 40.45, 40.25, 40.04, 39.83, 39.60.

MALDI-TOF mass: Anal. Calcd. *m/z* For [C₁₉H₁₃NNaO₃]⁺ = 326.08 Found *m/z* = 325.51

2.2.4 Synthesis of 6,6'-Disulfanediybis(hexan-1-ol) (S2)

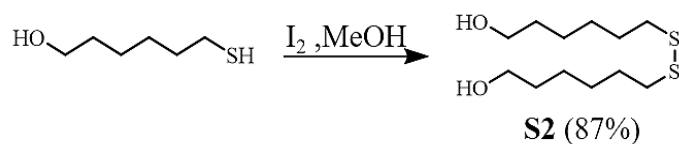


Figure 2.4 Synthesis pathway of 6,6'-Disulfanediybis(hexan-1-ol) (**S2**)

The 6-mercapto-1-hexanol (0.500 g, 3.72 mM) and iodine (1.00 g, 3.94 mM) were dissolved in 15 mL of methanol solution. The mixture was turned from colorless to dark-brown and subsequently stirred at room temperature overnight. After the reaction was completed, sodium thiosulfate pentahydrate was added to quench the reaction resulting in the color change of light-yellow solution. After that, the methanol was removed under the reduce pressure and purified by using column chromatography (100% dichloromethane) to afford the white solid of S2 was obtained in 87% yield.

¹H-NMR (400 MHz, *d*₃-CDCl₃): δ (in ppm) = 3.63 (t, *J* = 6.5 Hz, 2 H, CH₂), 2.67 (t, *J* = 7.3 Hz, 2 H, CH₂), 1.69 (t, *J* = 14.5, 7.2 Hz, 2 H, CH₂), 1.56 (t, *J* = 13.5, 6.8 Hz, 2 H, CH₂), 1.40 (m, *J* = 1.39 Hz, 4 H, CH₂)

¹³C-NMR (100 MHz, *d*₃-CDCl₃): 62.68, 39.05, 32.52, 29.12, 28.23

2.3 Qualitative discrimination of aldehydes using amine-functionalized and hydrazine-functionalized sensor

2.3.1 Screening studied of amine-functionalized and hydrazine-functionalized sensor with heptanal

The stock solutions of 0.1 M amine-functionalized or hydrazine-functionalized dye and 0.05 M heptanal were prepared in dried dimethyl formamide (DMF). The complexation was carried out by stirring at room temperature for 20 min. Consequently, the final volume of solution was adjusted to 3.0 mL and then collected the fluorescence spectra by using the following condition.

Table 2.1 amine-functionalized and hydrazine-functionalized sensor with heptanal

Amine-functionalized dye	Volume of dye	Volume of heptanal	Fluorescence condition
<i>o</i> -phenylenediamine	15 μ L	15 μ L	$\lambda_{\text{ex}} = 438 \text{ nm}$ Slit = 5.0 PMT 800
phenazine-2,3-diamine	15 μ L	15 μ L	$\lambda_{\text{ex}} = 360 \text{ nm}$ Slit = 5.0 PMT 800
4-hydrazinobenzoic acid	15 μ L	15 μ L	$\lambda_{\text{ex}} = 430 \text{ nm}$ Slit = 5.0 PMT 800

2.3.2 Fluorescence studies of 6-hydrazinyl-2-phenyl-1H-phenalene-1,3(2H)-dione (Naph-NH₂) with aldehydes

The stock solutions of 0.01 M **Naph-NH₂** and 0.05 M of 5 representative aldehyde compounds including formaldehyde, heptanal, benzaldehyde, 3-hydroxybenzaldehyde and 4-nitrobenzaldehyde were prepared in spectroscopic dimethyl sulfoxide (DMSO).

Table 2.2 The amounts of representative aldehyde compounds

Aldehydes	Molecular weight (g/mol)	Weight (g)	Final volume (mL)
Formaldehyde	30.03	0.0075	5.00
heptanal	114.19	0.0285	5.00
benzaldehyde	106.12	0.0265	5.00
3-hydroxybenzaldehyde	122.12	0.0305	5.00
4-nitrobenzaldehyde	151.12	0.0378	5.00

To study the complexation formation in organic solvent (100% DMSO), 15 μL of 0.01 M **Naph-NH₂** and 15 μL of aldehydes stock solution were stirred for 20 min at room temperature and subsequently diluted with DMSO to 3.0 mL.

In case of the sensor ability in an aqueous environment, the complexation formation between **Naph-NH₂** and heptanal was prepared by stirring 15 μL of M **Naph-NH₂** and 15 μL of aldehyde stock solutions at room temperature for 20 min. After that, the mixed solution was diluted to 3.0 mL in 2.5% DMSO/PBS buffer pH 7.4. The fluorescent emissions were detected by using the following condition

Start:	465 nm
End:	800 nm
Excitation:	445 nm
Excitation slit:	10.0
Emission slit:	10.0
PMT	550

2.3.3 Optimization of micellar system for 6-hydrazinyl-2-phenyl-1H-phenalene-1,3(2H)-dione (Naph-NH₂)

2.3.3.1 Optimization of surfactant for 6-hydrazinyl-2-phenyl-1H-phenalene-1,3(2H)-dione (Naph-NH₂)

The stock solutions of 0.01 M **Naph-NH₂** was prepared in spectroscopic dimethyl sulfoxide (DMSO). The 0.1 M stock solutions of surfactants including cetyltrimethylammonium bromide (CTAB), sodium dodecyl sulfate (SDS) and triton X-100 were prepared in 0.01 M PBS buffer pH 7.4.

Table 2.3 The amounts of surfactants for optimized micellar sensor

Surfactants	Molecular weight (g/mol)	Weight (g)	Final volume (mL)
CTAB	364.45	0.0729	2.00
SDS	288.37	0.0578	2.00
Triton X-100	647.00	0.1294	2.00

To prepare the micellar system for encapsulation of **Naph-NH₂** molecule, 200 μ L of 0.1 M surfactants in PBS buffer pH 7.4 and was stirred at room temperature for 10 min. After that, 15 μ L of 0.01 M **Naph-NH₂** was added to the mixture solution which was then diluted to 3.0 mL in 2.5% DMSO/PBS buffer pH 7.4. Finally, the solution was stirred for 20 min and the fluorescence spectra were recorded as the following condition.

Start:	465 nm
End:	800 nm
Excitation:	445 nm
Excitation slit:	10.0
Emission slit:	10.0
PMT	550

2.3.3.2 Critical micelle concentration (CMC) studies of CTAB

The 0.1 M stock solution of CTAB surfactant was prepared in 0.01 M PBS buffer pH 7.4. Firstly, the micellar system by CTAB was prepared by stirring the solution for 10 min. After that, 15 μL of 0.01 M **Naph-NH₂** was added to the above solution and then it was diluted to 3.0 mL in 2.5% DMSO/PBS buffer pH 7.4. Finally, the solution was stirring at room temperature for 20 min and the fluorescent emission spectra were record under the following condition.

Start: 465 nm
 End: 800 nm
 Excitation: 445 nm
 Excitation slit: 10.0
 Emission slit: 10.0
 PMT 550

Table 2.4 The critical micelle concentration (CMC) studies of **Naph-NH₂** in CTAB micellar system (2.5% DMSO/PBS buffer pH 7.4).

Entry	[CTAB], mM	Volume of CTAB (μL)	Total Volume (mL)
1	0	0	3.00
2	0.33	10	3.00
3	0.67	20	3.00
4	1.00	30	3.00
5	1.33	40	3.00
6	1.67	50	3.00
7	2.00	60	3.00
8	2.33	70	3.00
9	2.67	80	3.00
10	3.00	90	3.00
11	3.33	100	3.00

2.3.3.3 Optimization of co-surfactant in CTAB micellar system for encapsulation of Naph-NH₂

The stock solution of 0.01 M **Naph-NH₂** and 0.5 M co-surfactants (Table 2.5) were prepared in dimethyl sulfoxide (DMSO spectroscopic grade). Meanwhile, the stock solution of CTAB was dissolved in 0.01 M PBS buffer pH 7.4. In this experiment, the micellar system for encapsulation of **Naph-NH₂** by the mixture of CTAB and **S2** surfactants. For the preparation of **CTAB/co-surfactant** micellar system, 30 μ L of CTAB and 5 μ L of co-surfactant were stirred for 10 min. After that, 15 μ L of **Naph-NH₂** was added to and stirred above solution for 10 min. After the encapsulation of fluorescent dye, 15 μ L of 0.05 M heptanal was added to the solution which was kept stirring for 20 min. The fluorescence spectra were recorded as the following condition.

Start: 465 nm
 End: 800 nm
 Excitation: 445 nm
 Excitation slit: 10.0
 Emission slit: 10.0
 PMT 550

Table 2.5 The co-surfactants coupled with CTAB for encapsulation of **Naph-NH₂**

Entry	Co-surfactants	MW
1	ethanol	46.07
2	butanol	74.12
3	hexanol	102.23
4	octanol	130.23
5	6-mercapto-1-hexanol	134.24
6	ethylenediamine	60.10
7	ethanolamine	61.08
8	cysteamine	77.15

2.3.3.4 Critical micelle concentration (CMC) studies of S2

The stock solutions of 0.01 M **Naph-OMe** and 0.5 M **S2** were prepared in dimethyl sulfoxide (DMSO spectroscopic grade). First of all, the micellar system at various concentration of **S2** (Table 2.6) was prepared by stirring the solution for 10 min. After that, 15 μL of **Naph-OMe** stock solution was added to the above solution and then it was diluted to 3.0 mL in 2.5 % DMSO/PBS buffer pH 7.4. Finally, the solution was stirring at room temperature for 20 min, the fluorescence spectra were recorded under the following condition.

Start: 395 nm
 End: 800 nm
 Excitation: 385 nm
 Excitation slit: 5
 Emission slit: 5
 PMT 500

Table 2.6 The critical micelle concentration (CMC) studies of **Naph-OMe** in **S2** micellar system (2.5% DMSO/PBS buffer pH 7.4).

Entry	[S2], mM	Volume of S2 (μL)	Total Volume (mL)
1	0.33	2.00	3.00
2	0.50	3.00	3.00
3	0.67	4.00	3.00
4	0.83	5.00	3.00
5	1.00	6.00	3.00
6	1.17	7.00	3.00
7	1.33	8.00	3.00
8	1.50	9.00	3.00
9	1.67	10.00	3.00
10	1.83	11.00	3.00
11	2.00	12.00	3.00

2.3.3.5 Optimization of S2 concentration in CTAB micellar system for encapsulation of Naph-NH₂

The stock solution of 0.01 M **Naph-NH₂** and 0.5 M **S2** were prepared in dimethyl sulfoxide (DMSO spectroscopic grade). Meanwhile, the stock solution of CTAB was dissolved in 0.01 M PBS buffer pH 7.4. In this experiment, the micellar system for encapsulation of **Naph-NH₂** by the mixture of CTAB and **S2** surfactants. For the preparation of **CTAB/S2** micellar system, 30 μ L of CTAB and **S2** at various concentration were stirred for 10 min. After that, 15 μ L of **Naph-NH₂** was added to the above solution and stirred for 10 min. After the encapsulation of fluorescent dye, 15 μ L of 0.05 M heptanal was added to the solution which was kept stirring for 20 min. The fluorescence spectra were recorded under the following condition.

Start: 465 nm
 End: 800 nm
 Excitation: 445 nm
 Excitation slit: 10.0
 Emission slit: 10.0
 PMT 550

Table 2.7 The optimization of **S2** concentration for encapsulation **Naph-NH₂** in **CTAB/S2** micellar system. (2.5% DMSO/PBS buffer pH 7.4)

Entry	[CTAB], mM	Volume of CTAB (μ L)	[S2], mM	Volume of S2 (μ L)	Total Volume (mL)
1	1.00	30	0.00	0	3.00
2	1.00	30	0.50	3.00	3.00
3	1.00	30	0.83	5.00	3.00
4	1.00	30	1.17	7.00	3.00
5	1.00	30	1.50	9.00	3.00
6	1.00	30	2.00	12.00	3.00
7	1.00	30	2.50	15.00	3.00

2.3.3.6 Optimization of Naph-NH₂ concentration in CTAB/S2 micellar system

The stock solutions of 0.05 M Naph-NH₂, 0.5 M S2 and 0.05 M heptanal were prepared by dimethyl sulfoxide (DMSO spectroscopic grade). The stock solution of 0.1 M CTAB was dissolved in 0.01 M PBS buffer pH 7.4. The solution of 30 μ L of CTAB and 5 μ L of S2 was stirring at room temperature for 10 min. After that, Naph-NH₂ at various concentration (Table 2.8) was added to the solution. After that, 0.25 mM and 0.50 mM heptanal were introduced and the solution as stirred for 20 min at room temperature to complete reaction. Finally, the solution was diluted to 3.0 mL by 2.5% DMSO/PBS buffer pH 7.4 and the fluorescence spectra were recorded under the following condition.

Start: 465 nm
 End: 800 nm
 Excitation: 445 nm
 Excitation slit: 10.0
 Emission slit: 10.0
 PMT 550

Table 2.8 The various concentration of Naph-NH₂ for heptanal sensing in CTAB/S2 micellar system. (2.5% DMSO/PBS buffer pH 7.4)

Entry	[CTAB], mM	[S2], mM	[Naph-NH ₂], M	Volume of 0.05 M heptanal (μ L)	Concentration of heptanal (mM)
1	1.00	0.83	2.00×10^{-5}	0	0.00
				15	0.25
				30	0.50
2	1.00	0.83	5.00×10^{-5}	0	0.00
				15	0.25
				30	0.50
3	1.00	0.83	2.50×10^{-4}	0	0.00
				15	0.25
				30	0.50

Table 2.9 (continue)

Entry	[CTAB], mM	[S2], mM	[Naph-NH ₂] M	Volume of 0.05 M heptanal (μ L)	Concentration of heptanal (mM)
4	1.00	0.83	4.17×10^{-4}	0	0.00
				15	0.25
				30	0.50
5	1.00	0.83	7.50×10^{-4}	0	0.00
				15	0.25
				30	0.50

2.3.4 pH studies of Naph-NH₂ in micellar system for heptanal detection

The stock solutions of 0.05 M Naph-NH₂, 0.5 M S2, and 0.05 M heptanal were prepared in dimethyl sulfoxide (DMSO spectroscopic grade). The stock solution of 0.1 M CTAB was dissolved in 0.01 M PBS buffer pH 7.4.

The solution of 30 μ L of CTAB and 5.0 μ L of S2 were stirred at room temperature for 10 min to obtain a CTAB/S2 micellar system. After that, 15 μ L of Naph-NH₂ stock solution was added to the solution above. The mixture solution was stirred at room temperature for 20 min. Subsequently, 15 μ L of heptanal was introduced to the solution and then continuously stirred. Afterward, the mixture solution was diluted to 3.00 mL by buffer (Table 2.10) in 2.5% DMSO/ buffer. Finally, the fluorescence spectra were detected under the following the condition.

Start:	465 nm
End:	800 nm
Excitation:	445 nm
Excitation slit:	10.0
Emission slit:	10.0
PMT	550

Table 2.10 The types of buffer at various pH

pH	Types of buffer
5.0	0.01 M Sodiumacetate-acetic acid buffer
6.0, 7.4, 8.0	0.01 M PBS buffer
9.0	0.01 M Boric acid-KCl buffer

2.3.5 The role of hydrazine functional group of Naph-NH₂ on Naph-NH₂/CTAB/S2 micellar sensor

In order to investigate an important role of hydrazine group, **Naph-OMe** was used as a model of the fluorescent dye for aldehyde sensing. The stock solution of **Naph-OMe**, **S2**, and aldehydes (formaldehyde, heptanal, benzaldehyde, 3-hydroxybenzaldehyde, 4-nitrobenzaldehyde) were prepared in spectroscopic dimethyl sulfoxide (DMSO spectroscopic grade). The stock solution of 0.1 M CTAB was dissolved in 0.01 M PBS buffer pH 7.4. The solution of 30 μ L of CTAB and 5 μ L of **S2** was stirred at room temperature for 10 min. As an introduction of **Naph-OMe** as a fluorescent dye into **CTAB/S2** micelle, the solution was stirred for 10 min before adding the number of various aldehydes in 2.5% DMSO/PBS buffer pH 7.4. After that, the reaction mixture was stirred for 20 min to complete a reaction and the fluorescence spectra was recorded under the following condition.

Start:	395 nm
End:	800 nm
Excitation:	385 nm
Excitation slit:	5.0
Emission slit:	5.0
PMT	450

2.3.6 The kinetic profile of Naph-NH₂/CTAB/S2 micellar sensor

Naph-NH₂/PBS buffer, Naph-NH₂/CTAB/S2 in the absence and in the presence of 0.25 mM heptanal were evaluated by using the fluorescence spectroscopy. The stock solution of 0.05 M Naph-NH₂, 0.5 M S2, and 0.05 M heptanal were prepared in dimethyl sulfoxide (DMSO spectroscopic grade). The stock solution of 0.1 M CTAB was dissolved in 0.01 M PBS buffer pH 7.4. The emission spectra of Naph-NH₂/PBS buffer, Naph-NH₂/CTAB/S2 in the absence and in the presence of 0.25 mM heptanal at 542 nm were recorded every 10 min in 2.5% DMSO/PBS buffer pH 7.4. The condition of fluorescence measurement was assigned as the information below.

Start: 465 nm
 End: 800 nm
 Excitation: 445 nm
 Excitation slit: 10.0
 Emission slit: 10.0
 PMT 550

2.3.7 Determination for long-chain aldehyde detection by using Naph-NH₂/CTAB/S2 micellar sensor.

The stock solution of 0.05 M Naph-NH₂, 0.5 M S2, and 0.05 M long-chain aldehydes (hexanal, heptanal, octanal, nonanal) was prepared in dimethyl sulfoxide (DMSO spectroscopic grade). The stock solution of 0.1 M CTAB was dissolved in 0.01 M PBS buffer pH 7.4.

Table 2.11 The various aldehyde at concentration of 0.05 M

Aldehydes	Molecular weight (g/mol)	Weight (g)	Final volume (mL)
hexanal	100.16	0.0100	2.00
heptanal	114.19	0.0114	2.00
octanal	128.21	0.0128	2.00
nonanal	142.24	0.0142	2.00

Firstly, 30 μL of CTAB and 5.0 μL of **S2** was stirred at room temperature for 10 min to form the **CTAB/S2** micelle. 15 μL of **Naph-NH₂** stock solution was added to the solution of **CTAB/S2** and was stirred at room temperature for 20 min. Subsequently, long-chain aldehydes at various concentration were added to the corresponding solution and diluted 3.00 mL by 0.01 M buffer pH 7.4. The mixture was stirred for 20 min to complete reaction. Finally, the fluorescence spectra were recorded under the following the condition. The emission intensity at 542 nm in the absence and presence of long-chain aldehydes was assigned as I_0 and I , respectively. The standard calibration curve was constructed by the correlation between amount of long-chain aldehydes concentration and relative fluorescence intensity (I/I_0).

Start:	465 nm
End:	800 nm
Excitation:	445 nm
Excitation slit:	10.0
Emission slit:	10.0
PMT	500

2.3.8 Selectivity of **Naph-NH₂/CTAB/S2** nanomicellar sensor for long-chain aldehyde sensing

The stock solution of 0.05 M **Naph-NH₂**, 0.5 M **S2** and 0.05 M heptanal was prepared in dimethyl sulfoxide (DMSO spectroscopic grade). The stock solution of 0.1 M CTAB was dissolved in 0.01 M PBS buffer pH 7.4. The micellar system of **CTAB/S2** was prepared by stirring of 30 μL CTAB and 5.0 μL **S2**. After that, **Naph-NH₂** was added to the solution of **CTAB/S2** and then stirred for 10 min. Finally, the organic compound (Table 2.12) was introduced and stirred for 20 min before measurement of fluorescence emission under the following condition.

Start:	465 nm
End:	800 nm
Excitation:	445 nm
Excitation slit:	10.0
Emission slit:	10.0
PMT	550

Table 2.12 The various organic compounds actually found in breath of cancer patients.

Entry	Aldehydes	Molecular weight (g/mol)	Weight (g)	Final volume (mL)
1	formaldehyde	30.03	0.0030	2.00
2	propanal	58.08	0.0058	2.00
3	butanal	72.11	0.0072	2.00
4	pentanal	86.13	0.0086	2.00
5	hexanal	100.16	0.0100	2.00
6	heptanal	114.19	0.0114	2.00
7	octanal	128.21	0.0128	2.00
8	nonanal	142.24	0.0142	2.00
9	acetone	58.08	0.0058	2.00
10	benzaldehyde	106.12	0.0106	2.00
11	3-hydroxybenzaldehyde	122.12	0.0122	2.00
12	4-nitrobenzaldehyde	151.12	0.0151	2.00
13	xylene	106.16	0.0106	2.00
14	cyclohexane	84.16	0.0084	2.00
15	hexane	86.18	0.0086	2.00
16	benzene	78.11	0.0078	2.00
17	heptane	100.21	0.0100	2.00
18	phenol	94.11	0.0094	2.00
19	toluene	92.14	0.0092	2.00
20	acetonitrile	41.05	0.0041	2.00
21	cysteine	121.16	0.0121	2.00
22	homocysteine	135.18	0.0135	2.00
23	glutathione	307.32	0.0307	2.00
24	ascorbic acid	176.14	0.0176	2.00

2.3.9 The Naph-NH₂/CTAB/S2 micellar sensor for long-chain aldehyde detection in blood sample

Since the micellar sensor enabled to utilize for quantitative detection of long-chain aldehyde compounds, we consequently applied it to monitor the amount of heptanal in real sample. In this experiment, the whole blood sample of a healthy person was collected in heparin-coated blood collection tubes to prolong a blood coagulation. The whole blood sample was purified by centrifugation at 2000 rpm for 20 min in order to separate the white blood cell, red blood cell, protein and plasma. Subsequently, the plasma was collected and stored at 5 °C overnight. The **Naph-NH₂/CTAB/S2** micellar sensor was developed to the analytical application in blood sample by using standard addition method. Hence, the various concentration of heptanal was spiked into 50 μ L plasma in the optimal micellar system of **Naph-NH₂/CTAB/S2** in 2.5% DMSO/PBS buffer pH 7.4, as listed in Table 2.13. The mixture was stirred for 20 min to complete the reaction and the fluorescence spectra were recorded by using the following condition.

Start: 465 nm

End: 800 nm

Excitation: 445 nm

Excitation slit: 10.0

Emission slit: 10.0

PMT 500

Table 2.13 The **Naph-NH₂/CTAB/S2** micellar sensor for long-chain aldehyde detection in blood sample by using standard addition method.

Entry	Heptanal concentration (added, mM)	Volume of plasma (μL)	Naph-NH₂ (mM)	CTAB (mM)	S2 (mM)	Final volume (mL)
1	0.033	50.0	0.25	1.0	0.83	3.0
2	0.083	50.0	0.25	1.0	0.83	3.0
3	0.250	50.0	0.25	1.0	0.83	3.0
4	0.333	50.0	0.25	1.0	0.83	3.0
5	0.500	50.0	0.25	1.0	0.83	3.0
6	0.667	50.0	0.25	1.0	0.83	3.0
7	0.833	50.0	0.25	1.0	0.83	3.0
8	1.000	50.0	0.25	1.0	0.83	3.0
9	1.167	50.0	0.25	1.0	0.83	3.0

2.3.10 Cellular uptake of **Naph-NH₂/CTAB/S2** micellar sensor

A549 cells were cultured with 20,000 cells per cover slip in 8-well plate and incubated in Hyclone media (DMEM/High Glucose) for 20 h at 37 °C. After the incubation for 24 hr, the wells were washed with PBS buffer and incubated in media containing .0.0125 mM **Naph-NH₂/CTAB/S2** for 4 hr. After the completed incubation, the media was removed and washed with PBS buffer for 3 time to remove the excess **Naph-NH₂/CTAB/S2** material. After that, the cells were fixed by using cold ethanol 1% (V/V) for 1 min and then washed with PBS buffer for 3 times. Consequently, the A549 cells was incubated with the nuclei dye stain (DAPI; 4,6-diamidino-2-phenylindole) for 5 min and washed with PBS buffer again. Moreover, the MOWIOL (antiphase) was added to develop the fluorescent scanning microscopy. The cover slips were mounted on glass slide and left in a dark for 1 h at 5 °C before detecting the image by using a confocal laser scanning microscopy (CLSM). The **Naph-NH₂/CTAB/S2** and DAPI was measured by a green channel and a blue channel, respectively

2.4 Naph-NH₂/CTAB/S2@Gel 1 for long-chain aldehyde detection

2.4.1 Optimization of Gel 1

The gelation **1** behavior was reliably based on an important key of the gelator amount and solvent system. Hence, the various amounts of **Gel 1** gelator in three different solvent systems including 100% DMSO, 0.01 M PBS buffer pH 7.4 as well as the mixture of DMSO/PBS buffer pH 7.4 were investigated. The gelator (**Gel 1**) in the different solvent system was heated and then cooled down to self-assembly form gelation. Consequently, the gel formation was assessed by the simple ‘inversion’ test to check for a self-supporting solid-like material.

2.4.2 Optical property of Naph-NH₂/CTAB/S2@Gel 1

The stock solution of 0.05 M **Naph-NH₂**, 0.5 M **S2** and 0.05 M heptanal in dimethyl sulfoxide (DMSO spectroscopic grade). The stock solution of 0.1 M CTAB was dissolved in 0.01 M PBS buffer pH 7.4. The micellar system of **CTAB/S2** was prepared by stirring the solution of 30 μ L CTAB, 5.0 μ L **S2** and 2965 μ L PBS buffer pH 7.4. After that, **Naph-NH₂** was added to the corresponding solution which was stirred at room temperature for 10 min.

Consequently, 0.200 mL of **Naph-NH₂/CTAB/S2** micellar sensor was mixed with 1.94 wt% of **Gel 1** at 40 °C and was diluted to 2.5 mL in 60% DMSO/PBS buffer pH 7.4. The mixture solution was cooled down to self-assembly organize the **Naph-NH₂/CTAB/S2@Gel 1** for 10 min. Finally, the fluorescence spectra were recorded by using the following condition.

Start:	465 nm
End:	800 nm
Excitation:	445 nm
Excitation slit:	10.0
Emission slit:	10.0
PMT	500

2.4.3 Kinetic study of Naph-NH₂/CTAB/S2@Gel 1

The stock solution of 0.05 M Naph-NH₂, 0.5 M S2 and 0.05 M heptanal in spectroscopic dimethyl sulfoxide. The stock solution of 0.1 M CTAB was dissolved in 0.01 M PBS buffer pH 7.4. The micellar system of CTAB/S2 was prepared by stirring the solution of 30 μ L CTAB, 5.0 μ L S2 and 2965 μ L PBS buffer pH 7.4. After that, Naph-NH₂ was added to the corresponding solution which was stirred at room temperature for 10 min.

After that, 0.200 mL of Naph-NH₂/CTAB/S2 micellar sensor was stirred with 0.05 mM heptanal for 20 min. Then, 1.94 wt% of Gel 1 (40 °C) was added into the solution and the mixture solution was diluted to 2.5 mL by 60% DMSO/PBS buffer pH 7.4. The mixture solution was cooled down to self-assembly organize the Naph-NH₂/CTAB/S2@Gel 1 for 10 min. Finally, the fluorescent intensity at 535 nm was recorded every 10 min under the following condition.

Start:	465 nm
End:	800 nm
Excitation:	445 nm
Excitation slit:	10.0
Emission slit:	10.0
PMT	550

2.4.4 Determination of long-chain aldehydes by using Naph-NH₂/CTAB/S2@Gel 1

The stock solution of 0.05 M Naph-NH₂, 0.5 M S2 and 0.05 M heptanal in spectroscopic dimethyl sulfoxide. The stock solution of 0.1 M CTAB was dissolved in 0.01 M PBS buffer pH 7.4. The micellar system of CTAB/S2 was prepared by stirring the solution of 30 μ L CTAB and 5.0 μ L S2 and 2965 μ L PBS buffer pH 7.4. After that, Naph-NH₂ was added to the corresponding solution which was stirred at room temperature for 10 min.

Consequently, 0.200 mL of Naph-NH₂/CTAB/S2 micellar sensor was stirred with long-chain aldehydes (hexanal, heptanal, octanal, nonanal) at various concentration for 20 min. Then, 1.94 wt% of Gel 1 (40 °C) was added into the solution and then was diluted to 2.5 mL by 60% DMSO/PBS buffer pH 7.4. The mixture was

cooled down to self-assembly organized the **Naph-NH₂/CTAB/S2@Gel 1** for 10 min. Finally, the fluorescence response at 542 nm was recorded by using the following condition. The emission intensity at 535nm in the absence and presence of long-chain aldehydes were assigned as I_0 and I , respectively.

Start:	465 nm
End:	800 nm
Excitation:	445 nm
Excitation slit:	10.0
Emission slit:	10.0
PMT	550

2.4.5 Selectivity of **Naph-NH₂/CTAB/S2@Gel 1** sensor for long-chain aldehyde sensing

The stock solution of 0.05 M **Naph-NH₂**, 0.5 M **S2** and 0.05 M various organic compounds (Table 2.12) in dimethyl sulfoxide (DMSO spectroscopic grade). The stock solution of 0.1 M CTAB was dissolved in 0.01 M PBS buffer pH 7.4. The micellar system of **CTAB/S2** was prepared by stirring the solution of 30 μ L CTAB, 5.0 μ L **S2** and 2965 μ L PBS buffer pH 7.4. After that, **Naph-NH₂** was added to the corresponding solution which was stirred at room temperature for 10 min.

Consequently, 0.200 mL of **Naph-NH₂/CTAB/S2** micellar sensor was stirred with the organic compounds (Table 2.12) for 20 min. Then, 1.94 wt% of **Gel 1** (40 °C) was added into the solution and then was diluted to 2.5 mL by 60% DMSO/PBS buffer pH 7.4. The mixture was cooled down to self-assembly organize the **Naph-NH₂/CTAB/S2@Gel 1** for 10 min. Finally, the fluorescent intensity at 535 nm was recorded by using the following condition.

Start:	465 nm
End:	800 nm
Excitation:	445 nm
Excitation slit:	10.0
Emission slit:	10.0
PMT	550

CHAPTER III

RESULTS AND DISCUSSION

3.1 Conceptual design of fluorescent micellar probe for long-chain aldehydes sensing

In this research, we focused on the determination of long-chain aldehydes; hexanal, heptanal, octanal and nonanal, which are regarded as potential biomarkers of diseases progression for lung cancer [53-57]. Additionally, hexanal is greatly important quality indicator of fat and oil products due to the oxidation reaction during manufacturing process [58, 59]. Generally, long-chain aldehydes consist of hydrophobic tail of aliphatic hydrocarbon chain and hydrophilic head of aldehyde functional group. Hence, the long-chain aldehydes were expected to act as surfactants for self-assembly organized nanomicelle. In this research, the nanomicellar probes towards long-chain aldehydes have been achieved in the concept of fluorescent sensor incorporated in incomplete micellar-like particles promoting the complete micelle upon interaction with the long-chain aldehyde and a consequent fluorescence enhancement of fluorophore due to the well-entrapped dye-encapsulated nanomicelle.

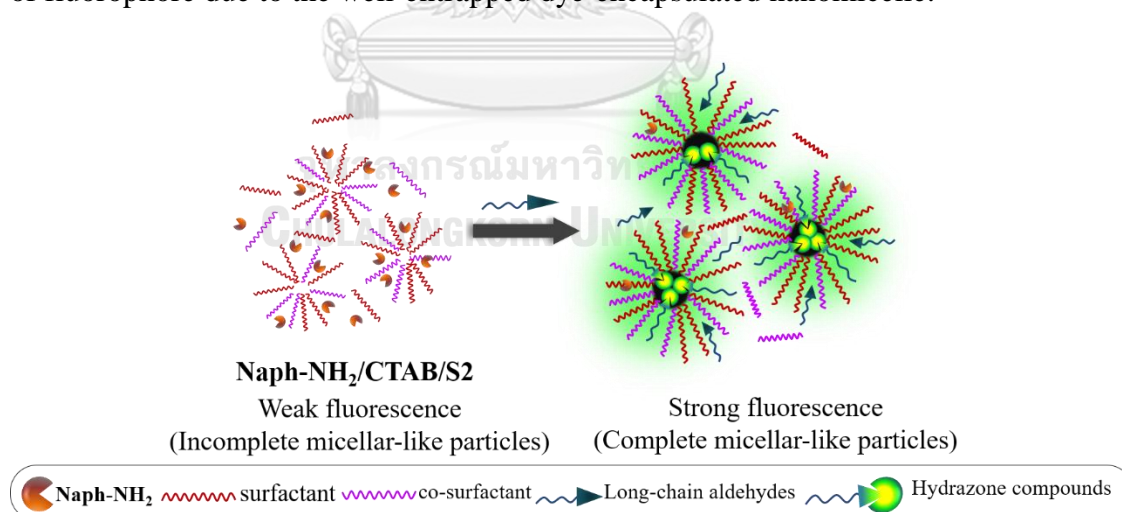


Figure 3.1 Conceptual design of fluorescent micellar probe for long-chain aldehydes sensing

In the case of the fluorescent dye doped in incomplete micellar-like particles, there are many binding sites for aldehyde coupling reaction such as amine and hydrazine functional group. Herein, the organic compounds containing amine or hydrazine were firstly examined to interact with aldehyde. Therefore, we have designed and synthesized fluorescence sensors composing of fluorophore coupled with amine or hydrazine binding site (Figure 3.2). Each fluorescence sensor was investigated the binding ability with aldehyde compound. The suitable fluorophore sensor was encapsulated in micellar particles under the optimizing condition. Upon the introduction of long-chain aldehydes into incomplete micellar sensor, we expected that the suitable long-chain aldehyde induced the self-organization of complete micelles and reacted to the binding site of fluorescent dye-doped nanomicelle resulting in fluorescence enhancement. Moreover, the micellar system of fluorescence sensor serves a high selectivity toward long-chain aldehydes such as heptanal.

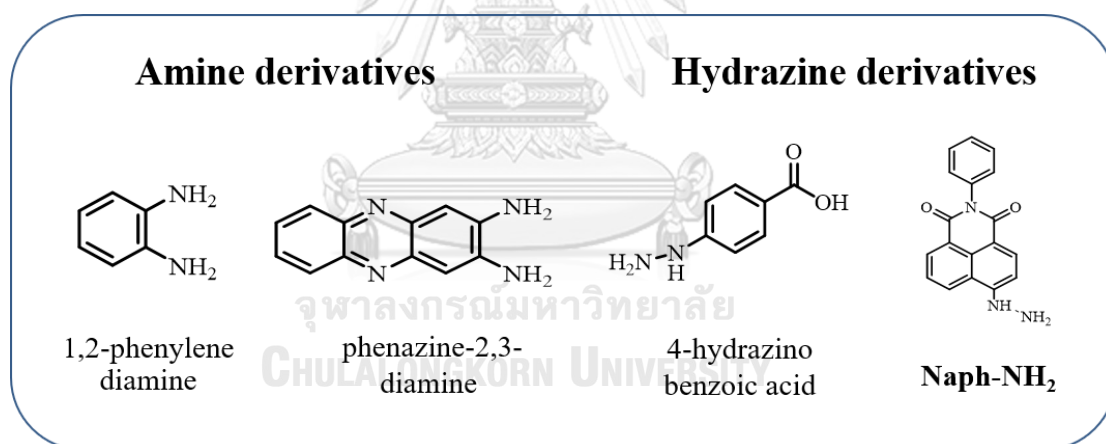
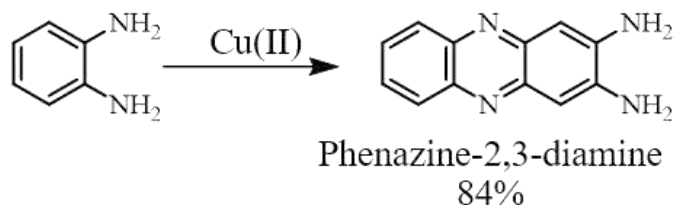


Figure 3.2 Chemical structures of fluorescence sensors for aldehyde sensing

3.2 Synthesis

3.2.1 Synthesis and characterization of phenazine-2,3-diamine [60]



The phenazine-2,3-diamine was synthesized by oxidation reaction of o-phenylenediamine using mild oxidant of Cu(II) under the room temperature for 24 h. The crude product was purified by extraction 3 times using dichloromethane to obtain the dark brown solid in 84% yield. The $^1\text{H-NMR}$ showed the additional signals at 7.86-6.88 ppm of aromatic protons and 6.20 ppm of $-\text{NH}_2$ protons which are evidence of the desired product of phenazine-2,3-diamine

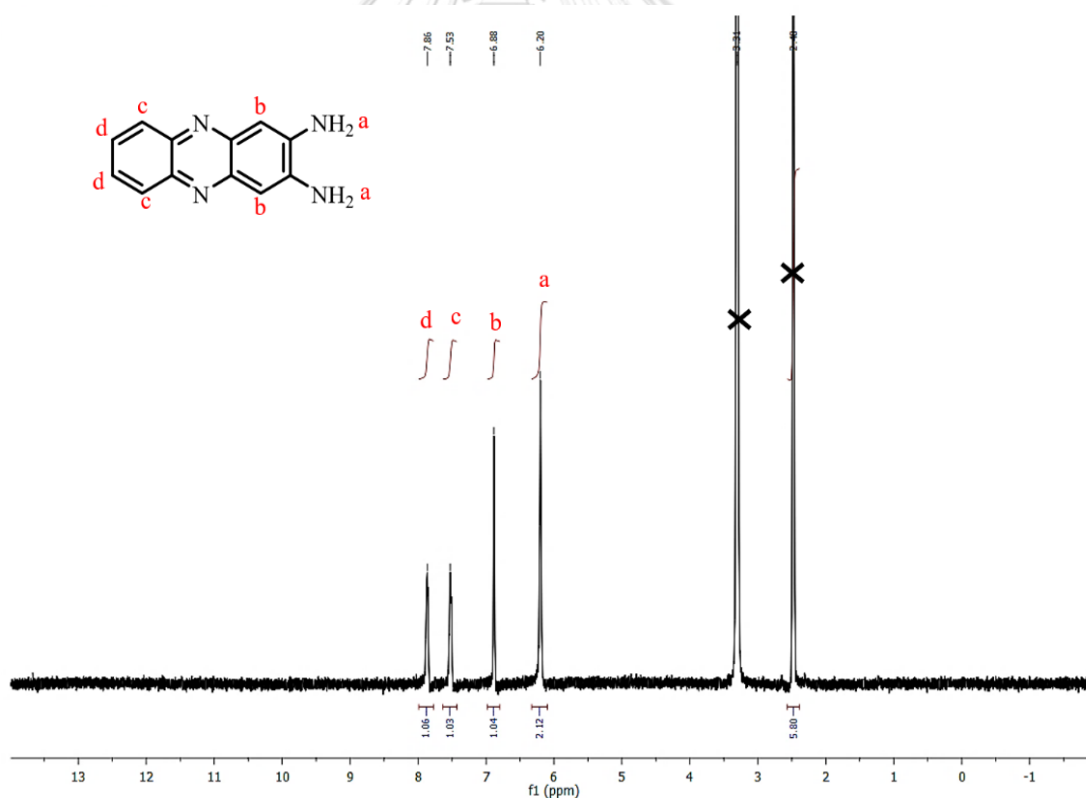
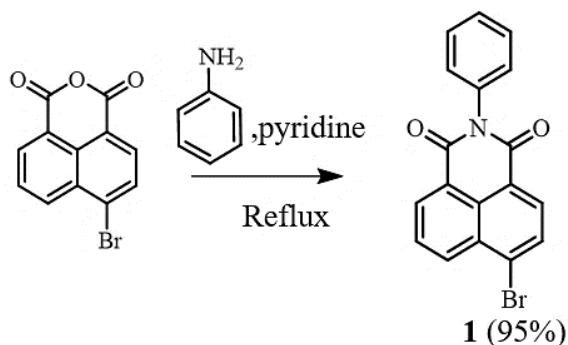


Figure 3.3 The $^1\text{H-NMR}$ spectrum of phenazine-2,3-diamine in d_6 -DMSO at 400 MHz

3.2.2 Synthesis and characterization of 6-Bromo-2-phenyl-1H-benzo[de]isoquinoline-1,3(2H)-dione (1)



The compound **1** was synthesized through condensation reaction between 4-bromo-1,8-naphthalic anhydride and aniline. In this reaction, pyridine was employed as a nucleophilic-covalent catalyst which could form a covalent intermediate with 4-bromo-1,8-naphthalic anhydride. After that, the nucleophile of primary amine on aniline could interact to an intermediate via nucleophilic substitution reaction. Subsequently, the compound **1** was recrystallized from methanol to afford the white solid in 95% yield. The ¹H-NMR spectrum of compound **1** showed the characteristic peak of aromatic protons in a range of 7.00 – 9.00 ppm. The signal of proton in the range of 7.64-7.37 ppm and 8.56-8.00 ppm were assigned as the aromatic photons of aniline and naphthalimide, respectively.

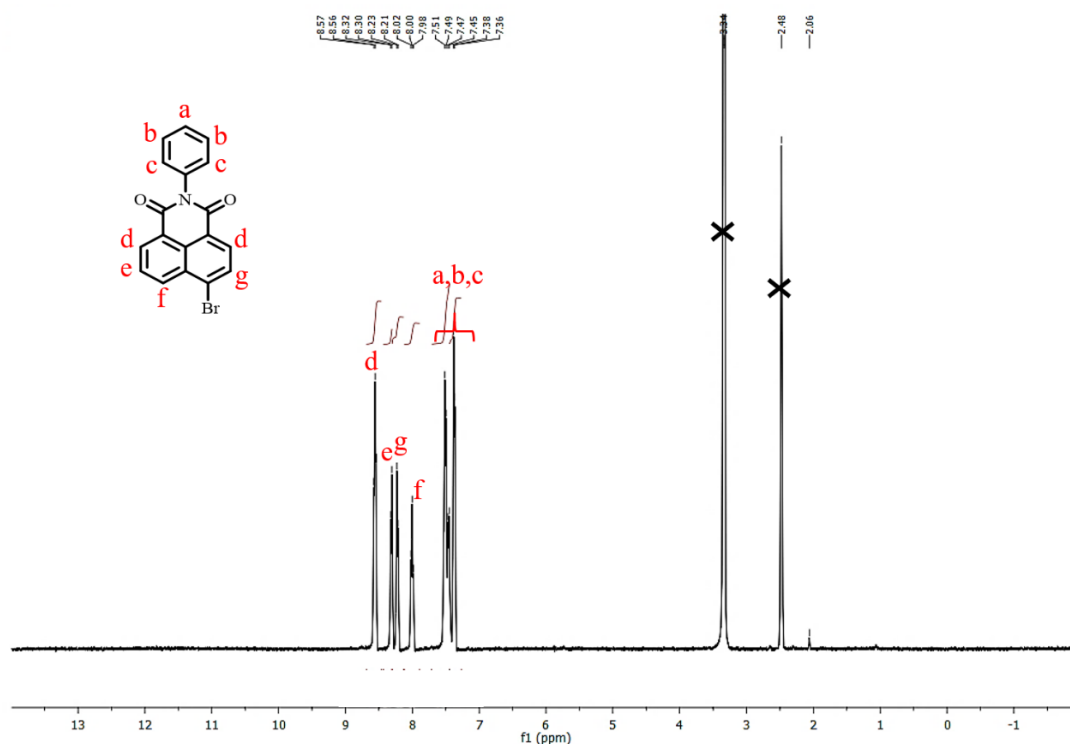
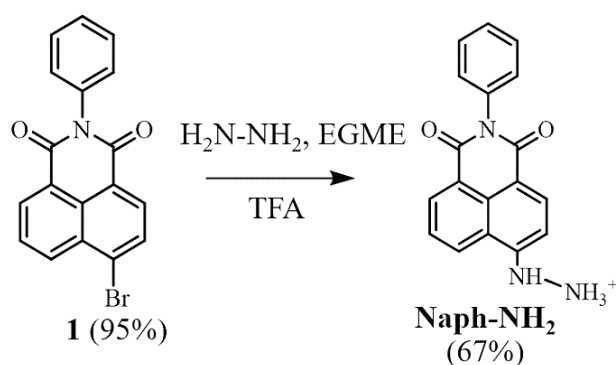


Figure 3.4 The $^1\text{H-NMR}$ spectrum of 6-bromo-2-phenyl-1H-benzo[de]isoquinoline-1,3(2H)-dione (**1**) in d_6 -DMSO at 400 MHz

3.2.3 Synthesis and characterization of 6-hydrazinyl-2-phenyl-1H-phenalene-1,3(2H)-dione (Naph-NH₂)



Naph-NH₂ was successfully synthesized via nucleophilic substitution reaction. The nucleophilic lone pair electron of nitrogen atom in hydrazine would substitute on the bromo atom based on compound **1** by using the magic solvent of ethylene glycol monomethyl ether (EGME) to afford **Naph-NH₂**. In order to improve the stability of

hydrazine derivative, amine functional group was also protonated with trifluoroacetic acid (TFA) to provide an orange-solid compound in 67% yield. $^1\text{H-NMR}$ spectrum displayed the additional protons at 9.24 and 5.53 ppm assigned to $-\text{NH}$ and $-\text{NH}_2$ of hydrazine functional groups, respectively. These proton signals are indicative of the **Naph-NH₂** compound.

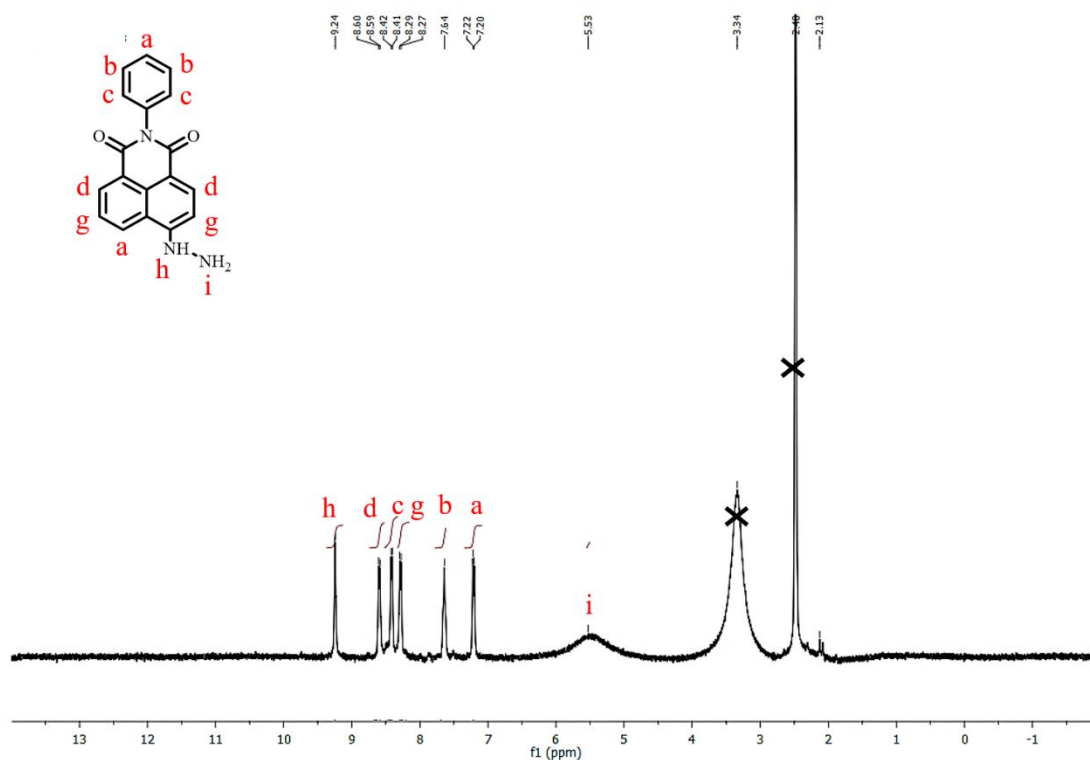
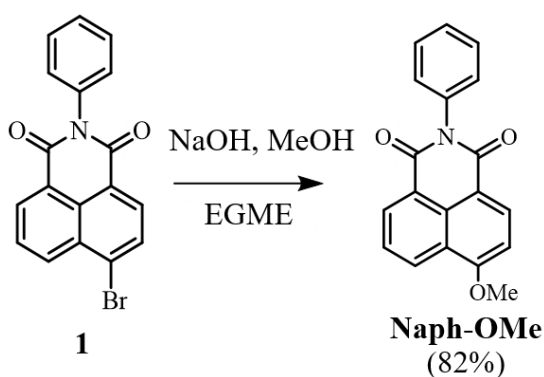


Figure 3.5 The $^1\text{H-NMR}$ spectrum of 6-hydrazinyl-2-phenyl-1H-phenalene-1,3(2H)-dione (**Naph-NH₂**) in d_6 -DMSO at 400 MHz

3.2.4 Synthesis and characterization of 6-Methoxy-2-phenyl-1H-benzo[de]isoquinoline-1,3(2H)-dione (**Naph-OMe**)



Naph-OMe was synthesized via substitution reaction of nucleophilic methoxy functional group. Firstly, methoxy group (-OMe) was generated by deprotonation of methanol under the strong basic condition of sodium hydroxide. Base on the strong nucleophilic methoxy, bromine atom of compound **1** was substituted by methoxy in ethylene glycol monomethyl ether (EGME) as a magic solvent to provide a yellow solid in 82% yield. $^1\text{H-NMR}$ spectrum of **Naph-OMe** showed the aromatic protons in a range of 8.63-7.16 ppm. The appearance of singlet proton at 4.16 ppm was assigned to the methoxy proton. Moreover, the aromatic photon of **Naph-OMe** in the range of 7.74 - 7.09 ppm was upfield shift compared to compound **1** due to electron-donating effect of methoxy group.

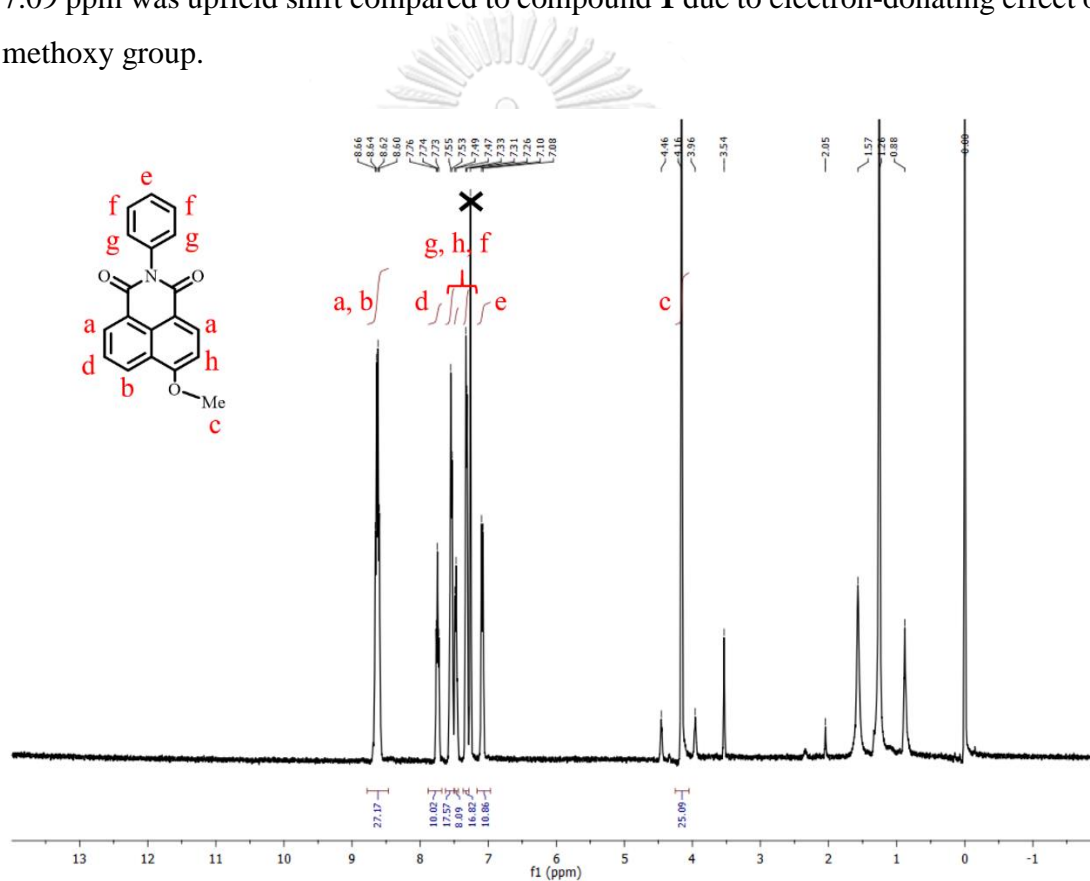
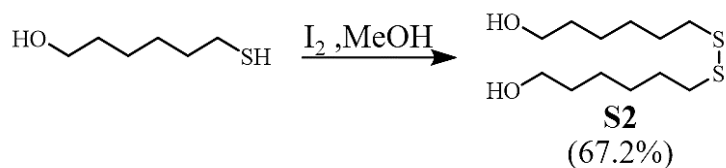


Figure 3.6 The $^1\text{H-NMR}$ spectrum of 6-Methoxy-2-phenyl-1H-benzo[de]isoquinoline-1,3(2H)-dione (**Naph-OMe**) in d_6 -DMSO at 400 MHz

3.2.5 Synthesis and characterization of 6,6'-Disulfanediylbis(hexan-1-ol) (S2)



6,6'-Disulfanediylbis(hexan-1-ol) or **S2** was synthesized by oxidation reaction of 6-mercapto-1-hexanol to produce the disulfide or **S2** by mild oxidant of I_2 under the room temperature. The product was purified by column chromatography to afford the yellow oil in % 67.2 yield. The $^1\text{H-NMR}$ spectrum showed the proton signal in a range of 3.36-1.40 ppm assigned to aliphatic protons. Compared to 6-mercapto-1-hexanol, the protons of **S2** showed downfield shift of CH_2 -proton adjacent to thiol group from 2.67 to 1.40 ppm. These results are indicative of the desired product of **S2**.

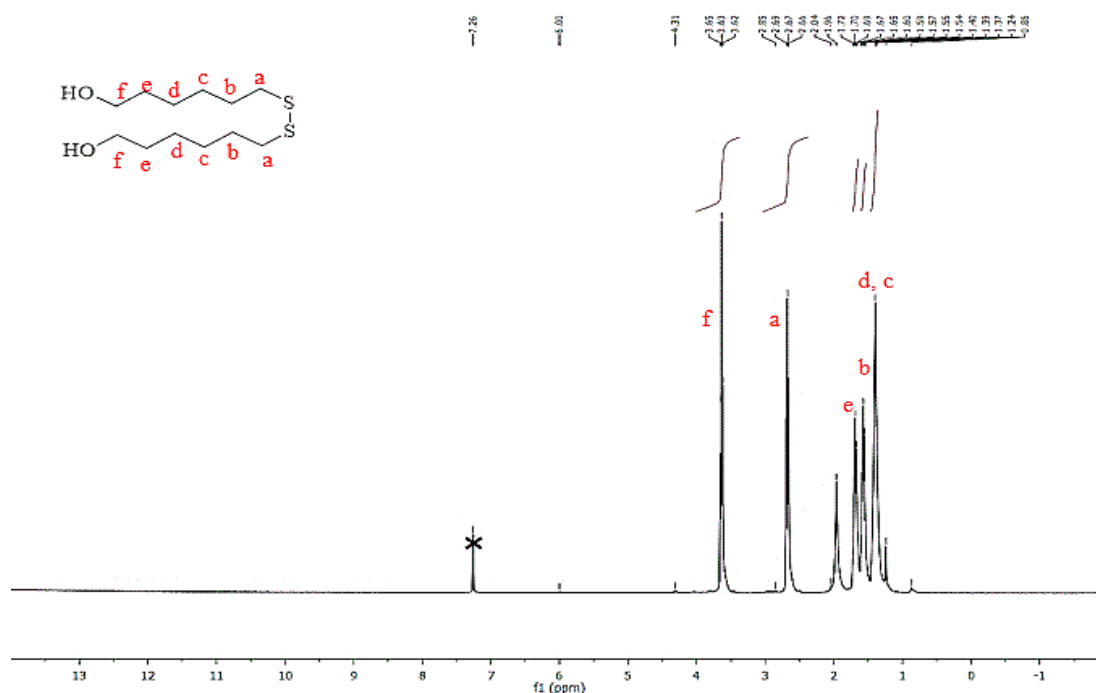


Figure 3.7 The $^1\text{H-NMR}$ spectrum of 6'-Disulfanediylbis(hexan-1-ol) (**S2**) in d_6 -DMSO at 400 MHz

3.3 Amine-functionalized fluorescence sensor

In general, the lone-pair electron on nitrogen atom is a nucleophile enabling to react with electrophile. Reaction of amine as a nucleophile and aldehyde as an electrophile, is known as schiff base reaction. Hence, we expected that amine on fluorescence sensor would react with aldehyde compound causing the change of fluorescence response.

For searching for the proper fluorescent dye, we firstly studied the sensing ability of 1,2-phenylenediamine as an amine-functionalized fluorescent sensor toward heptanal compound which is the representative of long-chain aldehyde. In this reaction, the mixture of 0.5 mM 1,2-phenylenediamine and 0.25 mM heptanal was vigorously stirred in DMF for 20 min before measuring an emission spectrum ($\lambda_{\text{ex}} = 428 \text{ nm}$). As shown in Figure 3.8, there is no change of fluorescent emission of 1,2-phenylenediamine after adding heptanal. It could be assumed that 1,2-phenylenediamine did not react with heptanal.

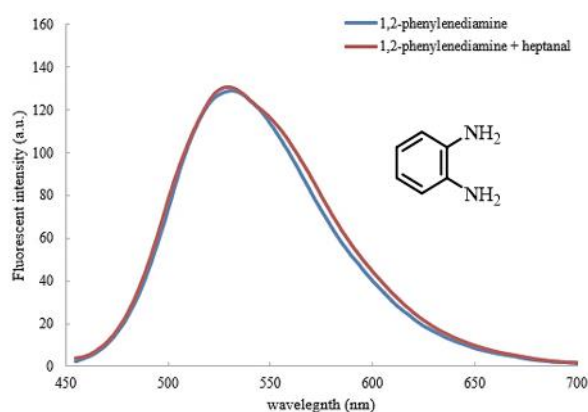


Figure 3.8 Fluorescence spectra of 0.5 mM 1,2-phenylenediamine after introduction of 0.25 mM heptanal in 100% DMF. ($\lambda_{\text{ex}} = 428 \text{ nm}$, PMT 800)

Due to the weak emission of 1,2-phenylenediamine, we further synthesized the phenazine-2,3-diamine via oxidative reaction using 1,2-phenylenediamine as a reactant. As shown in Figure 3.9, the fluorescent intensity was gradually quenched after adding of 0.25 mM heptanal. It indicated that heptanal interacted with 1,2-phenylenediamine via schiff base reaction causing the fluorescence quenching under the PET process. However, the continuously gradual decrease of fluorescent intensity was vanished at 350 min which is not convenient for real-time sensing purpose.

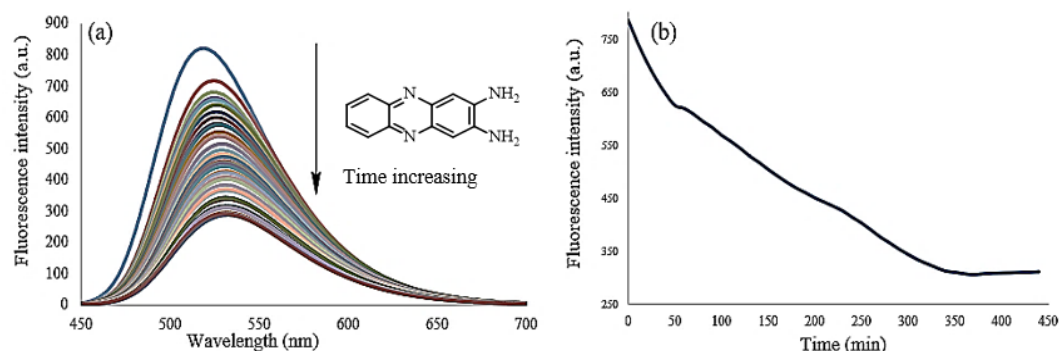


Figure 3.9 Fluorescence spectra (a) and the fluorescence response (b) of 0.5 mM phenazine-2,3-diamine after introduction of 0.25 mM heptanal in DMF. (10-450 min), ($\lambda_{\text{ex}} = 350 \text{ nm}$, PMT 800)

3.4 Hydrazine-functionalized fluorescence sensor

The hydrazine functional group was further considered as binding site for aldehyde reaction. 4-Hydrazinobenzoic acid was investigated as hydrazine-functionalized fluorescence sensor for heptanal sensing. The reaction mixture of 4-hydrazinobenzoic acid and heptanal was vigorously stirred in DMF. The fluorescence response at 524 nm was significantly enhanced after introduction of heptanal for 20 min, as illustrated in Figure 3.10(a). However, 4-hydrazinobenzoic acid showed the weak performance for heptanal detection in aqueous system as a respect of fluorescent change of dye-doped nanomicelle, as shown in Figure 3.10(b). In assumption, no interaction of 4-hydrazinobenzoic acid and heptanal was addressed by observation of remained unchanged emission band of dye. This behavior was possibly caused by the poor solubility of heptanal in aqueous solution

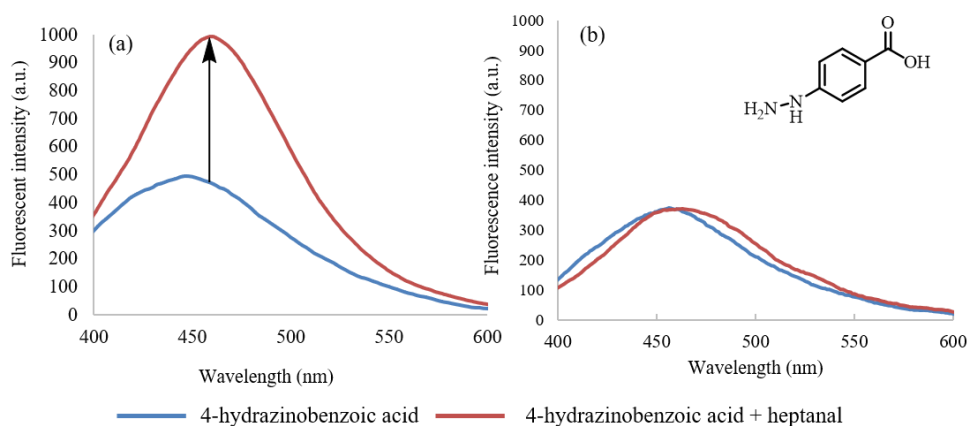


Figure 3.10 Fluorescence spectra of 0.5 mM 4-hydrazinobenzoic acid upon introduction of 0.25 mM heptanal in DMF (a) and in 2.5% DMF/PBS buffer pH 7.4 (b). (20 min, $\lambda_{\text{ex}} = 430$ nm)

According to the drawbacks of 4-hydrazinobenzoic acid in aqueous system (2.5% DMSO/ PBS buffer pH 7.4), we further designed and synthesized **Naph-NH₂** molecule as a fluorescence sensor for detection of long-chain aldehydes. In the past few years, 1,8-naphthalimide derivatives have been widely used as a fluorescent dye due to the excellent fluorescent property, good stability and easy modification. Hence, we designed **Naph-NH₂** consisting of naphthalimide and hydrazine functional group which typically acted as a fluorophore and binding site, respectively. To verify the selectivity of **Naph-NH₂** sensor for long-chain aldehyde detection, five aldehyde compounds including formaldehyde, heptanal, benzaldehyde, 3-hydroxybenzaldehyde and 4-nitrobenzaldehyde were selected as the representative aldehydes in this experiment (Figure 3.11). Generally, formaldehyde is a small molecule and highly reactive aldehyde group which is commonly employed as a precursor in various material industries. Meanwhile, heptanal containing seven-carbon chain and formyl group was chosen as a representative long-chain aldehyde for biomarker applications. In case of aromatic aldehydes, benzaldehyde was selected as a representative of aromatic aldehyde, and 3-hydroxybenzaldehyde as well as 4-nitrobenzaldehyde were selected to study the effect of electron donating group and electron withdrawing group, respectively.

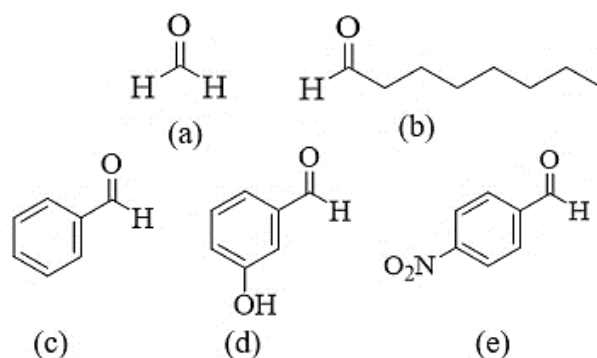


Figure 3.11 Chemical structures of representative aldehydes including; (a) formaldehyde (b) heptanal (c) benzaldehyde (d) 3-hydroxybenzaldehyde (e) 4-nitrobenzaldehyde

Naph-NH₂ was used as a fluorescence sensor for aldehyde detection in 100% DMSO. Upon the addition of various aldehyde compounds, the emission bands of **Naph-NH₂** at 542 nm remained unchanged as shown in Figure 3.12. It was assumed that **Naph-NH₂** did not interact with aldehydes in 100% DMSO due to the high viscosity of DMSO (1.996 cP at 20 °C) [61]. In order to decrease the effect of DMSO solvent, **Naph-NH₂** was also carried out for aldehyde sensing in 2.5% DMSO/PBS buffer pH 7.4. As illustrated in Figure 3.13, the emission intensity of **Naph-NH₂** was significantly enhanced under condition of 2.5% DMSO/PBS buffer pH 7.4 compared to 100% DMSO condition. This emissive increment of **Naph-NH₂** implied that the aggregation of **Naph-NH₂** was reduced in 2.5% DMSO/PBS buffer pH 7.4. Subsequently, we further studied aldehyde sensing of **Naph-NH₂** in 2.5% DMSO/PBS buffer pH 7.4. The results illustrated that **Naph-NH₂** sensor has a good selectivity toward formaldehyde over other aldehydes due to the high reactivity of its small size, as shown in Figure 3.14

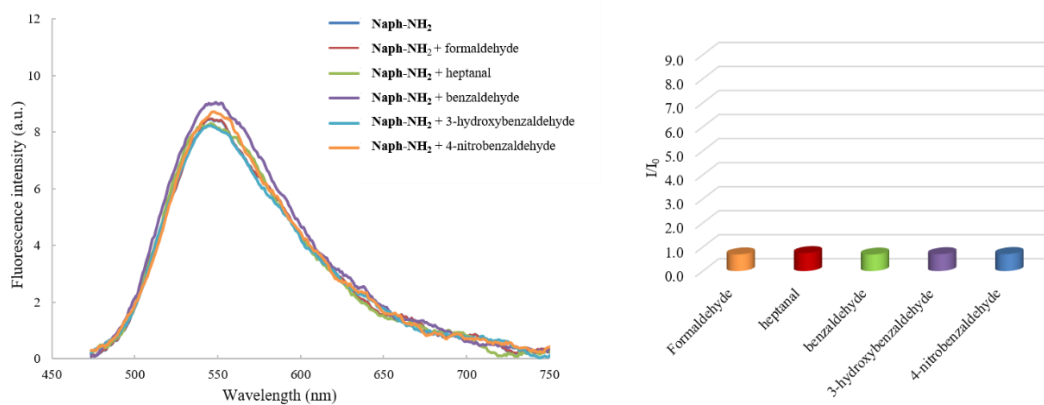


Figure 3.12 Relative fluorescence intensity (I/I_0) of 5.0×10^{-5} M Naph-NH_2 after introduction of various aldehydes (0.25 mM) in 100% DMSO. ($\lambda_{\text{ex}} = 445$ nm)

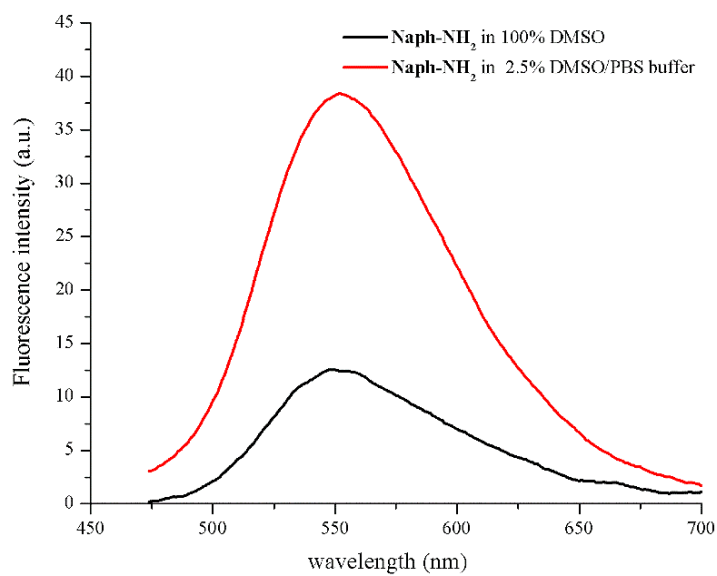


Figure 3.13 Fluorescence spectra of 5.0×10^{-5} M Naph-NH_2 in 100% DMSO (black line) and 2.5% DMSO/PBS buffer pH 7.4 (red line). ($\lambda_{\text{ex}} = 445$ nm)

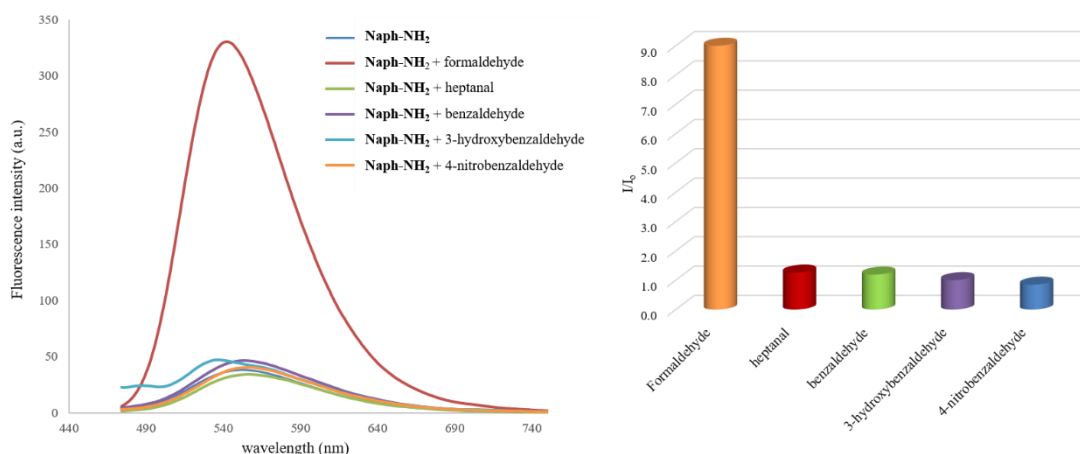


Figure 3.14 Relative fluorescence intensity (I/I_0) at 542 nm of 5.0×10^{-5} M **Naph-NH₂** upon introduction of various aldehydes (0.25 mM) in 2.5% DMSO/PBS buffer pH 7.4.

3.5 Optimization of micellar system for long-chain aldehyde detection

Due to no fluorescence changes for long-chain aldehyde sensing by using **Naph-NH₂**, we attempted to search for the platform for selective detection of long-chain aldehydes. Nowadays, nanomicelle is an alternative popular material of molecular nanosensors for detection in aqueous system due to good biocompatibility, highly dispersal ability and good stability. In general, nanomicelle is self-assembling organized by surfactants that commonly consists of hydrophobic tail and hydrophilic head. The center of nanomicelle has a hydrophobic-core property that are well-defined nanocarrier for hydrophobic organic dye. Hence, we proposed that **Naph-NH₂** was encapsulated in nanomicelle might improve the fluorescent efficiency and selectivity for long-chain aldehyde detection in aqueous solution.

Of particular finding the proper system for encapsulation of the **Naph-NH₂** was of great interest. The effectively commercial surfactants including cetyltrimethylammonium bromide (CTAB, positive-charge surfactant), sodium dodecyl sulfate (SDS, negative-charge surfactant) and Triton X-100 (neutral surfactant) were verified for self-assembled organized nanomicelle (Figure 3.15). The fluorescence spectra (Figure 3.16) illustrated that the emission of **Naph-NH₂** encapsulated in the three different micellar systems including CTAB, SDS and Triton X 100 in 2.5%

Furthermore, we studied the critical micelle concentration (CMC) of CTAB in 2.5% DMSO/PBS buffer pH 7.4. The solution of 5.0×10^{-5} M **Naph-NH₂** with a various CTAB concentration was stirred in 2.5% DMSO/PBS buffer pH 7.4 at room temperature for 20 min before a fluorescent measurement ($\lambda_{\text{ex}} = 445$ nm). The fluorescent emission of **Naph-NH₂** was rapidly enhanced and then kept constant at 2.25 mM of CTAB (Figure 3.17(a)). The fluorescent tendency attributed to the organization of nanomicelle for encapsulation of **Naph-NH₂** corresponding to the concentration of CTAB. Moreover, the relationship between CTAB concentration and fluorescent intensity revealed the CMC value of 1.25 mM, as shown in Figure 3.17(b). The CMC value of CTAB suggested that CTAB concentration ≥ 1.25 mM would form the completely self-organized nanomicelle. However, a nanomicellar fluorescent sensor towards long-chain aldehydes has been designed in the concept of incomplete micellar-like particle. Herein, 1.0 mM of CTAB at below its CMC value was selected as the optimal concentration to prepare an incomplete micellar-like sensor. Consequently, **Naph-NH₂** in 1.0 mM of CTAB (**Naph-NH₂/CTAB**) was carried out as a fluorescent micellar platform for aldehydes sensing in 2.5% DMSO/PBS buffer pH 7.4. As shown in Figure 3.17(c), the increments of relative fluorescent intensity (I/I_0) was demonstrated in the presence of 0.25 mM various aldehydes. The experimental results indicated that **Naph-NH₂/CTAB** micelle showed a poor selectivity for aldehyde detection.

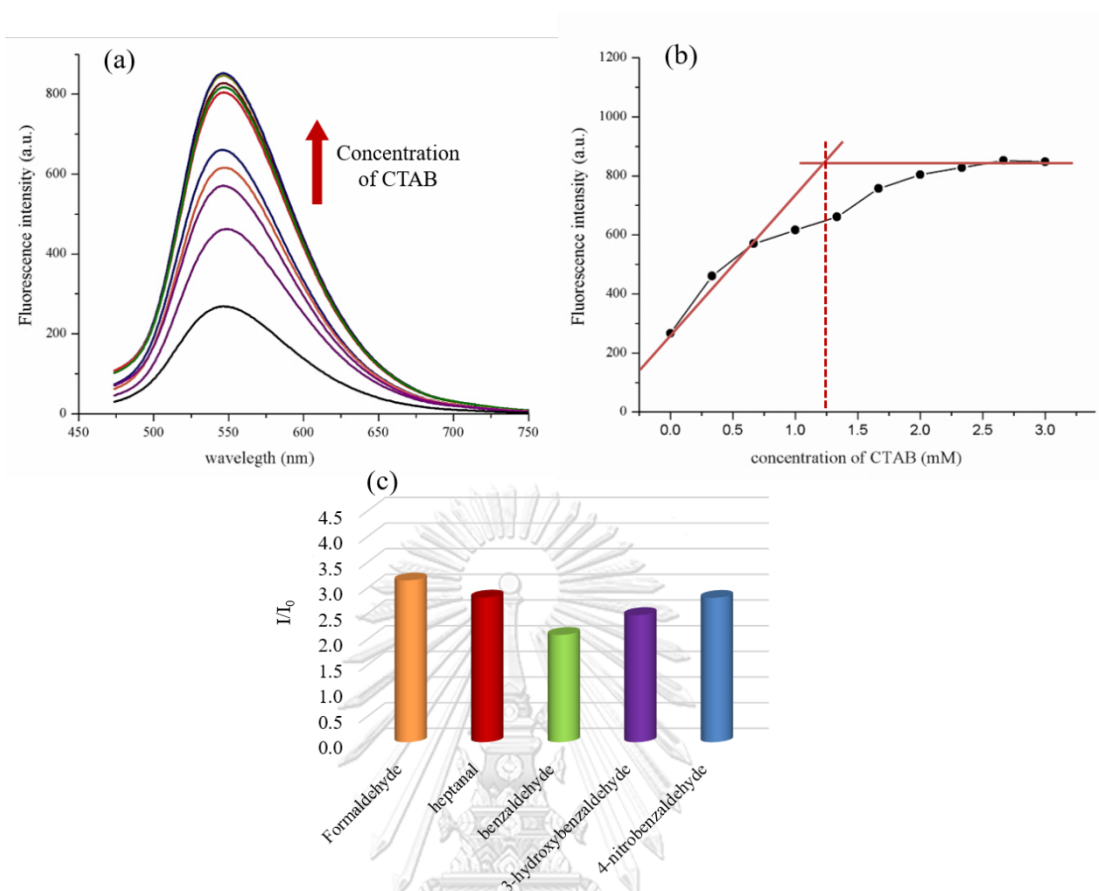


Figure 3.17 Fluorescence spectra (a) and fluorescent intensity (b) at 542 nm of 5.0×10^{-5} M Naph-NH₂ in CTAB micellar system at a concentration range from 0.0 mM to 3.0 mM. (c) Relative fluorescence intensity of Naph-NH₂/CTAB micelle at 542 nm (I/I_0) upon introduction of various aldehydes (2.5% DMSO/PBS buffer pH 7.4, $\lambda_{ex} = 445$ nm).

To further improve a selectivity of Naph-NH₂/CTAB sensor, we also studied co-surfactants which are organic molecules consisting of aliphatic long-chain hydrocarbon and hydroxy functional group, because these molecules could expose its hydroxy group to interact with water through H-bonding and easily organized a hydrophobic core through its hydrocarbon chain. Served long-chain hydrocarbons containing hydroxy, amine or thiol groups including ethanol, 1-butanol, 1-hexanol, 1-octanol, 6-mercapto-1-hexanol, S2, ethylenediamine and cysteamine were verified as a proper co-surfactant in Naph-NH₂/CTAB micellar system, as showed in Figure 3.18. Of particular bar graph revealed that Naph-NH₂/CTAB without co-surfactant provided

the poor selectivity for aldehydes sensing. The alcohol derivatives (ethanol, 1-butanol, 1-hexanol, 1-octanol) were employed as co-surfactant in **Naph-NH₂/CTAB** micelle in this study. They were found to induce the fluorescent enhancement upon the addition of both formaldehyde and heptanal. These emissive results suggested that the longer hydrocarbon-chain length of alcohol provided more effective selectivity for both of formaldehyde and heptanal sensing over other aromatic aldehydes. Additionally, we investigated the effect of functional group of co-surfactants for selective heptanal detection. The ethanolamine, ethylenediamine, cysteamine and **S2** were studied as a co-surfactant in **Naph-NH₂/CTAB** micellar system. These results suggested that the combination of surfactant of CTAB and thiol-derivatives for **Naph-NH₂** micellar-like sensor significantly enhanced the fluorescence at 542 nm in the case of 0.25 mM heptanal over other aldehydes. Herein, these results were presumed that thiol group possibly had the electronic effect on hydrophobic core of nanomicelle and then induced the long-chain aldehydes into nanomicelle, eventually causing a fluorescence enhancement. However, **S2** and 6-mercapto-1-hexanol exhibited the fluorescent enhancement over cysteamine possibly ascribing that long-chain hydrocarbon of thiol-derived co-surfactants also encouraged the hydrocarbon-self packing for long-chain aldehydes. Furthermore, the maximum emissive increment could be occurred by using **S2** molecule as a co-surfactant combined to **Naph-NH₂/CTAB**. These results were hypothesized that more hydrophobicity of **Naph-NH₂/CTAB/S2** enabled to induce heptanal to interact with fluorescence dye more than **Naph-NH₂/CTAB/6-mercapto-1-hexanol**. Hence, **S2** molecule was suitably employed as a co-surfactant for further studies in this research.

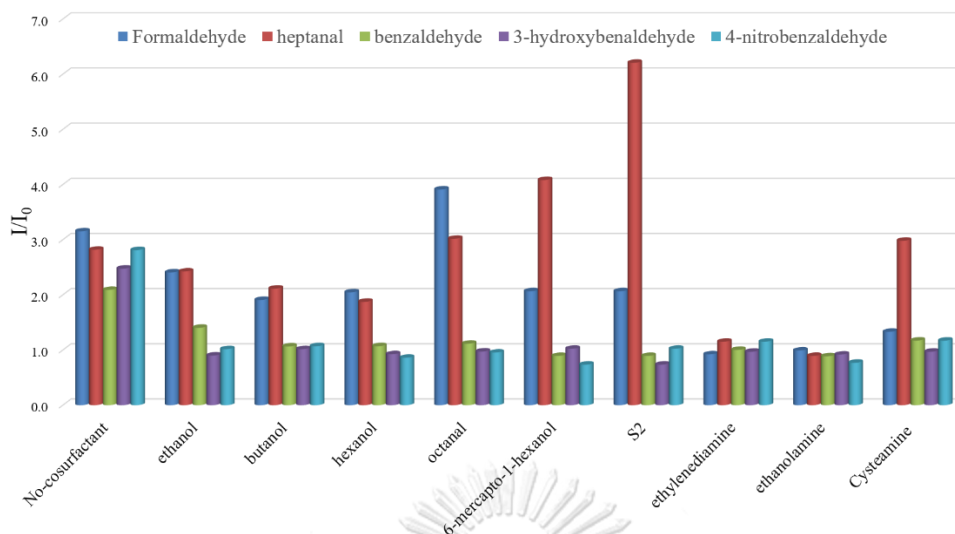


Figure 3.18 Fluorescence response at 542 nm of **Naph-NH₂/CTAB** micellar system with various co-surfactant including ethanol, butanol, hexanol, octanol, 6-mercapto-1-hexanol, **S2**, ethylenediamine, ethanolamine and cysteamine. (2.5% DMSO/PBS buffer pH 7.4, $\lambda_{\text{ex}} = 445$ nm).

Owing to the good co-surfactant of **S2** for this system, **Naph-NH₂ /CTAB/S2** was chosen as sensing platform for long-chain aldehydes. Therefore, CMC value of **S2** was first investigated by using fluorescence spectroscopy. Unfortunately, the fluorescent intensity of **Naph-NH₂** were continuously increased as a function of time in the **S2** addition. It was possibly the decomposition of hydrazine moiety in fluorescent dye due to its poor encapsulation in **S2**. This result indicated that **S2** is not suitable for dominant surfactant for encapsulation of **Naph-NH₂**. In order to solve the drawbacks, **Naph-OMe** which has a similar structure to **Naph-NH₂** was utilized as a fluorescent dye to determine the critical micelle concentration (CMC) of **S2** surfactant. As shown in Figure 3.19(a), the fluorescence emission of **Naph-OMe** dye at 458 nm ($\lambda_{\text{ex}} = 385$ nm) was gradually quenched upon increasing **S2** concentration. The results revealed the CMC of **S2** at approximately 1.30 mM. For incomplete micellar-like particle, the concentration of **S2** should be lower than CMC point (Figure 3.19(b)). Furthermore, we also optimized the **S2** concentration incorporated **Naph-NH₂/CTAB** micelle toward 0.25 mM heptanal. The appearance of the maximum fluorescence at 542 nm of sensory platform was observed by using 0.83 mM of **S2** as a co-surfactant. (Figure 3.19(c)). To

prove the good selectivity of **Naph-NH₂/CTAB/S2** toward long-chain aldehydes, the micellar-like sensing platform mediated by 1.0 mM CTAB, 0.83 mM **S2** and 5.0×10^{-5} M **Naph-NH₂** was employed to detect aldehydes in 2.5% DMSO/PBS buffer pH 7.4. The results showed the good selectivity for heptanal detection as shown in Figure 3.19(d).

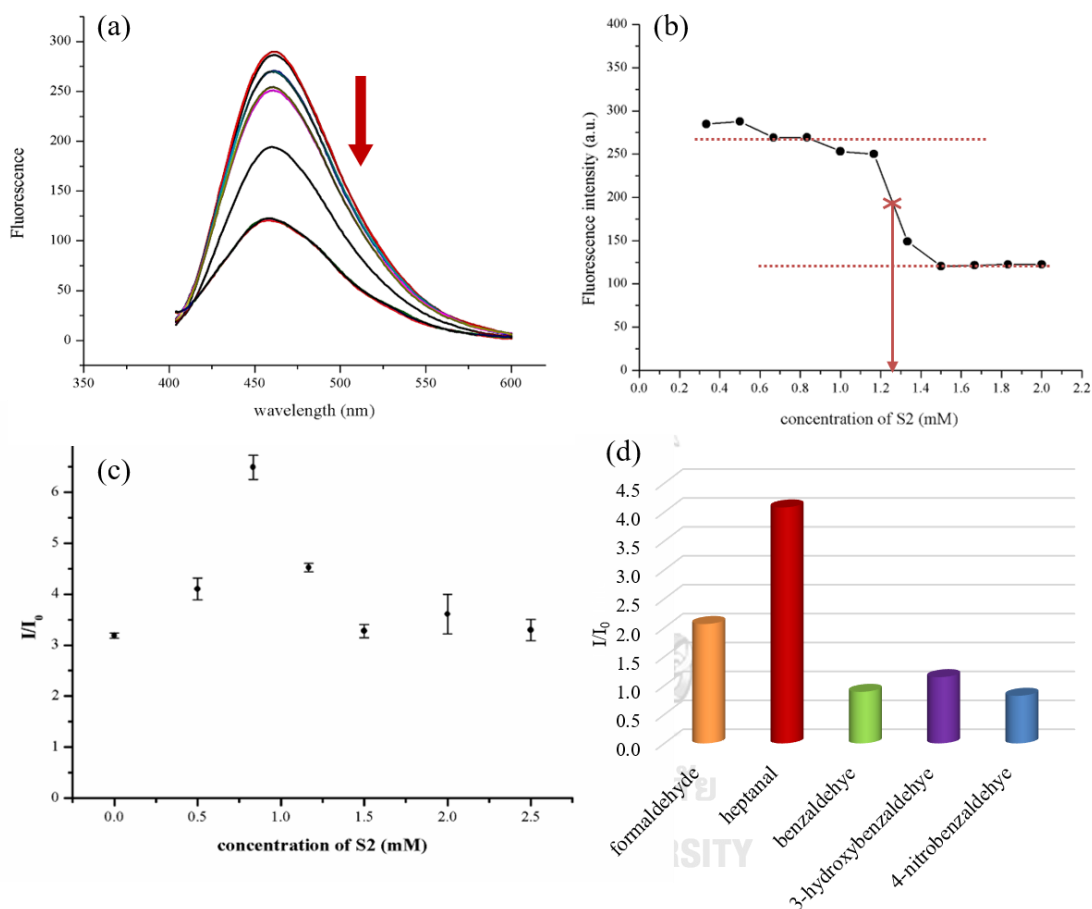


Figure 3.19 Fluorescence spectra (a) and fluorescent curve (b) at 458 nm of 5.0×10^{-5} M **Naph-OMe** in **S2** micellar system at a concentration range from 0.2 mM to 2.0 mM ($\lambda_{\text{ex}} = 385$ nm). (c) Relative fluorescence intensity at 542 nm (I/I_0) of **Naph-NH₂/CTAB** micelle with various **S2** concentration toward 0.25 mM heptanal. (d) Relative fluorescence intensity of **Naph-NH₂/CTAB/S2** micelle at 542 nm (I/I_0) after introduction of various aldehydes (2.5% DMSO/PBS buffer pH 7.4, $\lambda_{\text{ex}} = 445$ nm).

Moreover, we also studied the optimal concentration of **Naph-NH₂** in **CTAB/S2** micellar system for long-chain aldehyde sensing. The **Naph-NH₂**

concentration of 0.02, 0.05, 0.25, 0.42 and 0.75 mM were doped into **CTAB/S2** micellar-like particles. and then heptanal at concentration of 0.25 mM and 0.30 mM, were added to the solution of **Naph-NH₂/CTAB/S2** incomplete micellar sensor. The reaction mixture was stirred for 20 min in 2.5% DMSO/PBS buffer pH 7.4 prior to fluorescent measurement. The initial and final emission bands at 542 nm ($\lambda_{ex} = 445$ nm) corresponding to in the absence and presence of heptanal, were assigned as I_0 and I , respectively. The I/I_0 values were plotted against various concentrations of **Naph-NH₂**. Subsequently, the different fluorescence intensity with the addition 0.25 mM and 0.30 mM of heptanal were set as Δ value. In this experiment, Δ parameter was an essential parameter to optimize the **Naph-NH₂** concentration in **CTAB/S2** micellar-like platform for constructing the standard calibration curve in quantitative analysis of long-chain aldehyde detection. As illustrated in Figure 3.20, **Naph-NH₂** concentration of 0.02, 0.05, 0.25, 0.42 and 0.75 mM provided the Δ values of 0.46, 1.43, 1.62, 2.42 and 0.24, respectively. Hence, 0.42 mM of **Naph-NH₂** in **CTAB/S2** micellar-like particle showed a large Δ values of ~ 2.42 . However, the observation of a few precipitation of 0.42 and 0.75 mM **Naph-NH₂** in mixture solution indicated the poor water solubility of **Naph-NH₂**. Herein, 0.25 mM of **Naph-NH₂** with Δ value of 1.62 was chosen for long-chain aldehyde detection by **Naph-NH₂/CTAB/S2** incomplete micellar platform.

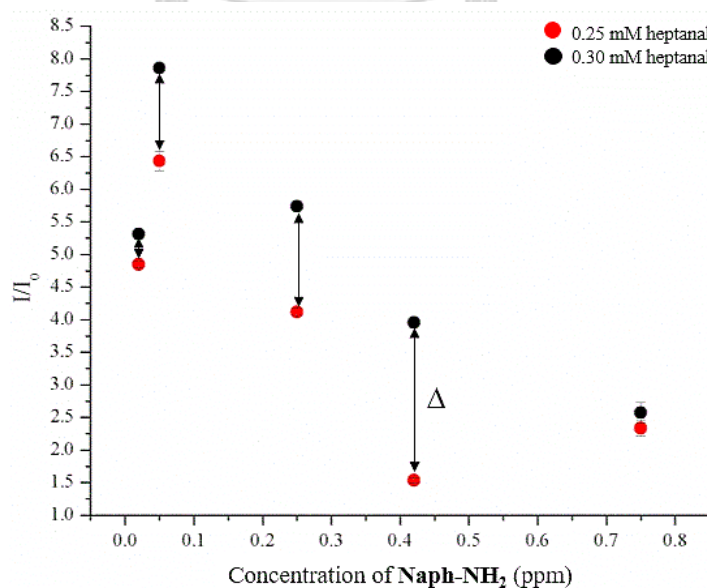


Figure 3.20 The studies of **Naph-NH₂** concentration of **CTAB/S2** micellar system in 2.5% DMSO/PBS buffer pH 7.4. ($\lambda_{ex} = 445$ nm)

3.6 The effect on pH of Naph-NH₂/CTAB/S2 micellar sensor for long-chain aldehyde detection

Apart from the concentration of dye, surfactants, the pH effect of **Naph-NH₂/CTAB/S2** sensor was a crucial factor for heptanal detection. We also studied pH influence on the sensing ability of this sensory platform at 5.0, 6.0, 7.4, 8.0 and 9.0, respectively. The fluorescent emission of nanosensor at 542 nm was examined under the reaction time of 20 min. The fluorescent intensity at 542 nm in the absence and presence of heptanal were assigned as I_0 and I , respectively. As illustrated in Figure 3.21, the relative fluorescence intensities (I/I_0) of **Naph-NH₂/CTAB/S2** toward 0.25 mM heptanal slightly decreased upon an increase of pH in a range of 5.0-7.4. Meanwhile, The I/I_0 values of **Naph-NH₂/CTAB/S2** toward heptanal were a large decrease in basic system (pH 8.0 - 9.0). These results implied the decomposition of hydrazone product in basic condition possibly under the Wolff-Kishner Reduction [62]. This is indicative of the pH-dependent fluorescence sensory system. Consequently, the PBS buffer pH 7.4 was chosen for sensing approach of this nonmicellar sensor which is a normal physical condition.

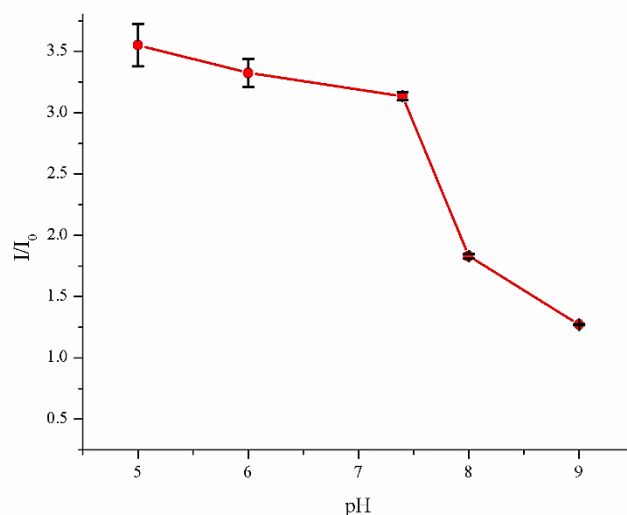


Figure 3.21 Determination of pH effect on **Naph-NH₂/CTAB/S2** toward 0.25 mM heptanal with various pH in the range of 5.0- 9.0. (2.5% DMSO/ buffer solution, λ_{ex} = 445 nm)

3.7 Characterization of Naph-NH₂/CTAB/S2 micellar sensor for long-chain aldehyde detection

To verify the morphology of **Naph-NH₂/CTAB/S2** material, plan-view images were studied by using Transmission Electron Microscopy (TEM). A single-layered film of diluted **Naph-NH₂/CTAB/S2** in 2.5% DMSO/PBS buffer pH 7.4 was collected on Copper-TEM grid. The TEM results of **Naph-NH₂/S2/CTAB** indicated the homogeneously spherical nanomicelles which had an average size in a range of 5.39 ± 1.03 nm (Figure 3.22(a1)) calculated from 200 particles by using Image J software (version 1.4.3.67). After introduction of 0.25 mM and 0.50 mM heptanal into **Naph-NH₂/CTAB/S2** nanomicelle (Figure 3.22(b) and Figure 3.22(c)), the average particle sizes of micelles was significantly increased to 22.38 ± 5.49 nm and 30.19 ± 7.28 nm, respectively. These increments in particle size of micelles was proposed that heptanal penetrated into the core of incomplete micellar-like particle to react with **Naph-NH₂** incorporated in incomplete **CTAB/S2** micelle inducing the completed micellar formation and a consequent fluorescent enhancement. These results confirmed that heptanal formed a well-induced fit aggregation of micellar form.

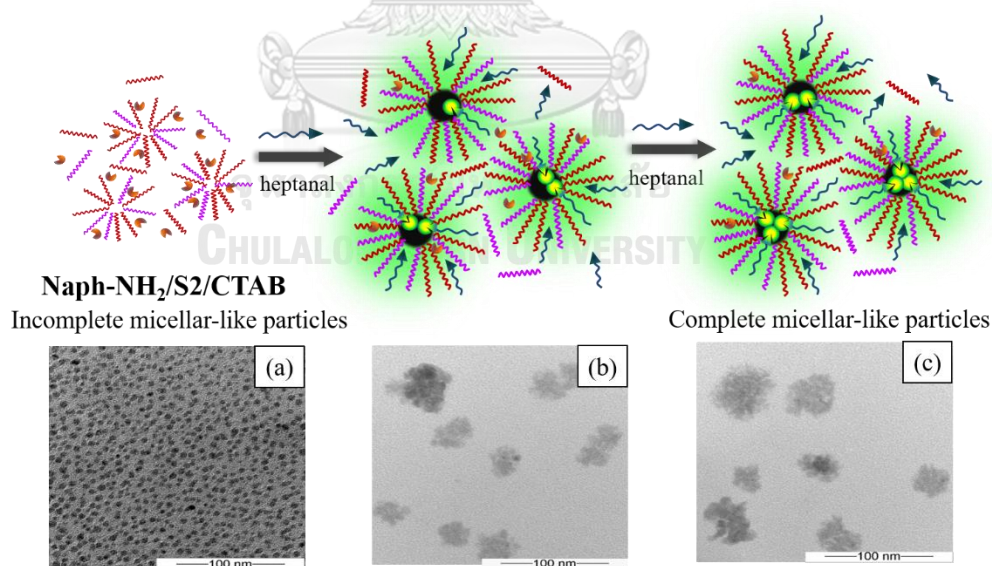


Figure 3.22 TEM photographs of **Naph-NH₂/CTAB/S2** micelles (a), **Naph-NH₂/CTAB/S2** micelle after introduction of 0.25 mM heptanal (b) and 0.50 mM heptanal (c).

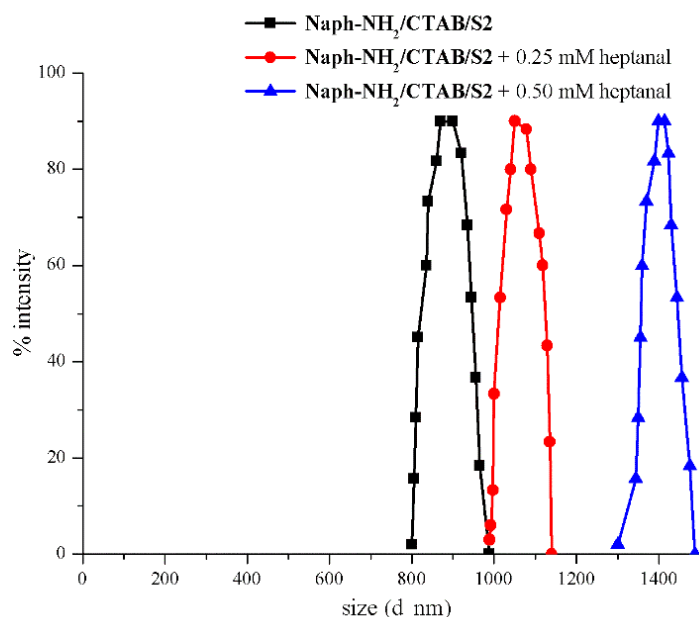


Figure 3.23 DLS of **Naph-NH₂/S2/CTAB** micelles before (black line) and after introduction of 0.25 mM (red line) and 0.50 mM (blue line) heptanal, respectively., in 2.5% DMSO/ 0.01 M PBS buffer pH 7.4

Additionally, the particles sizes of micelle in solution have been investigated by Dynamic Light Scattering (DLS) technique. As shown in Figure 3.23 and Table 3.1, the trend of average size of **Naph-NH₂/S2/CTAB** micelles with and without heptanal in 0.25 mM and 0.50 mM in solution is consistent with the particle size measured by TEM image. The results demonstrated a larger size of **Naph-NH₂/S2/CTAB** platform in the presence of heptanal. However, very big particle size of nanomicelle in solution indicated the apparent size of the dynamic hydrated/solvated particle assuming a hydration layer surrounding the particle.

Table 3.1 Size distribution of **Naph-NH₂/S2/CTAB** micellar sensor by DLS

Entry	System components	Size diameter (nm)
1	Naph-NH₂/CTAB/S2	899
2	Naph-NH₂/CTAB/S2 + 0.25 heptanal	1078
3	Naph-NH₂/CTAB/S2 + 0.50 heptanal	1414

Table 3.2 Zeta potential measurement of **Naph-NH₂/S2/CTAB** micellar sensor

Entry	System components	Zeta potential (mV)
1	CTAB/S2	27.23 ± 0.81
2	Naph-NH₂/CTAB/S2	4.10 ± 0.78
3	Naph-NH₂/CTAB/S2 + heptanal	25.80 ± 0.26

In our hypothesis about the aggregation behaviour by charge changing, **Naph-NH₂/CTAB/S2** was examined by using zeta potential analysis. In view of colloidal dispersion, zeta potential value of the particles is known as the electric potential at the boundary of the double layer surrounding particles. In case of zeta potential analysis of micellar fluorescent sensor (Table 3.2), the results showed the zeta potential of **CTAB/S2** micelle at 27.23 ± 0.81 mV ascribing the positive charge of particle surface from CTAB surfactant exposed to water. Upon the addition of **Naph-NH₂**, the zeta potential value significantly decreases to 4.10 ± 0.78 mV. The reduction of zeta potential value could be assumed that the positive charge of CTAB was balanced by lone-paired electron of hydrazine in **Naph-NH₂** base. Surprisingly, the presence of heptanal predominantly enhanced the zeta potential values to 25.80 ± 0.26 mV. Notably, this result was assumed that heptanal was induced to interact with **Naph-NH₂** to form hydrazone compound which is high degree of hydrophobic compound causing a complete micellar formation and an increase of encapsulation of fluorescent dye in nanomicelle. Eventually, the positive charge of CTAB was apparently dominant. The results from TEM, DLS and Zeta potential are the powerful evidences to support our concept that heptanal performed an effectively induced-fit aggregation by reacting with hydrazine group of fluorescent dye-doped incomplete micellar form and subsequently, induced the complete nanomicelle formation and enhanced the fluorescent intensity of dye-doped material.

3.8 The optical studies of Naph-NH₂/CTAB/S2 micellar sensor

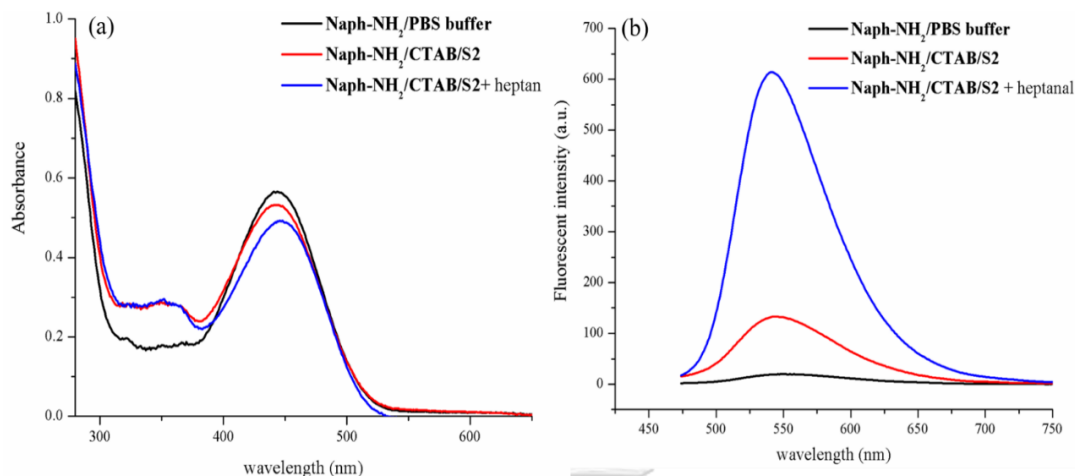


Figure 3.24 UV-visible (a) and fluorescence (b) spectra of **Naph-NH₂/PBS buffer** (black line), **Naph-NH₂/CTAB/S2** before (red line) and after (blue line) introduction of 0.25 mM heptanal in 2.5% DMSO/PBS buffer pH 7.4 ($\lambda_{\text{ex}} = 445$ nm).

The optical property of **Naph-NH₂/CTAB/S2** was studied by using UV-visible and fluorescence spectroscopy in 2.5% DMSO/PBS buffer pH 7.4, as shown in Figure 3.24. The absorption spectra of **Naph-NH₂/PBS buffer** and **Naph-NH₂/CTAB/S2** exhibited the maximum absorption band at 445 nm. Meanwhile, the absorption peak of **Naph-NH₂/CTAB/S2** was slightly red shift to 448 nm after introduction of 0.25 mM heptanal. These results implied that heptanal enabled to induce self-assembled organization to form a complete micelle [63] resulting in the environmental change in **Naph-NH₂/CTAB/S2** micellar system.

According to fluorescence properties, the **Naph-NH₂/PBS buffer** and **Naph-NH₂/CTAB/S2** showed the maximum emission bands at 550 nm and 545 nm, respectively. However, the observation of a small fluorescence enhancement of **Naph-NH₂/CTAB/S2** was due to the effect of dye-doped micellar system which protect the interaction of water and reduced free rotation of benzene ring in dye [63, 64]. Interestingly, the heptanal addition induced a slightly blue shift to 542 nm with a concomitant of a large fluorescent enhancement of the fluorescence response for **Naph-NH₂/CTAB/S2**.

In addition, the fluorescence intensity of **Naph-NH₂/CTAB/S2** was blue shift to 542 nm and further enhanced after adding 0.25 mM heptanal. There are two possible hypothesis; i) the inhibition of PET process of dye after reacting with heptanal [43, 65] ii) reducing free rotation of benzene ring of dye by complete encapsulation from heptanal induced-fit aggregation of nanomicelle [63, 64].

3.9 The kinetic profiles of **Naph-NH₂/CTAB/S2** micellar sensor

Furthermore, we have investigated the kinetic profiles of **Naph-NH₂/PBS buffer** and **Naph-NH₂/CTAB/S2** in the absence and in the presence of 0.25 mM heptanal by using fluorescence spectroscopy. The reaction mixture was continuously stirred at room temperature for 90 min. The fluorescent intensity of sensory platforms at 542 nm was measured every 10 min under the excitation of 445 nm and the fluorescence intensity at 542 nm was plotted against time, as illustrated in Figure 3.25. The kinetic profiles revealed that the fluorescence intensity of **Naph-NH₂/PBS buffer** showed a small increase while that of **Naph-NH₂/CTAB/S2** were gradually enhanced as a function of time. This is possibly due to a poor encapsulation of **Naph-NH₂** in the incomplete micellar-like material without the heptanal addition. On the other hand, the case of the heptanal addition could react with hydrazine moiety based **Naph-NH₂** and subsequently induced the complete micelle aggregation resulting in the effective encapsulation of **Naph-NH₂**. This phenomenon showed no change of fluorescent intensity upon increment of time over 20 min. Hence, the fluorescent intensity of **Naph-NH₂/CTAB/S2** was constant within 20 min after adding 0.25 mM of heptanal. This result suggested that the reaction time of 20 min is suitable for long-chain aldehyde detection by using **Naph-NH₂/CTAB/S2** platform.

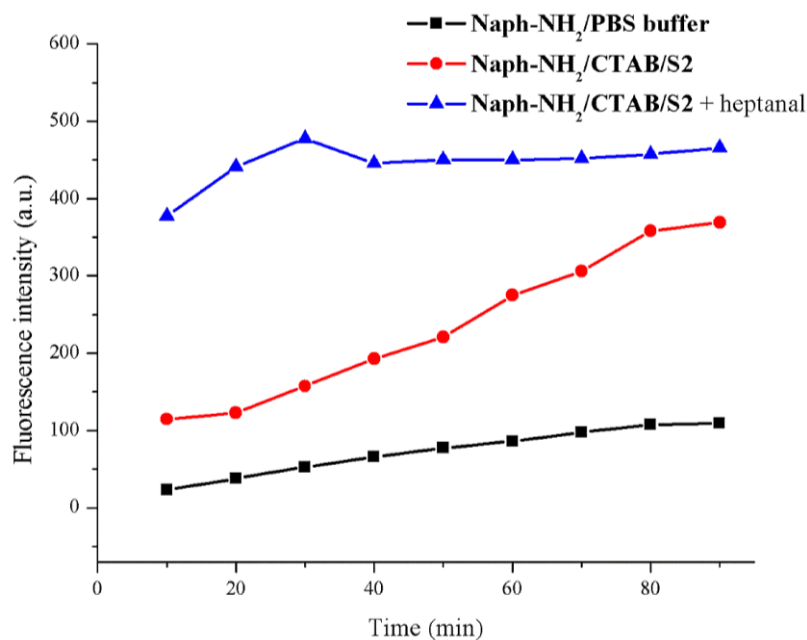


Figure 3.25 The kinetic profiles of **Naph-NH₂/PBS buffer** (black line) and **Naph-NH₂/CTAB/S2** in the absence (red line) and in the presence (blue line) of 0.25 mM heptanal. (2.5% DMSO/PBS buffer pH 7.4, $\lambda_{\text{ex}} = 445 \text{ nm}$)

3.10 The effect of hydrazine functional group on Naph-NH₂/CTAB/S2 micellar sensor

To clarify the important role of hydrazine functional group on **Naph-NH₂** for aldehyde detection, **Naph-OMe** was the model compound without hydrazine group for studying the aldehyde detection in micellar system. From Figure 3.26, the fluorescence intensity of **Naph-OMe/CTAB/S2** was quenched compared to that of bare **Naph-OMe** in PBS buffer solution while no fluorescent change of **Naph-OMe/CTAB/S2** with various aldehyde compounds were observed. These results suggested that the hydrazine group of **Naph-NH₂** played an important role as a reactive site for aldehyde detection via condensation reaction.

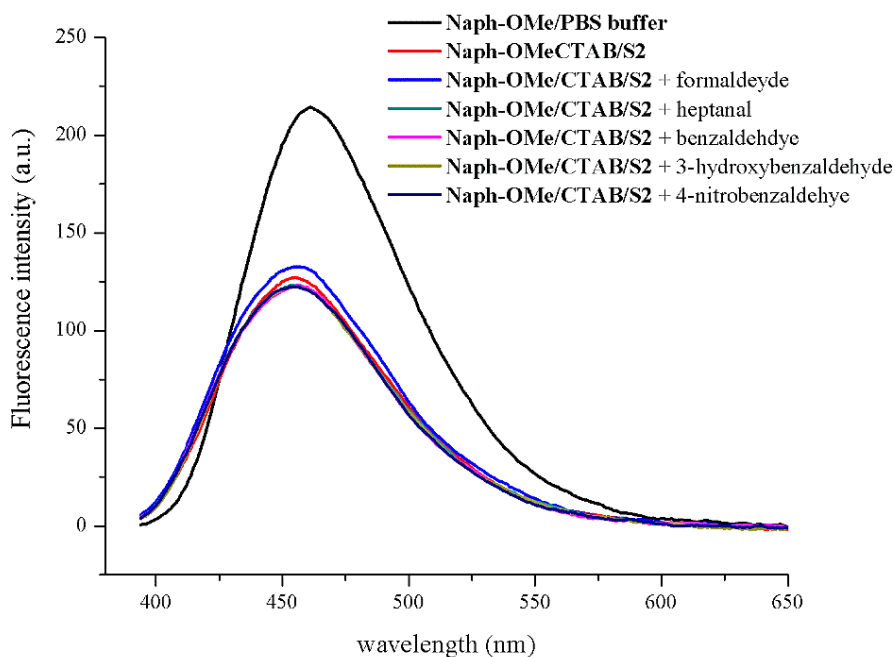


Figure 3.26 Fluorescence spectra of **Naph-OMe/PBS buffer** and **Naph-OMe/CTAB/S2** micelle after introduction of 0.25 mM various aldehydes including formaldehyde, heptanal, benzaldehyde, 3-hydroxybenzaldehyde and 4-nitrobenzaldehyde. (2.5% DMSO/PBS buffer pH 7.4, $\lambda_{\text{ex}} = 385 \text{ nm}$)

3.11 Determination of long-chain aldehydes using Naph-NH₂/CTAB/S2 sensor

In our further attempt, we designed fluorescent probe for long-chain aldehydes sensing by incomplete micellar-like particles, which prepared by 1.0 mM CTAB and 0.83 mM **S2** surfactant. **Naph-NH₂** acting as a fluorophore containing hydrazine binding site was encapsulated into the incomplete micellar-like particles. In this approach, we expected that long-chain aldehydes would perform as the induce-fit aggregation to form a completely self-assembling nanomicelle with a concomitant of reacting with **Naph-NH₂** via a condensation reaction as shown in Figure 3.27. Subsequently, the interaction of hydrazine-derivative dye and aldehyde caused the fluorescent change corresponding to the concentration of aldehydes.

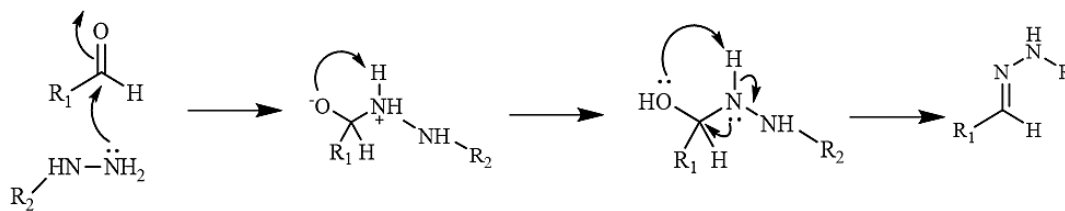


Figure 3.27 Mechanism of condensation reaction between hydrazine and aldehyde [66]

In case of long-chain aldehydes; hexanal, heptanal, octanal and nonanal were regarded as a biomarker for lung cancer disease. Hence, we have focused on determination of a considerable amount of these aldehydes using **Naph-NH₂/CTAB/S2** micellar platform. In quantitative analysis for sensing approach, the fluorescent titration of **Naph-NH₂/CTAB/S2** micellar platform toward long-chain aldehydes was carried out in 2.5% DMSO/PBS buffer pH 7.4. The relation between the amounts of long-chain aldehydes and emissive signal was illustrated in term of standard calibration curve which was plotted under various aldehyde concentrations versus the relative fluorescence intensities (I/I_0) of **Naph-NH₂/CTAB/S2** sensor. The emission intensity at 542 nm in the absence and presence of heptanal were assigned as I_0 and I , respectively. Based on the calibration curve, the limit of detection (LOD) and limit of quantification (LOQ) were calculated by method validation procedure using equation 3.1 and equation 3.2. The signal of blank was measured in 10 times to set a standard derivation (SD) of baselines.

$$\text{LOD} = \frac{3\text{SD}}{\text{slope}} \quad 3.1$$

$$\text{LOQ} = \frac{10\text{SD}}{\text{slope}} \quad 3.2$$

The LOD and LOQ values for long-chain aldehyde detection of **Naph-NH₂/CTAB/S2** micellar platform was in the range of 64-81 μM , (Table 3.3). Moreover, the percent recovery of aldehyde concentration was also evaluated in the range of 83-110 % under the SD values of 2.18-8.55 which were acceptable for sensing aspect. As shown in Table 3.4, the results showed that the **Naph-NH₂/CTAB/S2** micellar system provided the high percent recovery for long-chain aldehyde detection in 2.5% DMSO/PBS buffer pH 7.4. Hence, these relationship between the fluorescent

enhancement and the amounts of long-chain aldehydes could be applied for further cancer diagnosis.

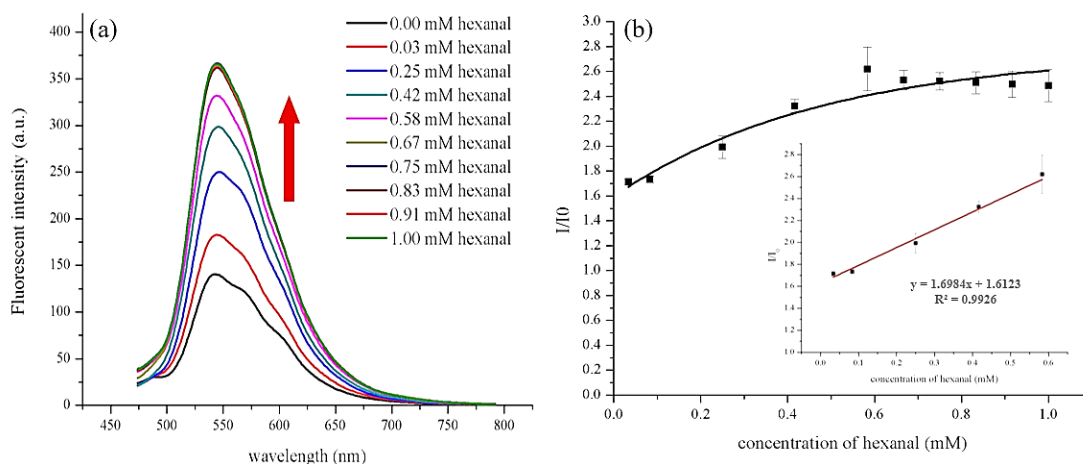


Figure 3.28 (a) Fluorescence titration spectra and (b) relative fluorescence intensity (I/I_0) after introduction of various hexanal concentration. The inset showed the linear range of hexanal detection from 0.03 to 0.67 mM (0.03-1.00 mM) in 2.5% DMSO/PBS buffer pH 7.4 ($\lambda_{\text{ex}} = 445$ nm).

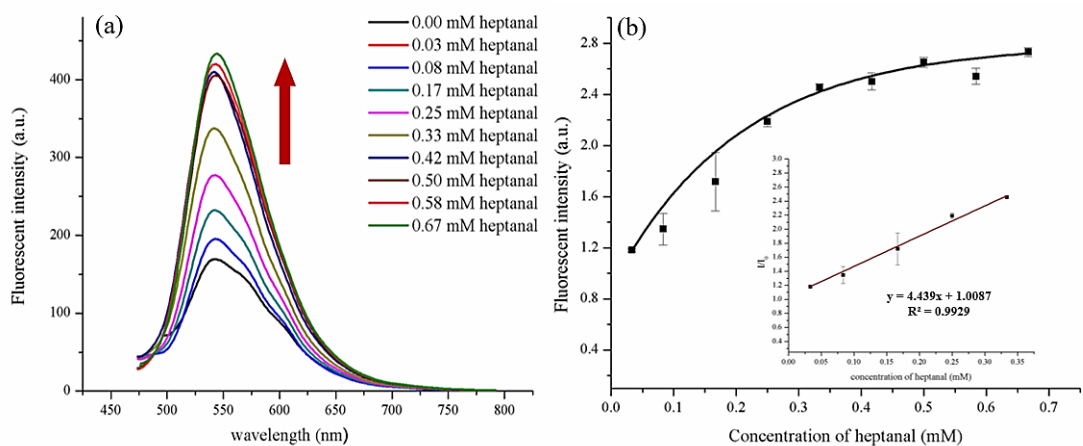


Figure 3.29 (a) Fluorescence titration spectra and (b) relative fluorescence intensity (I/I_0) after introduction of various heptanal concentration. The inset showed the linear range of heptanal detection from 0.03 to 0.33 mM (0.03-0.67 mM) in 2.5% DMSO/PBS buffer pH 7.4 ($\lambda_{\text{ex}} = 445$ nm).

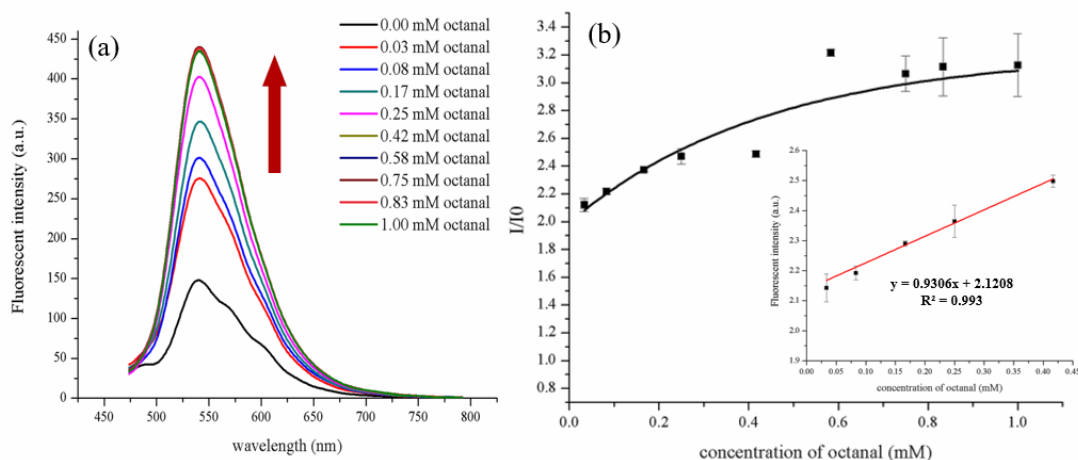


Figure 3.30 (a) Fluorescence titration spectra and (b) relative fluorescence intensity (I/I_0) after introduction of various octanal concentration. The inset showed the linear range of octanal detection from 0.03 to 0.42 mM (0.03-1.00 mM) in 2.5% DMSO/PBS buffer pH 7.4 ($\lambda_{\text{ex}} = 445$ nm).

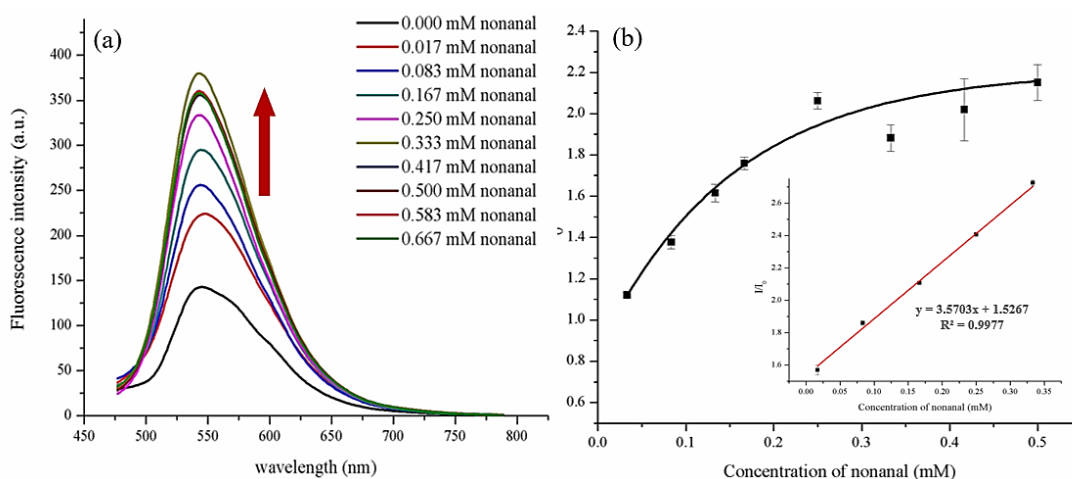


Figure 3.31 (a) Fluorescence titration spectra and (b) relative fluorescence intensity (I/I_0) after introduction of various nonanal concentration. The inset showed the linear range of nonanal detection from 0.017 to 0.33 mM (0.017-0.667 mM) in 2.5% DMSO/PBS buffer ($\lambda_{\text{ex}} = 445$ nm).

Table 3.3 limit of detection (LOD) and limit of quantification (LOQ) for long-chain aldehyde detection by using **Naph-NH₂/CTAB/S2** incomplete micellar sensor

Entry	Long-chain aldehydes	Linear range (mM)	Equation	R ²	LOD (μM)	LOQ (μM)
1	hexanal	0.03 - 0.67	$y = 1.6984x + 1.6123$	0.9926	74.38	251.27
2	heptanal	0.03 - 0.33	$y = 4.4390x + 1.0087$	0.9929	80.38	267.92
3	octanal	0.03 - 0.42	$y = 0.9306x + 2.1208$	0.9930	80.98	269.86
4	nonanal	0.017 - 0.33	$y = 17.851x + 1.5267$	0.9977	64.09	213.65

Table 3.4 Percent recovery of **Naph-NH₂/CTAB/S2** for long-chain aldehyde detection.

Entry	Long-chain aldehydes	Concentration (added)	% recovery ± SD
1	hexanal	0.33 mM	105.32 ± 8.55
		0.50 mM	83.38 ± 2.91
2	heptanal	0.13 mM	85.64 ± 6.77
		0.20 mM	96.94 ± 4.93
3	octanal	0.12 mM	87.62 ± 5.57
		0.35 mM	110.02 ± 2.18
4	nonanal	0.15 mM	95.43 ± 5.76
		0.20 mM	101.50 ± 4.09

3.12 Selectivity of Naph-NH₂/CTAB/S2 micellar sensor

Apart from the sensitivity of **Naph-NH₂/CTAB/S2** micellar platform, its selectivity with various organic compounds is very important role for sensing approach. We focused on studying on the organic compounds which are actually found in exhale breath of lung cancer patients [67-75], including formaldehyde, propanal, butanal, pentanal, hexanal, heptanal, octanal, nonanal, acetone, benzaldehyde, 4-hydroxybenzaldehyde, 3-nitrobenzaldehyde, xylene, cyclohexane, benzene, heptane, phenol, toluene, acetonitrile, cysteine, homocysteine, glutathione, and ascorbic acid. The solution of **Naph-NH₂/CTAB/S2** sensor and 0.25 mM of various organic compounds was stirred at room temperature for 20 min before fluorescent measurement. The results illustrated that the relative fluorescent intensity (I/I_0) was enhanced in the presence of hexanal, heptanal, octanal and nonanal. These implied that **Naph-NH₂/CTAB/S2** micellar platform offered a good selectivity for long-chain aldehydes, as shown in Figure 3.32. However, butanal and pentanal was able to interfere a **Naph-NH₂/CTAB/S2** micellar sensor towards long-chain aldehydes. These results indicated that **Naph-NH₂/CTAB/S2** micellar sensor was able to detect aliphatic aldehydes comprising more than four carbon atoms in their structures.

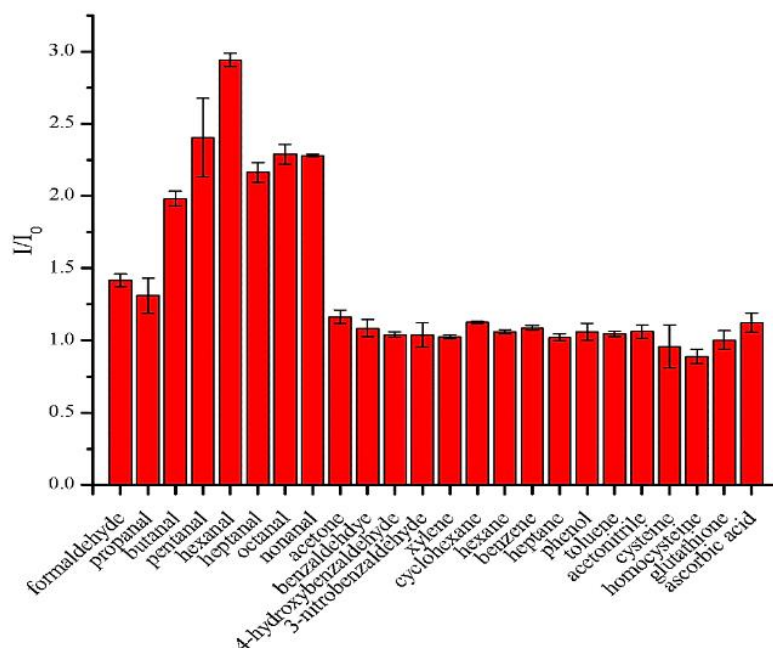


Figure 3.32 Fluorescence response at 542 nm **Naph-NH₂/CTAB/S2** micellar toward organic compounds which were found in breath of lung cancer patients. (2.5% DMSO/PBS buffer pH 7.4, $\lambda_{ex} = 445$ nm).

3.13 Determination of long-chain aldehydes in real blood sample

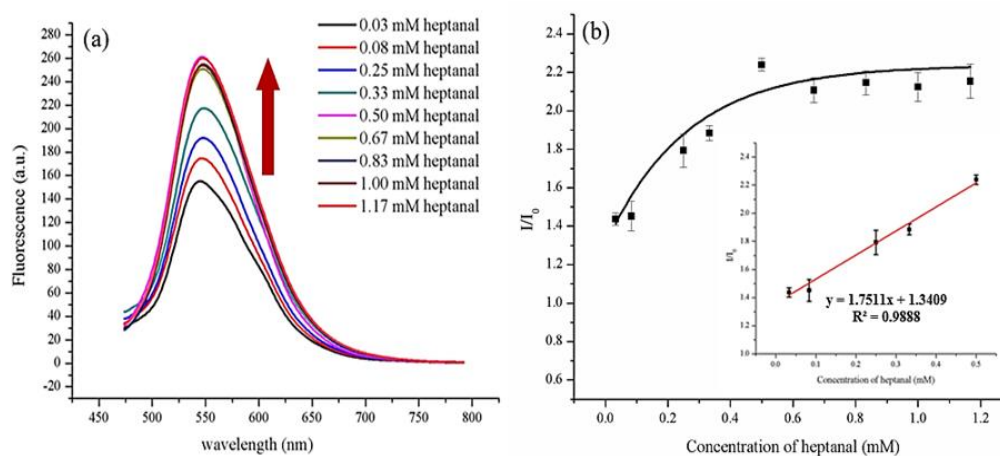


Figure 3.33 (a) Fluorescence titration spectra and (b) relative fluorescence intensity (I/I_0) after spiked of various heptanal concentration in real blood sample. The inset showed the linear range of heptanal detection from 0.03 to 0.50 mM (0.03-1.17 mM) in 2.5% DMSO/PBS buffer pH 7.4 ($\lambda_{ex} = 445$ nm).

To further gain more benefits of **Naph-NH₂/CTAB/S2** material in diagnosis application, we also applied it to determine heptanal in blood sample using standard addition method. With the preparation of blood plasma samples, blood was collected in heparin-coated collection tubes from a healthy candidate person. The plasma was separated by centrifugation at 2000 rpm for 20 min and then the supernatant was stored at 5 °C until use. Subsequently, various heptanal concentrations were spiked into the plasma prior to fluorescence measurement. As illustrated in **Figure 3.33**, the results showed the fluorescence enhancement corresponding to spiked-heptanal concentration with percent recovery in a range of 94.01-102.4 (Table 3.5). In this regard, the **Naph-NH₂/CTAB/S2** was able to detect heptanal in blood sample by using the standard addition method, even though there were many interference compounds in the sample. Hence, the **Naph-NH₂/CTAB/S2** platform served as a medical application for diagnosis disease.

Table 3.5 Percent recovery of **Naph-NH₂/CTAB/S2** for long-chain aldehyde detection.

Concentration of heptanal (add)	Concentration of heptanal (found)	% recovery	Average %recovery	SD	% RSD
0.00	ND	-	-	-	-
0.167	0.158	94.87	94.01	3.83	4.08
	0.152	91.39			
	0.160	95.78			
0.217	0.217	100.15	102.48	2.16	2.11
	0.226	104.42			
	0.222	102.86			

ND = Not detectable

3.14 Biological application in lung cancer cell (A549)

According to the aldehyde sensing ability of **Naph-NH₂/CTAB/S2** micellar sensor in blood sample, we further applied it to determine the long-chain aldehydes in human adenocarcinoma lung cell (A549) [76]. In this study, A549 cancer cells were seeded at density 10^5 cells/mL in each well plate of 8-well plates and treated with **Naph-NH₂/CTAB/S2** micellar sensor for 4 h. Moreover, 4,6-diamino-2-phenylindole (DAPI) was incubated for 5 min in order to serve as a blue fluorescent stain for labeling of nucleus region. These micrographs were detected under excitation wavelength at 405 and 488 nm.

For the cell imaging, the green fluorescence was clearly observed indicating the efficient cover of the A549 cancer cell. This satisfied an excellent intracellular uptake and high green emission contrast. The blue emissive areas were also found in cells indicating the location of cell nuclei. The above results further suggested that **Naph-NH₂/CTAB/S2** micelle could easily penetrated into A549 cancer cell and located in both nucleus and cytoplasm. Moreover, **Naph-NH₂/CTAB/S2** micelle after introduction of 0.125 mM heptanal showed a stronger fluorescence. The green channel confirmed that the **Naph-NH₂/CTAB/S2** was internalized into all cells. The merged images of three channels (right column) showed that the **Naph-NH₂/CTAB/S2** were localized in the cytoplasm and nucleus. Consequently, **Naph-NH₂/CTAB/S2** micellar

sensor was successfully applied to cell imaging and promising for further biological applications.

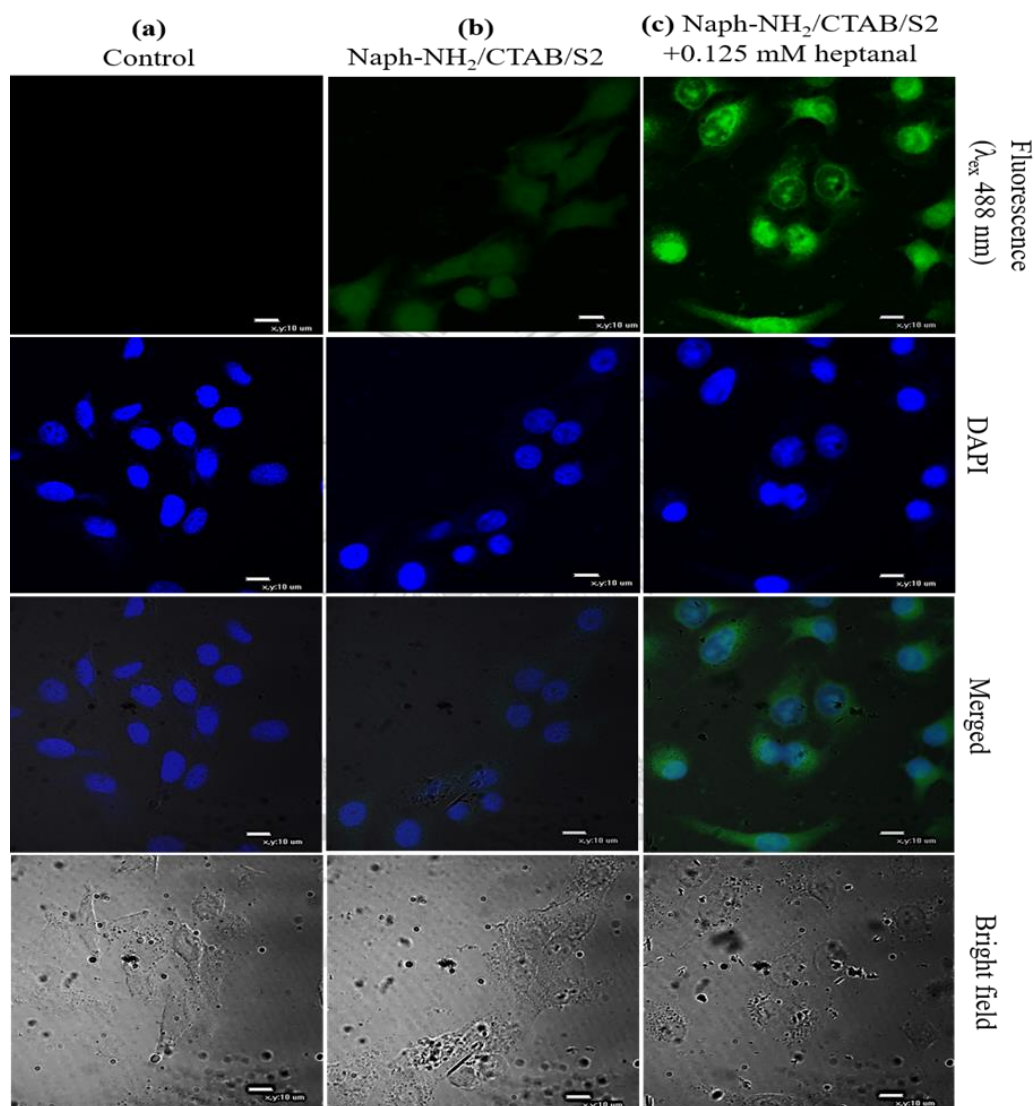
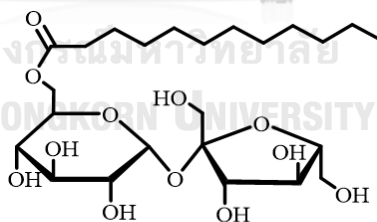


Figure 3.34 Confocal images of A549 cancer cells (a) control, (b) incubation of **Naph-HN₂/CTAB/S2**, (C) **Naph-HN₂/CTAB/S2** and heptanal for 4 h using confocal fluorescence microscopy.

3.15 Naph-NH₂/CTAB/S2 based gel (Naph-NH₂/CTAB/S2 @gel) for long-chain aldehyde detection

Although Naph-NH₂/CTAB/S2 platform is achievable a pioneer optical sensing aspect for long-chain aldehyde compounds with high selectivity among all kinds of aldehyde compounds, the sensitivity did not advantageously touch in the efficacy of cancer diagnosis. To solve the weak point of sensitivity, we attempt to integrate our sensing platform with supramolecular hydrogels which are flexible materials arise from the self-assembly of hydrophobic gelator and large amount of water (typically higher than 99%) using non-covalent interactions, inducing the formation of a hydrophobic fibrillar network and large hydrophilic cavities of water [77-80]. Meanwhile, the gels behave as solid-like materials on an analytical time scale but also exhibit fluid behavior promoting diffusion of solutes in the gel phase. Fortunately, in our laboratory, we have sucrose laurate monoester (**Gel 1**) which contained the sucrose and octane chain. This is expected to be gelator for hydrogel materials due to its aliphatic long-chain hydrocarbon of lauric acid-containing molecule. Regarding to works by Guijun Wang group [81], they reported the gelation properties of low molecular weight gelators (LMWGs) or molecular gelators containing carbohydrate based system because they suggested that carbohydrate based gelator was synthesized from naturally abundant and readily available starting material and a benefit-compatible material.



Gel 1

Figure 3.35 The Chemical structure of **Gel 1**

In this approach, **Naph-NH₂/CTAB/S2** micellar material was prepared by cooperating CTAB and **S2** as a surfactant and co-surfactant, respectively. Subsequently, **Naph-NH₂/CTAB/S2** material was employed as a probe for detection of long-chain aldehydes. After the reaction of **Naph-NH₂/CTAB/S2** sensor and heptanal was completed in 20 min, the **Gel 1** gelator was added to the mixture solution and diluted by 60% DMSO/PBS buffer pH 7.4. Finally, the mixture self-assembly form gel in 10 min before measurement of the fluorescence spectrum ($\lambda_{\text{ex}} = 445 \text{ nm}$). The gelation procedure was illustrated in Figure 3.36

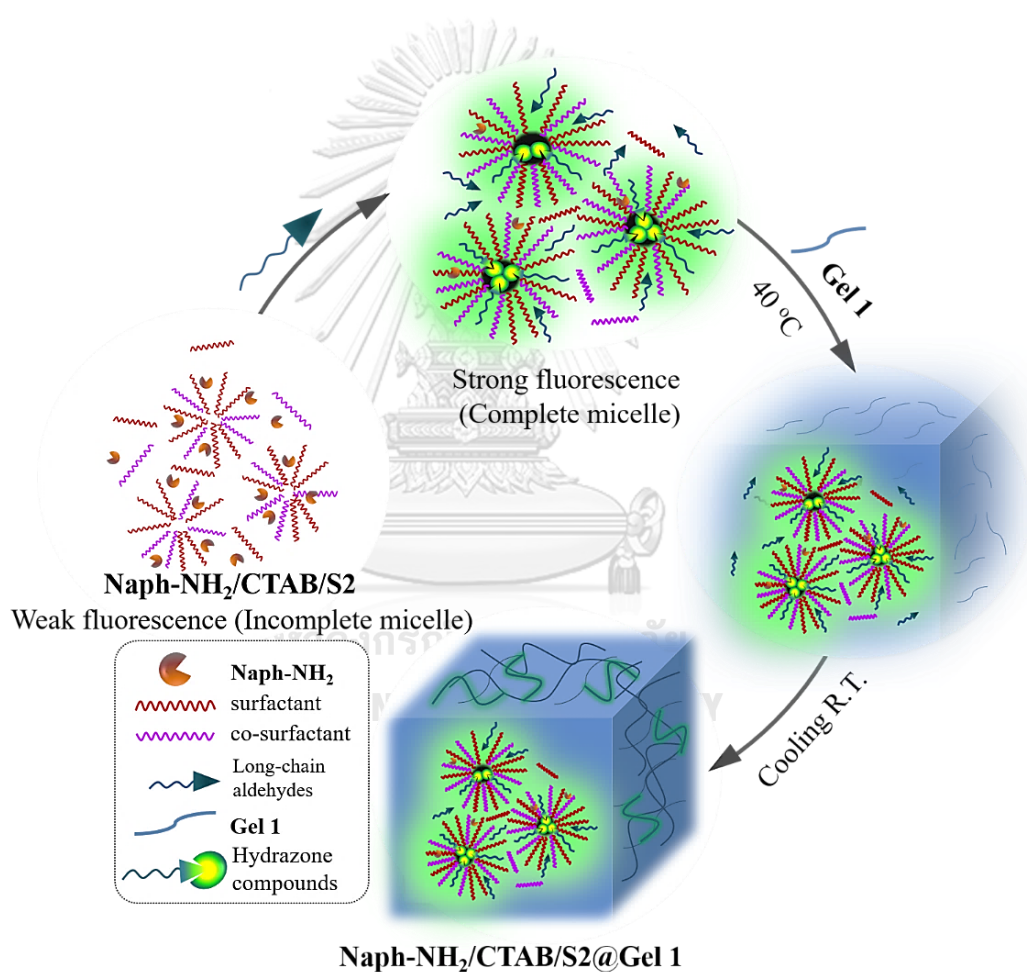


Figure 3.36 Schematic representation of the gelation mechanism of **Naph-NH₂/CTAB/S2@Gel 1** for long-chain aldehydes sensing

3.15.1 Optimization conditions of Gel 1 for gelation

In case of the optimal condition of gel, 100% DMSO and 0.01 M PBS buffer pH 7.4 were employed as the solvent for dissolving **Gel 1** at various concentrations. The gelator (**Gel 1**) was heated and then cooled down to self-assembly form gel. The gelation behavior of **Gel 1** was tested in a range of **Gel 1** concentration as shown in Table 3.6 and Table 3.7. Gel formation was assessed by the simple 'inversion' test to check for a self-supporting solid-like material. Base on studying the gel behavior, the total solution did not form gel assigned as "S" but the partial of solution formed gel assigned as partial gel or "PG" and the total solution forms translucent gel assigned as "G" and the total solution self-assembly organized an opaque gel assigned as "OG"

Ongoing systematic studies of the gelation behavior was reliably realized based on a key importance of the gelator amount and solvent system. Since gelator (**Gel 1**) is well dissolved in DMSO. The solvent system, thus, was investigated including three systems of 100% DMSO, 0.01 M PBS buffer pH 7.4 and the mixed DMSO and 0.01 M. PBS buffer pH 7.4. Considering of Table 3.6 and Table 3.7, the gel was completed formed at the 1.94 wt% **Gel 1** at 1 h in 100% DMSO while an opaque gel was observed at 22.90 wt% **Gel 1** at 3 h in 0.01 M. PBS buffer pH 7.4. By the visual observation of the gelation behavior, the **Gel 1** in 100% DMSO displayed an organized 3D translucent gel under condition of 1.94 wt% gelator at 1 h and the robust gel was remarkably observed under condition of over 22.90 wt% gelator at 2 h in 0.01 M PBS buffer pH 7.4. In general, the robust gel is not suitable for sensing application because of its opaque-gel material. Moreover, most of sensing approach are advantageously used in aqueous solution. Consequently, the mixed solvent of DMSO and PBS buffer pH 7.4 was hold out tremendous investigation for gel formation behavior, as shown in Table 3.8 and Table 3.9. In this experimental, 0.98 wt% and 1.94 wt% of **Gel 1** were studied. Deeply considerable, it was found that **Gel 1** enables to form an effective gel under condition of 1.94 wt% in 60% DMSO/PBS buffer pH 7.4. This condition is reasonably proper for incorporating our sensing platform in hydrogel because the gelation time at 30 min induced the partial gel which is an efficient stage for penetration of the sensing platform through the gel and further process to form the complete hydrogel in 1 h.

Table 3.6 The self-assembled studies of **Gel 1** chelator in 100% DMSO

% wt	Time				
	30 min	1 hr	2 hr	1 day	2 days
0.198	S	S	S	S	S
0.296	S	S	S	S	S
0.394	S	S	S	S	S
0.591	S	S	PG	PG	PG
0.786	PG	PG	PG	PG	PG
0.980	PG	PG	PG	PG	PG
1.942	PG	OG	OG	OG	OG

G = gel, PG = partial gel, S = solution, OG = opaque gel

Table 3.7 The self-assembled studies of **Gel 1** chelator in 0.01 M PBS buffer pH 7.4

% wt	Time				
	30 min	1 hr	2 hr	1 day	2 days
0.198	S	S	S	S	S
0.980	S	S	S	S	S
1.942	S	S	S	S	S
2.885	S	S	S	S	S
4.717	S	S	S	S	S
9.009	S	S	S	S	S
22.901	S	S	OG	OG	OG
33.113	S	OG	OG	OG	OG
37.267	S	OG	OG	OG	OG
40.936	S	OG	OG	OG	OG
49.751	S	OG	OG	OG	OG

G = gel, PG = partial gel, S = solution, OG = opaque gel

Table 3.8 The self-assembled organized studies of 0.98 wt % **Gel 1** gelator in various ratio of mixed solvent

% (V/V) DMSO/PBS buffer pH 7.4	% wt	Time				
		30 min	1 hr	2 hr	1 day	2 days
20	0.98	S	S	S	S	S
25	0.98	S	S	S	S	S
30	0.98	S	S	S	S	S
35	0.98	S	S	S	S	S
40	0.98	S	PG	PG	PG	PG
60	0.98	S	PG	PG	PG	PG
80	0.98	S	PG	PG	PG	PG
100	0.98	P	PG	PG	PG	PG

G = gel, PG = partial gel, S = solution, OG = opaque gel

Table 3.9 The self-assembled organized studies of 1.94 wt % **Gel 1** in various ratio of mixed solvent

% (V/V) DMSO/PBS buffer pH 7.4	% wt	Time				
		30 min	1 hr	2 hr	1 day	2 days
20	1.94	S	S	S	S	S
30	1.94	S	S	S	S	S
40	1.94	S	S	S	S	S
60	1.94	PG	G	G	G	G
80	1.94	PG	G	G	G	G
100	1.94	PG	G	G	G	G

G = gel, PG = partial gel, S = solution, LG = robust gel

3.15.2 Characterization of Naph-NH₂/CTAB/S2@Gel 1

The morphology of material sensor was also studied using Scanning Electron Microscopy (SEM) under the condition; 20.0 kV, WD 10 mm and PC 60, The hybrid material of **Naph-NH₂/CTAB/S2** cooperated with **Gel 1** was prepared in 60% DMSO/PBS buffer pH 7.4 and then left it to dry overnight on the Whatman Filter paper No.1 at 40 °C.

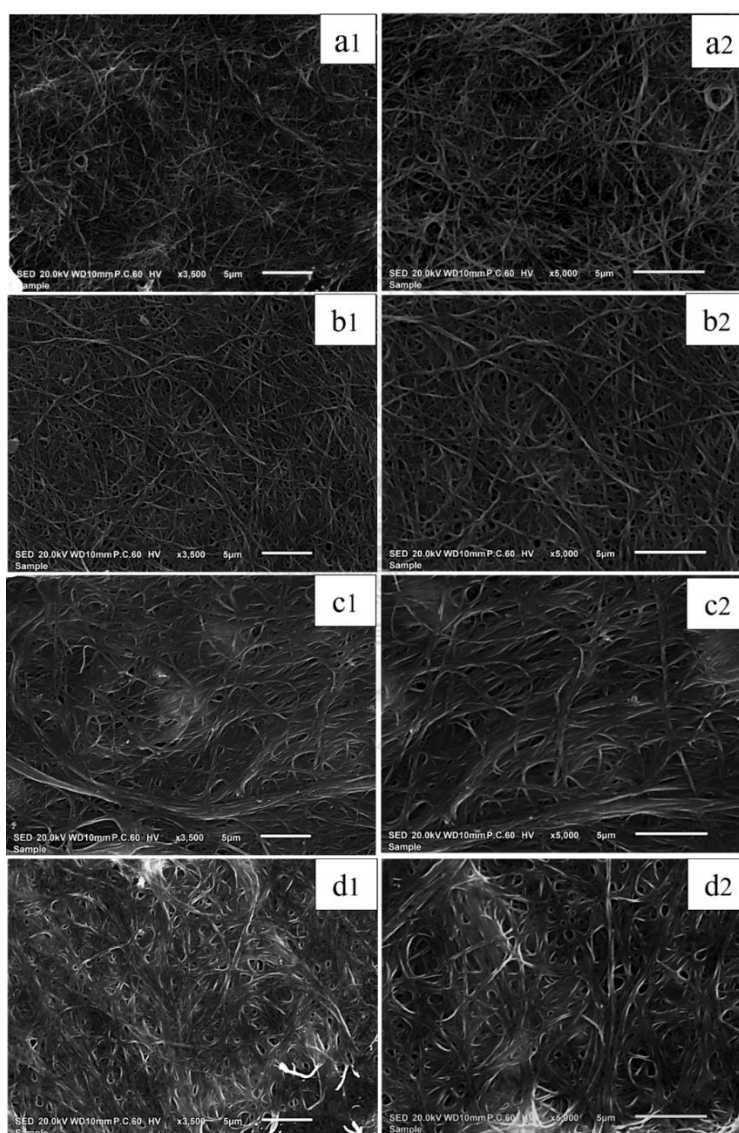


Figure 3.37 SEM images of gelator (**Gel 1**) (a), **Naph-NH₂/CTAB/S2@Gel 1** (b), **Naph-NH₂/CTAB/S2@Gel 1** after introduction of 0.05 mM (c) and 0.3 mM heptanal (d). (1.94 wt % **Gel 1** in 60% DMSO/PBS buffer pH 7.4)

According to visualization of gel from gelator (**Gel 1**) without **Naph-NH₂/CTAB/S2** by using SEM technique, the SEM image illustrated the fibers with an average diameter size of $0.254 \pm 0.10 \mu\text{M}$ as shown in Figure 3.37(a). Upon introduction of **Naph-NH₂/CTAB/S2** into gel, the fiber network was denser than fibers of gel without **Naph-NH₂/CTAB/S2**. The fibers had an average diameter size of $0.313 \pm 0.11 \mu\text{M}$ and partially exhibited a few aggregations, as shown in Figure 3.37(b). These possibly caused by the penetration of **Naph-NH₂/CTAB/S2** into 3D-fiber network and a consequent deposition on the fiber surface via H-bonding and hydrophobic interaction. In the presence of 0.05 mM and 0.30 heptanal, the overall diameter size of **Naph-NH₂/CTAB/S2@Gel 1** was partially swelled and enlarged as shown in Figure 3.37 (c) and Figure 3.37(d), respectively. These results could be explained that heptanal was not only induced to react with **Naph-NH₂/CTAB/S2** micelle platform, but also promoted a **Gel 1** to form hydrogel via H-bonding and hydrophobic interaction.

Furthermore, the **NH₂/CTAB/S2@Gel 1** was characterized by Fourier Transform (FT-IR) spectroscopy as shown in Figure 3.38. Comparing the FT-IR spectra of **Naph-NH₂/CTAB/S2@Gel 1** hybrid material to **Naph-NH₂** and **Gel 1**, the relative intensity at 3330 and 3220.7 cm^{-1} indicated the N-H vibration of hydrazine functional group on **Naph-NH₂**. Moreover, the broad peak characteristic in a range of 3000-3500 cm^{-1} and the sharp peak at 1577.0 cm^{-1} was possibly assigned to the O-H stretching vibration of hydroxy group and carbonyl group on **Gel 1**, respectively. The CH₂ bending of **NH₂/CTAB/S2@Gel 1** was observed as the peak around 1422.7 cm^{-1} corresponding to the **Gel 1**. These results proved that **Naph-NH₂/CTAB/S2** was penetrated to the supramolecular **Gel 1**.

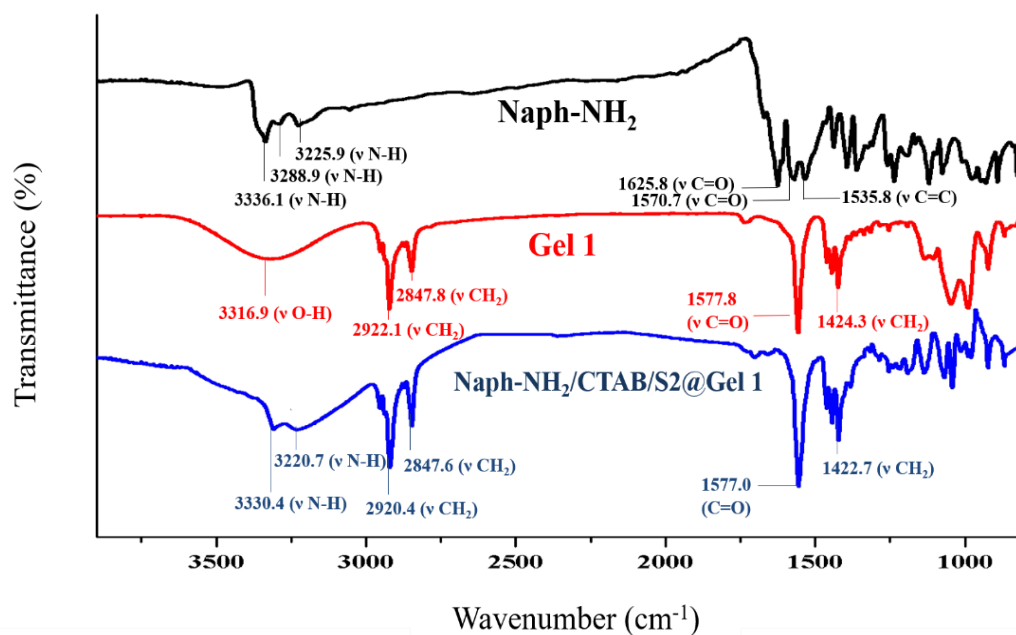


Figure 3.38 FT-IR spectra of **Naph-NH₂** (black line), **Gel 1** (red line) and **Naph-NH₂/CTAB/S2@Gel 1** (blue line)

3.15.3 Optical property of Naph-NH₂/CTAB/S2@Gel 1

To further verify the optical property of hybrid material, **Naph-NH₂/CTAB/S2@Gel 1** was examined compared to **Naph-NH₂/CTAB/S2**, as shown in Figure 3.40. The fluorescence spectra were collected upon an excitation of 445 nm in 60% DMSO/PBS buffer pH 7.4. Compared to **Naph-NH₂/CTAB/S2**, the maximum emission band of **Naph-NH₂/CTAB/S2@Gel 1** platform was significantly enhanced. Moreover, the sensing ability of **Naph-NH₂/CTAB/S2** and **Naph-NH₂/CTAB/S2@Gel 1** towards heptanal was also investigated. Heptanal enabled to react to hydrazine group in **Naph-NH₂/CTAB/S2** inducing the complete micellar platform and a significant increase of fluorescence intensity with a concomitant red-shift emission band of sensing platform after penetrating in gel. This result is analog to **Naph-NH₂/CTAB/S2** upon the addition of heptanal. Remark increase of fluorescence intensity of **Naph-NH₂/CTAB/S2@Gel 1** \subset heptanal can be possibly described that; i) heptanal interacted with **Naph-NH₂/CTAB/S2** also promoted the well-organized gel formation. ii) the fluorophore in gel is likely to be rigid reducing the energy loss from rotation.

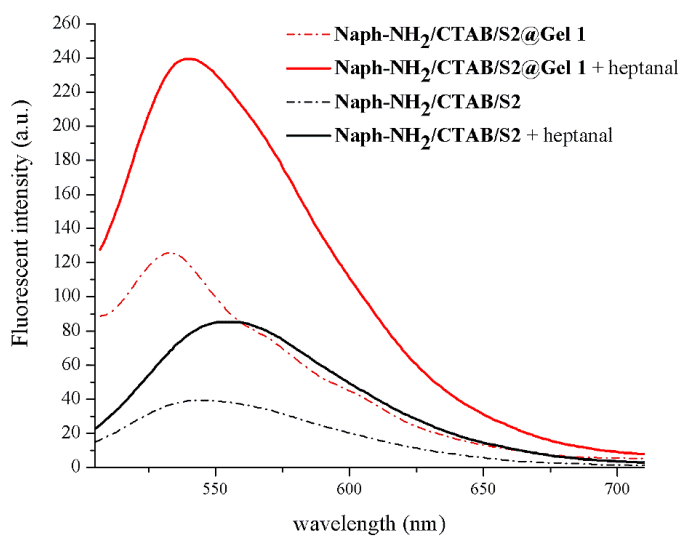


Figure 3.39 Fluorescence spectra of **Naph-NH₂/CTAB/S2@Gel 1** (red line) and **Naph-NH₂/CTAB/S2** (black line) in the absence (dash line) and in the presence (solid line) of 0.05 mM heptanal ($\lambda_{\text{ex}} = 445 \text{ nm}$).

With the good gelation properties of our platform, we have investigated a great deal of sensing application of **Naph-NH₂/CTAB/S2@Gel 1** for long-chain aldehyde detection. The results demonstrated the strong fluorescent intensity by **NH₂/CTAB/S2@Gel 1** upon the addition of 0.05 mM heptanal (Figure 3.40(a)). Compared to **Naph-NH₂/CTAB/S2@Gel 1** platform, other platform with and without heptanal in hydrogel displayed the weak emission band. In comparison, the **Naph-NH₂/CTAB/S2@Gel 1** platform and **Naph-NH₂/CTAB/S2** micellar platform with heptanal addition presented the significantly different fluorescence responses. The observation of high fluorescent intensity in hydrogel system offered an advantageously promising sensitivity for sensing approach by **Naph-NH₂/CTAB/S2@Gel 1** micellar platform. Hence, these findings could confirm that the gel system enables to improve the sensitivity of **Naph-NH₂/CTAB/S2** micellar sensor for long-chain aldehyde detection.

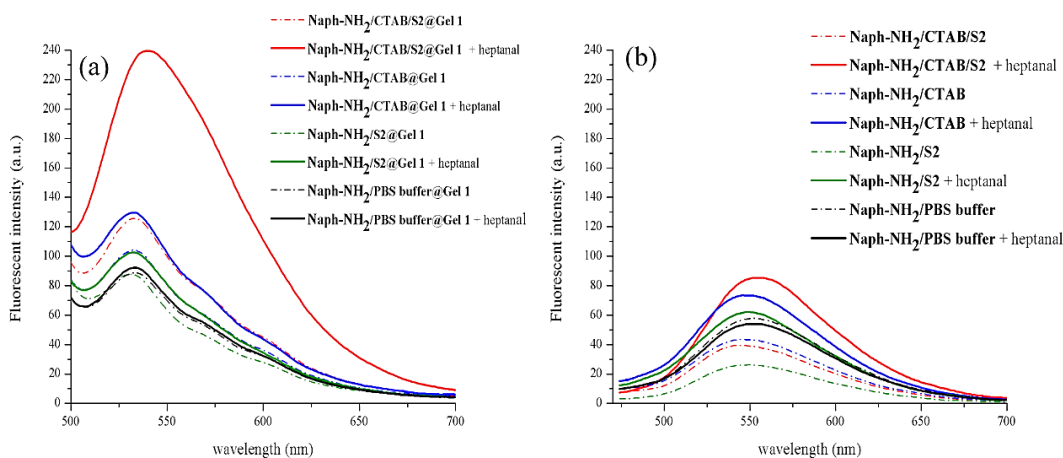


Figure 3.40 Fluorescence spectra of **Naph-NH₂/CTAB/S2@Gel 1** (a) and **Naph-NH₂/CTAB/S2** (b) ($\lambda_{\text{ex}} = 445 \text{ nm}$). (1.94 wt % **Gel 1** in 60% DMSO/PBS buffer pH 7.4)

3.15.4 Kinetic studies of **Naph-NH₂/CTAB/S2@Gel 1** for long-chain detection

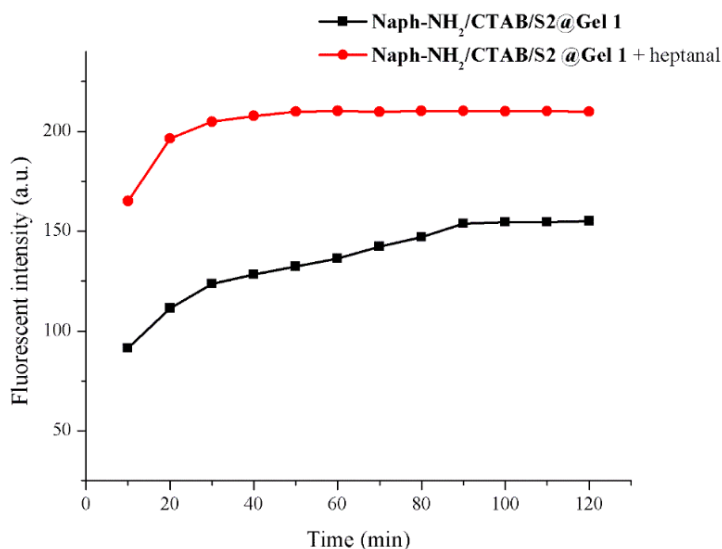


Figure 3.41 The kinetic profiles of **Naph-NH₂/CTAB/S2@Gel 1** in the absence (black line) and in the presence (red line) of 0.05 mM heptanal. (1.94 wt % **Gel 1** in 60% DMSO/PBS buffer pH 7.4)

With a kinetically interaction study of **Naph-NH₂/CTAB/S2@Gel 1** for long-chain aldehyde detection, the mixture solution of **Naph-NH₂/CTAB/S2** and heptanal was stirred for 20 min in 60% DMSO/PBS buffer pH 7.4. The **Gel 1** was added to the mixture solution to self-assembly organize the 3D-fibrous network. The fluorescence intensity at 535 nm was monitored under excitation wavelength of 445 nm. As illustrated in Figure 3.41, the emission intensity of **Naph-NH₂/CTAB/S2@Gel 1** in the presence of heptanal was gradually increased until 20 min. In contrast, the case of sensor material without heptanal showed the gradually change of fluorescence response until 80 min. These results suggested that heptanal was induced into **Naph-NH₂/CTAB/S2** micelle promoting the complete micelle and a well-organized gel formation with a regard of a significant fluorescent enhancement.

3.15.5 Determination of long-chain aldehydes using **Naph-NH₂/CTAB/S2@Gel 1**

To further determine the amounts of long-chain aldehydes using **Naph-NH₂/CTAB/S2@Gel 1**, the fluorescent titrations of **Naph-NH₂/CTAB/S2@Gel 1** and long-chain aldehydes were carried out in 60% DMSO/PBS buffer pH 7.4. From Figure 3.41, the fluorescent intensity of sensing platform in hydrogel was gradually increased in a proportional of the amount of long-chain aldehyde. For quantitative application, the limit of detection (LOD) and limit of quantification (LOQ) were calculated by method validation procedure using equation 4.1 and equation 4.2, respectively. The standard derivation (SD) of baselines was calculated by monitoring the blank signal in 10 times. The fluorescence intensity at 535 nm in the absence and presence of heptanal was set as I and I_0 , respectively. The standard calibration curve was plotted between I/I_0 values and various concentrations of long-chain aldehydes. In case of experimental approach, **Naph-NH₂/CTAB/S2** material was carried out as fluorescent probe for long-chain aldehydes. During the reaction of **Naph-NH₂/CTAB/S2** sensor and heptanal for 20 min, the **Gel 1** was added to the mixture reaction and was diluted by 60% DMSO/PBS buffer pH 7.4. The mixture was kept to stand for organizing 3D fibrous gel for 10 min before measuring the fluorescence spectra ($\lambda_{ex} = 445$ nm).

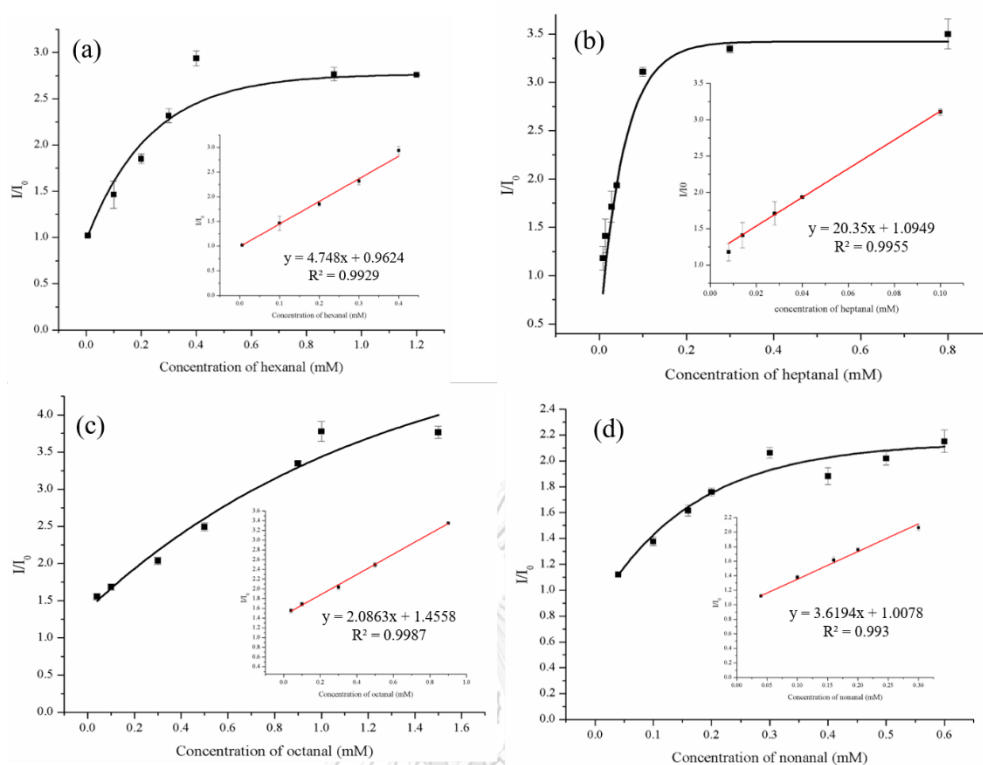


Figure 3.42 Fluorescent titration curves of **Naph-NH₂/CTAB/S2@Gel 1** toward hexanal (a), heptanal (b), octanal (c) and nonanal (d) under condition of 60% DMSO/PBS buffer pH 7.4 (1.94 wt % **Gel 1**, $\lambda_{\text{ex}} = 445 \text{ nm}$).

As shown in Figure 3.42, the amounts of long-chain aldehydes; including hexanal, heptanal, octanal and nonanal were proportional to I/I_0 values. The limit of detection (LOD) and limit of quantification (LOQ) of **Naph-NH₂/CTAB/S2@Gel 1** for long-chain aldehyde sensing was collected. These results indicated that both LOD and LOQ values of **Naph-NH₂/CTAB/S2@Gel 1** provided more efficient values with broader linear range than **Naph-NH₂/CTAB/S2** micelle platform. Moreover, the %recovery of sensing aspect of **Naph-NH₂/CTAB/S2@Gel 1** towards long-chain aldehyde demonstrated the range of 93.40-101.92 which was acceptable for sensing application. It was suggested that gel-like system encouraged the sensing approach of **Naph-NH₂/CTAB/S2** micellar platform. Taking on a broad from the improvement of sensitivity in gel-like system, the **Naph-NH₂/CTAB/S2@Gel 1** served as a potential sensing platform for diagnosis treatment of lung cancer disease.

Table 3.10 limit of detection (LOD) and limit of quantification (LOQ) for long-chain aldehyde detection of **Naph-NH₂/CTAB/S2@Gel 1** in 60% DMSO/PBS buffer pH 7.4

Entry	Long-chain aldehydes	Linear range (mM)	Equation	R ²	LOD (μM)	LOQ (μM)
1	hexanal	0.005-0.33	Y = 4.748X+0.9624	0.9929	7.48	24.94
2	heptanal	0.008-0.10	Y = 20.300X+1.0949	0.9953	7.59	25.32
3	octanal	0.03-0.75	Y = 2.0863X+1.4558	0.9987	13.61	45.37
4	nonanal	0.03-0.25	Y = 3.6194X+1.0078	0.9930	21.69	72.28

Table 3.11 Percent recovery for long-chain aldehyde detection by **Naph-NH₂/CTAB/S2@Gel 1**

Entry	Long-chain aldehydes	Concentration (added)	% recovery ± SD
1	hexanal	0.07 mM	93.40 ± 0.73
		0.28 mM	101.91 ± 1.39
2	heptanal	0.02 mM	101.92 ± 1.57
		0.036 mM	95.01 ± 0.41
3	octanal	0.09 mM	98.80 ± 1.84
		0.30 mM	99.65 ± 7.15
4	nonanal	0.12 mM	96.17 ± 2.62
		0.26 mM	97.19 ± 0.64

3.15.6 The selectivity of Naph-NH₂/CTAB/S2@Gel 1 toward long-chain aldehyde

To study the selectivity of Naph-NH₂/CTAB/S2@Gel, the organic compounds which are actually found in exhale breath of lung cancer patients [65-73] including formaldehyde, propanal, butanal, pentanal, hexanal, heptanal, octanal, nonanal, acetone, benzaldehyde, 4-hydroxybenzaldehyde, 3-nitrobenzaldehyde, xylene, cyclohexane, benzene, heptane, phenol, toluene, acetonitrile, cysteine, homocysteine, glutathione, and ascorbic acid were also examined. As illustrated in Figure 3.43, the relative fluorescent intensity (I/I_0) was enhanced in the presence of hexanal, heptanal, octanal and nonanal. Interestingly, the Naph-NH₂/CTAB/S2@Gel 1 gives a good selectivity toward long-chain aldehydes.

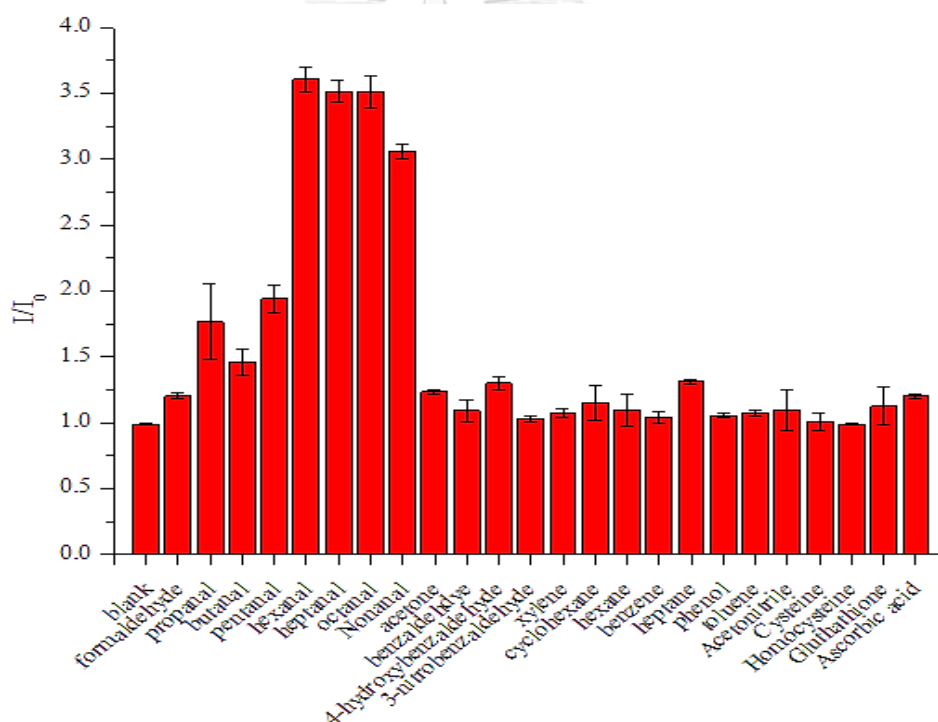


Figure 3.43 Fluorescence response at 542 nm Naph-NH₂/CTAB/S2@Gel micellar toward organic compounds which were found in breath of lung cancer patients. (60% DMSO/PBS buffer pH 7.4 (1.94 wt %, Gel 1, λ_{ex} = 445 nm).

Therefore, Naph-NH₂/CTAB/S2@Gel 1 material served as a promising sensitivity and selectivity for long-chain aldehyde detection and also highlighted a high effective optical sensing approach for biomedical application.

CHAPTER IV

Conclusion

With the selective recognition of long-chain aldehyde compounds; hexanal, heptanal, octanal, and nonanal, which were regarded as a biomarker of lung cancer disease and an indicator of fat-oil products, we have successfully developed the novel micellar sensor for long-chain aldehydes discrimination by using fluorescence spectroscopy. In this research, the fluorescent micellar probes toward long-chain aldehydes have been achieved in the concept of long-chain aldehyde are induced-fit compound to incorporate the complete micelle-like particles which give a fluorescent change of dye-doped nanomicelle. The incomplete micelle was prepared by cationic surfactant (CTAB) and co-surfactant (S2) in the concentration ratio of 1:0.83. The hydrazine functionalized fluorescent dye (**Naph-NH₂**) was encapsulated in incomplete nanomicelle. After introduction of aldehydes as a target molecule, long-chain would be induced into the core of micelle via hydrophobic effect and also interacted with hydrazine functional group of **Naph-NH₂**. Subsequently, the complete self-assembly micelle-like aggregation was achieved and promoted the good entrapment of fluorescent dye (**Naph-NH₂**) resulting in the fluorescent enhancement by aggregation. This sensing platform served as a high selectivity of self-assembling micellar sensor toward long-chain aldehydes over other organic compounds especially formaldehyde. Importantly, the fluorescent enhancement of dye-doped micelle is proportional to the amounts of long-chain aldehyde added under the reaction time of 20 min in PBS buffer pH 7.4. Moreover, the quantitative analysis of this system toward long-chain aldehyde such as hexanal, heptanal, octanal, and nonanal offered the limit of detection (LOD) of 74.38, 80.38, 80.98 and 64.09 μM , respectively. Interestingly, **Naph-NH₂/CTAB/S2** is capable of detecting of long-chain aldehydes such as heptanal in blood sample by using the standard addition method with percent recovery in a range of 94.01-102.4 which is acceptable for sensing application. Hence, the **Naph-NH₂/CTAB/S2** platform served as a medical application for diagnosis disease. Furthermore, the **Naph-NH₂/CTAB/S2** showed an excellent intracellular uptake with a strong green fluorescence in pulmonary lung cancer cell (A549), which applied for cell imaging and promising in further biological imaging applications. To improve the sensitivity of this micellar sensing

platform, the supramolecular hydrogel network was an excellent alternative material for improvement of sensitivity of nanomicelle. The sucrose laurate monoester (**Gel 1**) containing the sucrose and octane hydrocarbon chain was used as gelator for long-chain aldehyde approach. The **Naph-NH₂/CTAB/S2@Gel 1** under the optimal condition of 1.94 wt% in 2.5% DMSO/ PBS buffer pH 7.4. successfully developed in approximately 10-fold improved sensitivity with LOD of 7.48, 7.59, 13.61 and 21.69 μM , respectively. Consequently, this **Naph-NH₂/CTAB/S2** fluorescent micellar platform offers the promising selective determination of the long-chain aldehyde detection and a benefit for easy checking in real samples.



REFERENCES

- [1] Lehn, J.-M. Perspectives in Supramolecular Chemistry—From Molecular Recognition towards Molecular Information Processing and Self-Organization. Angewandte Chemie International Edition in English 29(11) (1990): 1304-1319.
- [2] Balzani, V., Gómez-López, M., and Stoddart, J.F. Molecular Machines. Accounts of Chemical Research 31(7) (1998): 405-414.
- [3] Ikeda, T. and Stoddart, J.F. Electrochromic materials using mechanically interlocked molecules. Science and Technology of Advanced Materials 9(1) (2008): 014104.
- [4] Zhang, S. Fabrication of novel biomaterials through molecular self-assembly. Nature Biotechnology 21 (2003): 1171.
- [5] L Dickert, F. and Hayden, O. Molecular imprinting in chemical sensing. Vol. 18, 1999.
- [6] Lehn, J.-M. From Molecular to Supramolecular Chemistry. in Supramolecular Chemistry, pp. 1-9: Wiley-VCH Verlag GmbH & Co. KGaA, 2006.
- [7] Parkin, I.P. Supramolecular chemistry. J.W. Steed and J.L. Atwood. John Wiley & Sons Ltd., Applied Organometallic Chemistry 15(3) (2001): 236-236.
- [8] Liu, T., Han, L.-L., Du, C.-M., and Yu, Z.-Y. Redox potentials of dopamine and its supramolecular complex with aspartic acid. Russian Journal of Physical Chemistry A 88(7) (2014): 1085-1090.
- [9] Wang, K., Yang, X., and Yang, R. Optical chemical sensors based on supramolecular chemistry. Sensors and Actuators B: Chemical 66(1) (2000): 263-265.
- [10] Resendiz, M.J.E., Noveron, J.C., Disteldorf, H., Fischer, S., and Stang, P.J. A Self-Assembled Supramolecular Optical Sensor for Ni(II), Cd(II), and Cr(III). Organic Letters 6(5) (2004): 651-653.
- [11] Chen, Z., Wang, Q., Wu, X., Li, Z., and Jiang, Y.-B. Optical chirality sensing using macrocycles, synthetic and supramolecular oligomers/polymers, and nanoparticle based sensors. Chemical Society Reviews 44(13) (2015): 4249-4263.
- [12] Dsouza, R.N., Pischel, U., and Nau, W.M. Fluorescent Dyes and Their Supramolecular Host/Guest Complexes with Macrocycles in Aqueous Solution. Chemical Reviews 111(12) (2011): 7941-7980.
- [13] Siraj, N., et al. Fluorescence, Phosphorescence, and Chemiluminescence. Analytical Chemistry 88(1) (2016): 170-202.
- [14] Rabinowitch, E. Fluorescence and phosphorescence. Journal of Chemical Education 28(8) (1951): 446.
- [15] McGlynn, S.P. Fluorescence and Phosphorescence Analysis. Principles and Applications. Journal of the American Chemical Society 88(23) (1966): 5688-5688.
- [16] Diamandis, E.P. Fluorescence Spectroscopy. Analytical Chemistry 65(12) (1993): 454-459.
- [17] Ellis, D.W. Fluorescence theory, instrumentation, and practice (Guilbault, George G., ed). Journal of Chemical Education 45(5) (1968): A442.

- [18] Baryshnikov, G., Minaev, B., and Ågren, H. Theory and Calculation of the Phosphorescence Phenomenon. Chemical Reviews 117(9) (2017): 6500-6537.
- [19] Kappaun, S., Slugovc, C., and List, E.J.W. Phosphorescent Organic Light-Emitting Devices: Working Principle and Iridium Based Emitter Materials. International Journal of Molecular Sciences 9(8) (2008): 1527-1547.
- [20] Minaev, B., Baryshnikov, G., and Agren, H. Principles of phosphorescent organic light emitting devices. Physical Chemistry Chemical Physics 16(5) (2014): 1719-1758.
- [21] Wasielewski, M.R. Photoinduced electron transfer in supramolecular systems for artificial photosynthesis. Chemical Reviews 92(3) (1992): 435-461.
- [22] de Silva, A.P., Moody, T.S., and Wright, G.D. Fluorescent PET (Photoinduced Electron Transfer) sensors as potent analytical tools. Analyst 134(12) (2009): 2385-2393.
- [23] Talelli, M., Barz, M., Rijcken, C.J.F., Kiessling, F., Hennink, W.E., and Lammers, T. Core-crosslinked polymeric micelles: Principles, preparation, biomedical applications and clinical translation. Nano Today 10(1) (2015): 93-117.
- [24] Tanford, C. Theory of micelle formation in aqueous solutions. The Journal of Physical Chemistry 78(24) (1974): 2469-2479.
- [25] Maibaum, L., Dinner, A.R., and Chandler, D. Micelle Formation and the Hydrophobic Effect. The Journal of Physical Chemistry B 108(21) (2004): 6778-6781.
- [26] Wang, L., et al. Modeling micelle formation and interfacial properties with iSAFT classical density functional theory. The Journal of Chemical Physics 146(12) (2017): 124705.
- [27] Petcu, A.R., Rogozea, E.A., Lazar, C.A., Olteanu, N.L., Meghea, A., and Mihaly, M. Specific interactions within micelle microenvironment in different charged dye/surfactant systems. Arabian Journal of Chemistry 9(1) (2016): 9-17.
- [28] Dominguez, A., Fernandez, A., Gonzalez, N., Iglesias, E., and Montenegro, L. Determination of Critical Micelle Concentration of Some Surfactants by Three Techniques. Journal of Chemical Education 74(10) (1997): 1227.
- [29] Santos, M.S., Tavares, F.W., and Biscaia Jr, E.C. Molecular Thermodynamics of micellization: Micelle size distribution and geometry transitions. Brazilian Journal of Chemical Engineering 33 (2016): 515-523.
- [30] Fisicaro, E., Compari, C., Duce, E., Biemmi, M., Peroni, M., and Braibanti, A. Thermodynamics of micelle formation in water, hydrophobic processes and surfactant self-assemblies. Physical Chemistry Chemical Physics 10(26) (2008): 3903-3914.
- [31] Ambrose, R.J. Surfactants and interfacial phenomena—second edition, by Milton J. Rosen, John Wiley & Sons, 1989, 431 Journal of Polymer Science Part C: Polymer Letters 27(12) (1989): 503-503.
- [32] Bag, S.S. and Kundu, R. Sensing of micellar microenvironment with dual fluorescent probe, triazolylpyrene (TNDMBPy). Journal of fluorescence 23(5) (2013): 929-938.
- [33] Ding, L., Bai, Y., Cao, Y., Ren, G., Blanchard, G.J., and Fang, Y. Micelle-Induced Versatile Sensing Behavior of Bispyrene-Based Fluorescent Molecular Sensor for Picric Acid and PYX Explosives. Langmuir 30(26) (2014): 7645-7653.

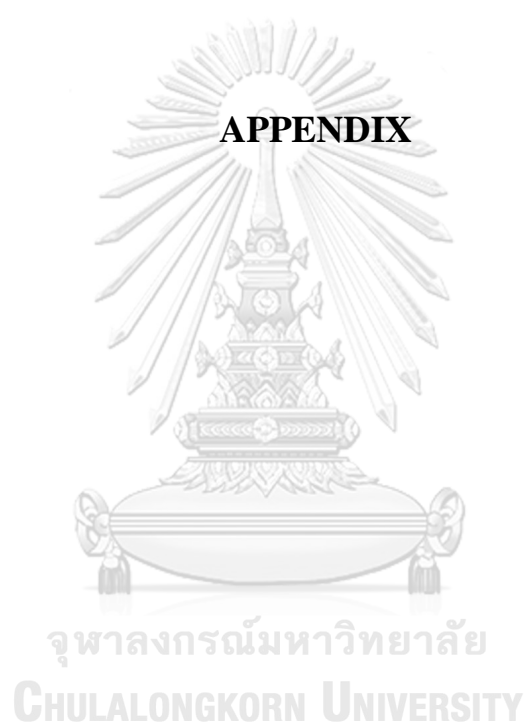
- [34] Alai, M.S., Lin, W.J., and Pingale, S.S. Application of polymeric nanoparticles and micelles in insulin oral delivery. Journal of Food and Drug Analysis 23(3) (2015): 351-358.
- [35] Su, F., et al. Nanostructured Oxygen Sensor - Using Micelles to Incorporate a Hydrophobic Platinum Porphyrin. PLOS ONE 7(3) (2012): 33390.
- [36] Ahmed, E.M. Hydrogel: Preparation, characterization, and applications: A review. Journal of Advanced Research 6(2) (2015): 105-121.
- [37] Ibrahim, M.M., Hafez, S.A., and Mahdy, M.M. Organogels, hydrogels and bigels as transdermal delivery systems for diltiazem hydrochloride. Asian Journal of Pharmaceutical Sciences 8(1) (2013): 48-57.
- [38] Satapathy, S., et al. Development and characterization of gelatin-based hydrogels, emulsion hydrogels, and bigels: A comparative study. Journal of Applied Polymer Science 132(8) (2015).
- [39] Elharfaoui, N., Djabourov, M., and Babel, W. Molecular Weight Influence on Gelatin Gels: Structure, Enthalpy and Rheology. Macromolecular Symposia 256(1) (2007): 149-157.
- [40] Ozlem Dilek, S.L.B. Turn on Fluorescent Probes for Selective Targeting of Aldehydes. Chemosensors 4(1)(5) (2016): 4010005.
- [41] Aksornneam, L., Kanatharana, P., Thavarungkul, P., and Thammakhet, C. 5-Aminofluorescein doped polyvinyl alcohol film for the detection of formaldehyde in vegetables and seafood. Analytical Methods 8(6) (2016): 1249-1256.
- [42] Song, X., Han, X., Yu, F., Zhang, J., Chen, L., and Lv, C. A reversible fluorescent probe based on C=N isomerization for the selective detection of formaldehyde in living cells and in vivo. Analyst 143(2) (2018): 429-439.
- [43] Tang, Y., Kong, X., Liu, Z.-R., Xu, A., and Lin, W. Lysosome-Targeted Turn-On Fluorescent Probe for Endogenous Formaldehyde in Living Cells. Analytical Chemistry 88(19) (2016): 9359-9363.
- [44] Mukherjee, K., et al. Benzocoumarin Hydrazine: A Large Stokes Shift Fluorogenic Sensor for Detecting Carbonyls in Isolated Biomolecules and in Live Cells. ACS Sensors 2(1) (2017): 128-134.
- [45] Tian, H., Qian, J., Bai, H., Sun, Q., Zhang, L., and Zhang, W. Micelle-induced multiple performance improvement of fluorescent probes for H₂S detection. Analytica Chimica Acta 768 (2013): 136-142.
- [46] Miki, R., et al. Glucose Responsive Rheological Change and Drug Release from a Novel Worm-like Micelle Gel Formed in Cetyltrimethylammonium Bromide/Phenylboronic Acid/Water System. Molecular Pharmaceutics 15(3) (2018): 1097-1104.
- [47] Wang, T., et al. Ultrasound accelerated sugar based gel for in situ construction of a Eu³⁺-based metallogel via energy transfer in a supramolecular scaffold. RSC Advances 5(130) (2015): 107694-107699.
- [48] Cao, X., et al. Strong Blue Emissive Supramolecular Self-Assembly System Based on Naphthalimide Derivatives and Its Ability of Detection and Removal of 2,4,6-Trinitrophenol. Langmuir 33(31) (2017): 7788-7798.
- [49] Wada, A., Tamaru, S.-i., Ikeda, M., and Hamachi, I. MCM-Enzyme-Supramolecular Hydrogel Hybrid as a Fluorescence Sensing Material for Polyanions of Biological Significance. Journal of the American Chemical Society 131(14) (2009): 5321-5330.

- [50] Cano, M.E., Di Chenna, P.H., Lesur, D., Wolosiuk, A., Kovensky, J., and Uhrig, M.L. Chirality inversion, supramolecular hydrogelation and lectin binding of two thiolactose amphiphiles constructed on a di-lauroyl-1-tartaric acid scaffold. New Journal of Chemistry 41(23) (2017): 14754-14765.
- [51] Clemente, M.J., Tejedor, R.M., Romero, P., Fitremann, J., and Oriol, L. Maltose-based gelators having azobenzene as light-sensitive unit. RSC Advances 2(30) (2012): 11419-11431.
- [52] Sun, J., Wang, B., Zhao, X., Li, Z.-J., and Yang, X. Fluorescent and Colorimetric Dual-Readout Assay for Inorganic Pyrophosphatase with Cu²⁺-Triggered Oxidation of o-Phenylenediamine. Analytical Chemistry 88(2) (2016): 1355-1361.
- [53] Hakim, M., et al. Volatile Organic Compounds of Lung Cancer and Possible Biochemical Pathways. Chemical Reviews 112(11) (2012): 5949-5966.
- [54] Toyokuni, S., Okamoto, K., Yodoi, J., and Hiai, H. Persistent oxidative stress in cancer. FEBS Letters 358(1) (1995): 1-3.
- [55] Fuchs, P., Loeseken, C., Schubert, J.K., and Miekisch, W. Breath gas aldehydes as biomarkers of lung cancer. International Journal of Cancer 126(11) (2010): 2663-2670.
- [56] Corradi, M., et al. Aldehydes in Exhaled Breath Condensate of Patients with Chronic Obstructive Pulmonary Disease. American Journal of Respiratory and Critical Care Medicine 167(10) (2003): 1380-1386.
- [57] Del Rio, D., Stewart, A.J., and Pellegrini, N. A review of recent studies on malondialdehyde as toxic molecule and biological marker of oxidative stress. Nutrition, Metabolism and Cardiovascular Diseases 15(4) (2005): 316-328.
- [58] Shahidi, F. and Pegg, R.B. Hexanal as an Indicator of the Flavor Deterioration of Meat and Meat Products. in Lipids in Food Flavors, pp. 256-279: American Chemical Society, 1994.
- [59] Ribeiro-Santos, R., et al. Whey protein active films incorporated with a blend of essential oils: Characterization and effectiveness. Packaging Technology and Science 31(1) (2018): 27-40.
- [60] Khattar, R., Yadav, A., and Mathur, P. Copper(II) complexes as catalyst for the aerobic oxidation of o-phenylenediamine to 2,3-diaminophenazine. Spectrochimica Acta Part A: Molecular and Biomolecular Spectroscopy 142 (2015): 375-381.
- [61] O'Neil and (ed.), M.J. The Merck Index An Encyclopedia of Chemicals, Drugs, and Biologicals (2013): 593.
- [62] Hutchins, R.O. and Hutchins, M.K. 1.14 - Reduction of CX to CH₂ by Wolff-Kishner and Other Hydrazone Methods. in Trost, B.M. and Fleming, I. (eds.), Comprehensive Organic Synthesis, pp. 327-362. Oxford: Pergamon, 1991.
- [63] Macedo, E.R., De Boni, L., Misoguti, L., Mendonça, C.R., and de Oliveira, H.P. Dye aggregation and influence of pre-micelles on heterogeneous catalysis: A photophysical approach. Colloids and Surfaces A: Physicochemical and Engineering Aspects 392(1) (2011): 76-82.
- [64] Gopikrishna, P., Meher, N., and Iyer, P.K. Functional 1,8-Naphthalimide AIE/AIEEgens: Recent Advances and Prospects. ACS Applied Materials & Interfaces 10(15) (2018): 12081-12111.

- [65] Liu, C., et al. Nanomolar fluorescent quantitative detection of formaldehyde with a 8-hydroxyquinoline derivative in aqueous solution and electrospun nanofibers. Sensors and Actuators B: Chemical 219(Supplement C) (2015): 185-191.
- [66] Sayer, J.M., Pinsky, B., Schonbrunn, A., and Washtien, W. Mechanism of carbinolamine formation. Journal of the American Chemical Society 96(26) (1974): 7998-8009.
- [67] Lim, J.H., Park, J., Oh, E.H., Ko, H.J., Hong, S., and Park, T.H. Nanovesicle-Based Bioelectronic Nose for the Diagnosis of Lung Cancer from Human Blood. Advanced Healthcare Materials 3(3) (2014): 360-366.
- [68] Filipiak, W., et al. TD-GC-MS Analysis of Volatile Metabolites of Human Lung Cancer and Normal Cells Cancer Epidemiology Biomarkers & Prevention 19(1) (2010): 182-195.
- [69] Schmidt, K. and Podmore, I. Current Challenges in Volatile Organic Compounds Analysis as Potential Biomarkers of Cancer. Journal of Biomarkers 2015 (2015): 16.
- [70] Zhou, J., Huang, Z.-A., Kumar, U., and Chen, D.D.Y. Review of recent developments in determining volatile organic compounds in exhaled breath as biomarkers for lung cancer diagnosis. Analytica Chimica Acta 996 (2017): 1-9.
- [71] Deng, C., Zhang, X., and Li, N. Investigation of volatile biomarkers in lung cancer blood using solid-phase microextraction and capillary gas chromatography–mass spectrometry. Journal of Chromatography B 808(2) (2004): 269-277.
- [72] Li, J., et al. Investigation of potential breath biomarkers for the early diagnosis of breast cancer using gas chromatography–mass spectrometry. Clinica Chimica Acta 436 (2014): 59-67.
- [73] Yazdanpanah, M., Luo, X., Lau, R., Greenberg, M., Fisher, L.J., and Lehotay, D.C. Cytotoxic Aldehydes as Possible Markers for Childhood Cancer. Free Radical Biology and Medicine 23(6) (1997): 870-878.
- [74] Peter, J.M. Exhaled breath volatile organic compound biomarkers in lung cancer. Journal of Breath Research 6(2) (2012): 027106.
- [75] Sakumura, Y., et al. Diagnosis by Volatile Organic Compounds in Exhaled Breath from Lung Cancer Patients Using Support Vector Machine Algorithm. Sensors (Basel, Switzerland) 17(2) (2017): 287.
- [76] Song, M.-K., Choi, H.-S., Lee, H.-S., and Ryu, J.-C. Transcriptome Profile Analysis of Saturated Aliphatic Aldehydes Reveals Carbon Number-Specific Molecules Involved in Pulmonary Toxicity. Chemical Research in Toxicology 27(8) (2014): 1362-1370.
- [77] Liang, H., et al. Co-immobilization of multiple enzymes by metal coordinated nucleotide hydrogel nanofibers: improved stability and an enzyme cascade for glucose detection. Nanoscale 8(11) (2016): 6071-6078.
- [78] Ulijn, R.V. and Smith, A.M. Designing peptide based nanomaterials. Chemical Society Reviews 37(4) (2008): 664-675.
- [79] Weiss, R.G. The Past, Present, and Future of Molecular Gels. What Is the Status of the Field, and Where Is It Going? Journal of the American Chemical Society 136(21) (2014): 7519-7530.
- [80] Estroff, L.A. and Hamilton, A.D. Water Gelation by Small Organic Molecules. Chemical Reviews 104(3) (2004): 1201-1218.

- [81] Mangunuru, H.P.R., Yerabolu, J.R., and Wang, G. Synthesis and study of N-acetyl d-glucosamine triazole derivatives as effective low molecular weight gelators. Tetrahedron Letters 56(23) (2015): 3361-3364.





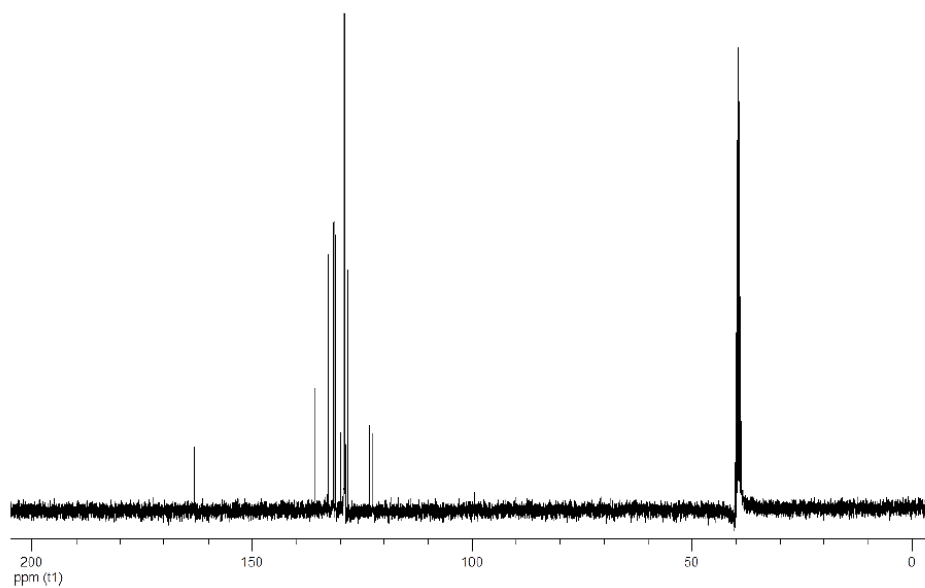


Figure A1 The ^{13}C -NMR spectrum of **1** in d_6 -DMSO at 100 MHz

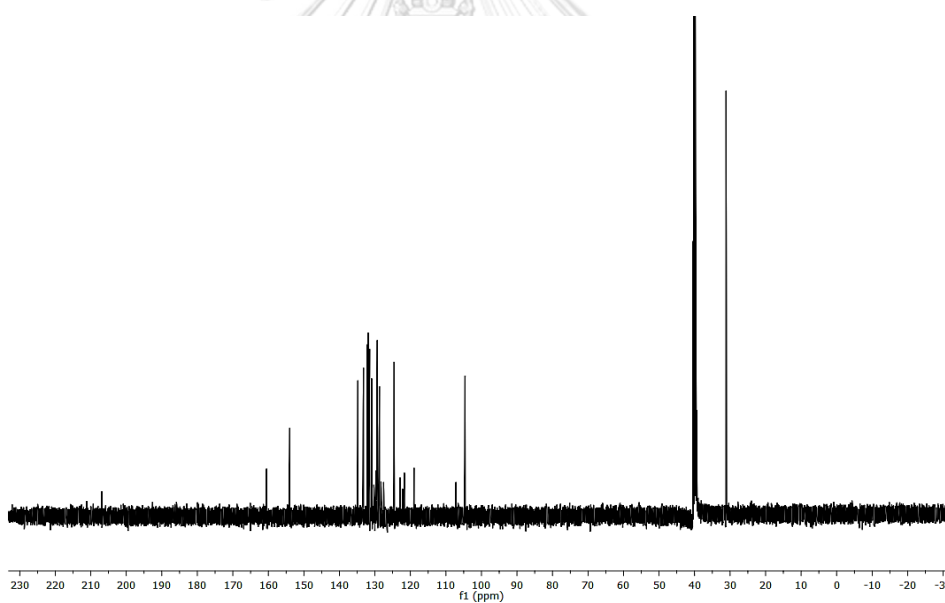


Figure A2 The ^{13}C -NMR spectrum of **Naph-NH₂** in d_6 -DMSO at 100 MHz

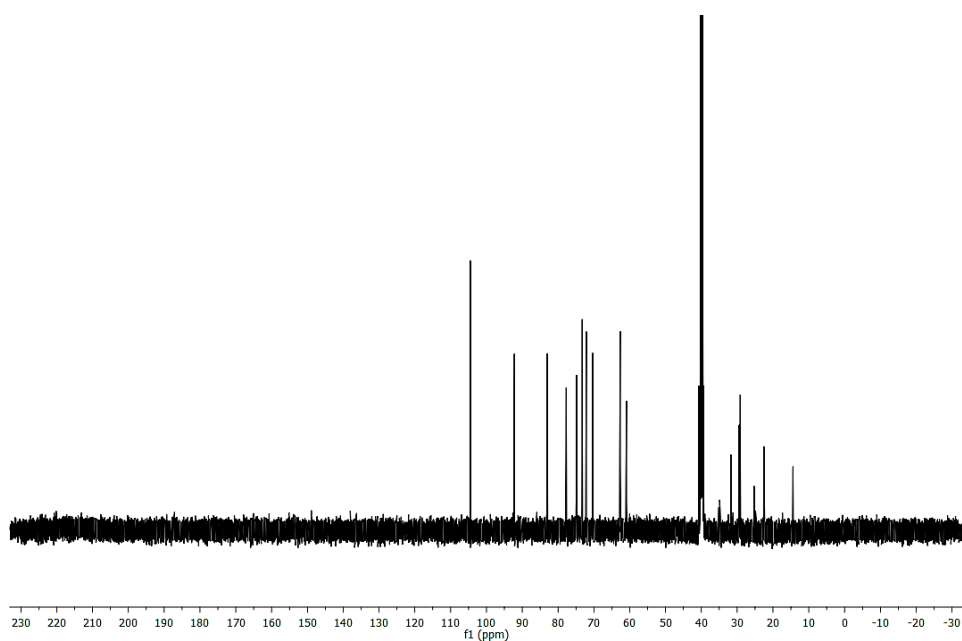


Figure A3 The ^{13}C -NMR spectrum of **SL** in d_6 -DMSO at 100 MHz

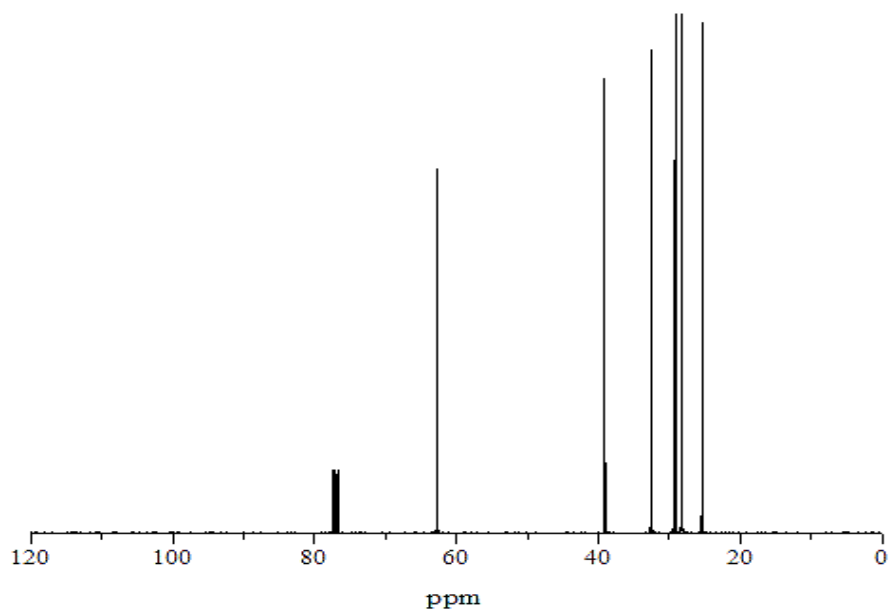


Figure A4 The ^{13}C -NMR spectrum of **S2** in d_6 -CDCl₃ at 100 MHz

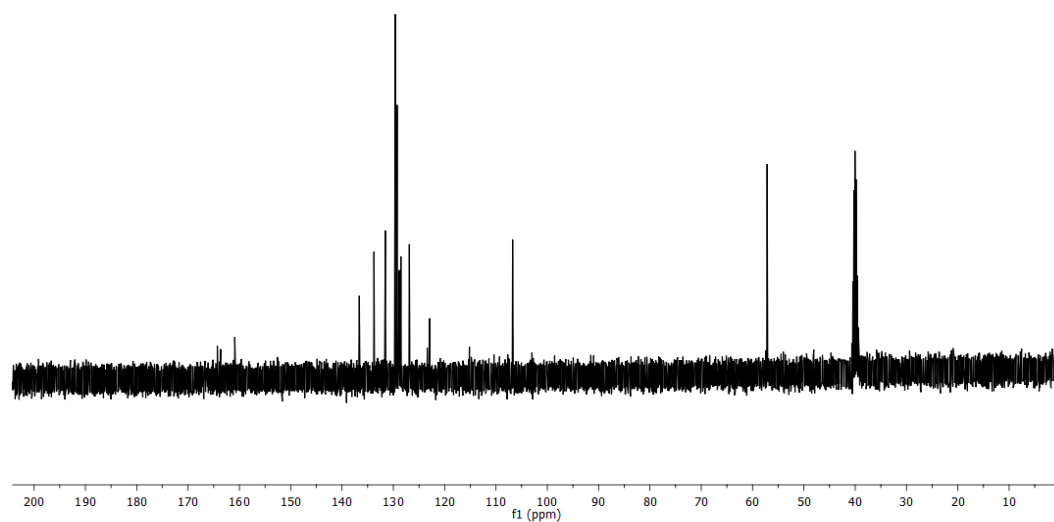


Figure A5 The ^{13}C -NMR spectrum of **Naph-OMe** in $d_6\text{-CDCl}_3$ at 100 MHz

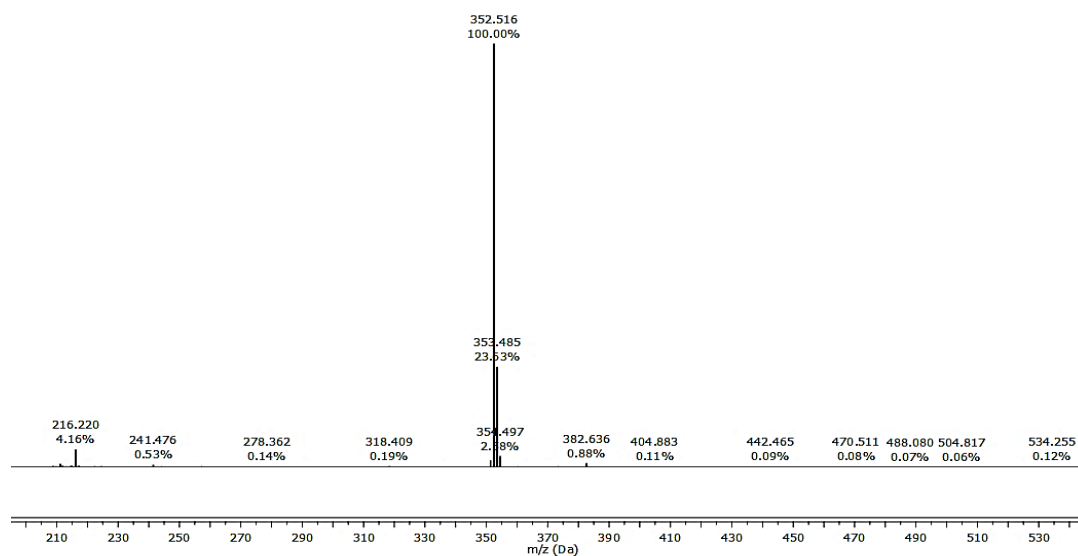


Figure A6 The mass spectrum spectrum of **1** at m/z 352.52

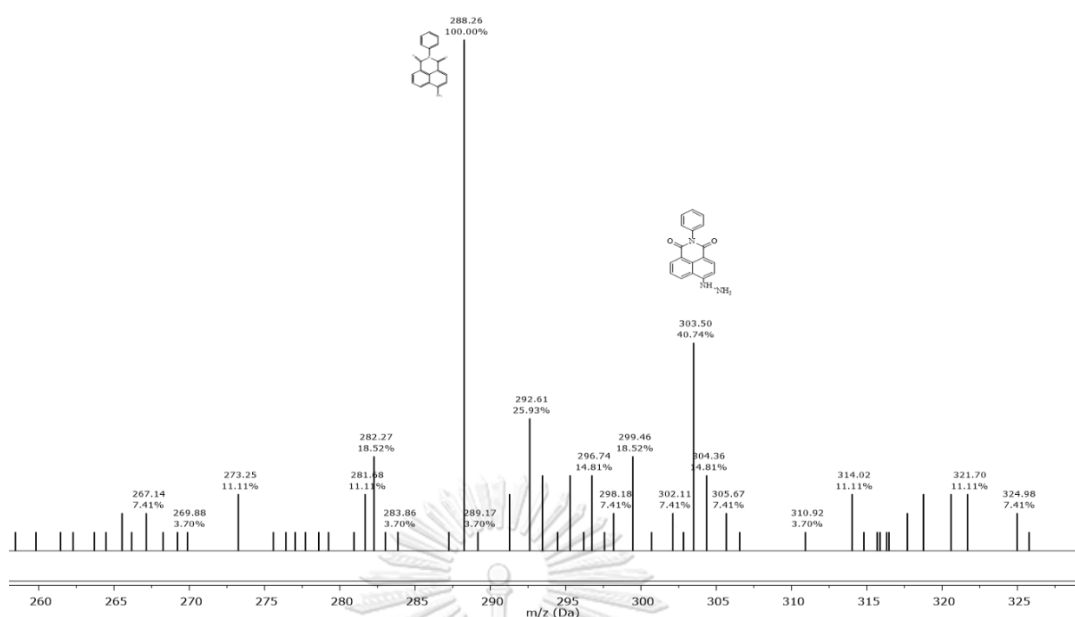


Figure A7 The mass spectrum spectrum of **Naph-NH₂** at m/z 303.50

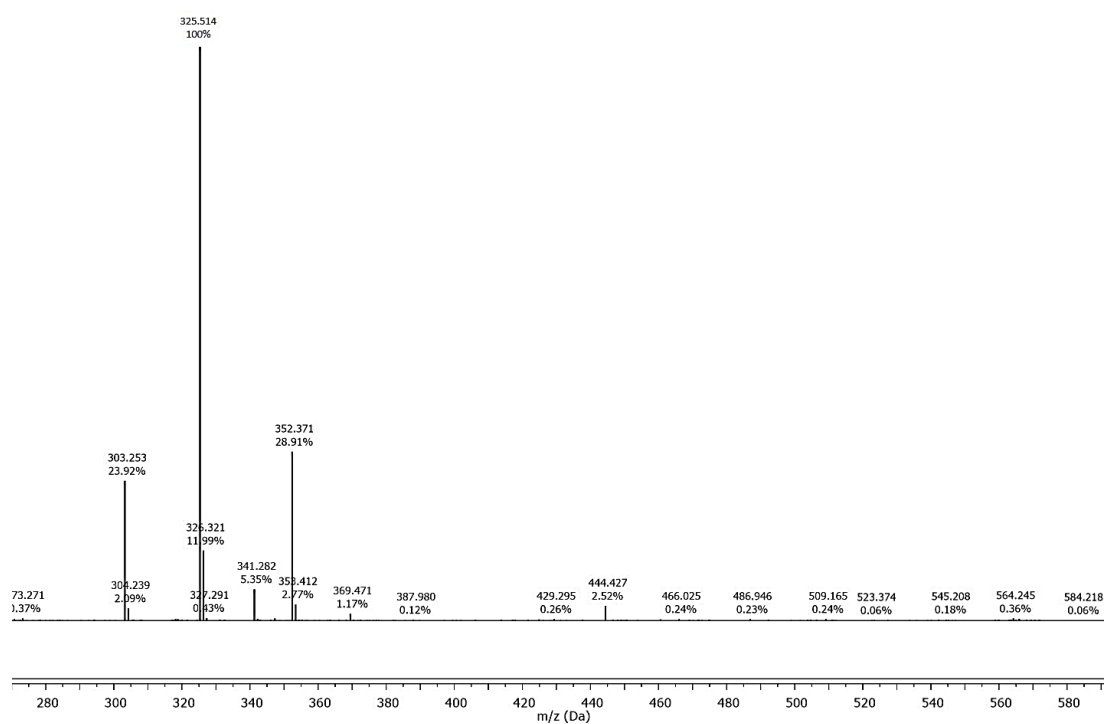


Figure A8 The mass spectrum of **Naph-OMe** at m/z 325.51

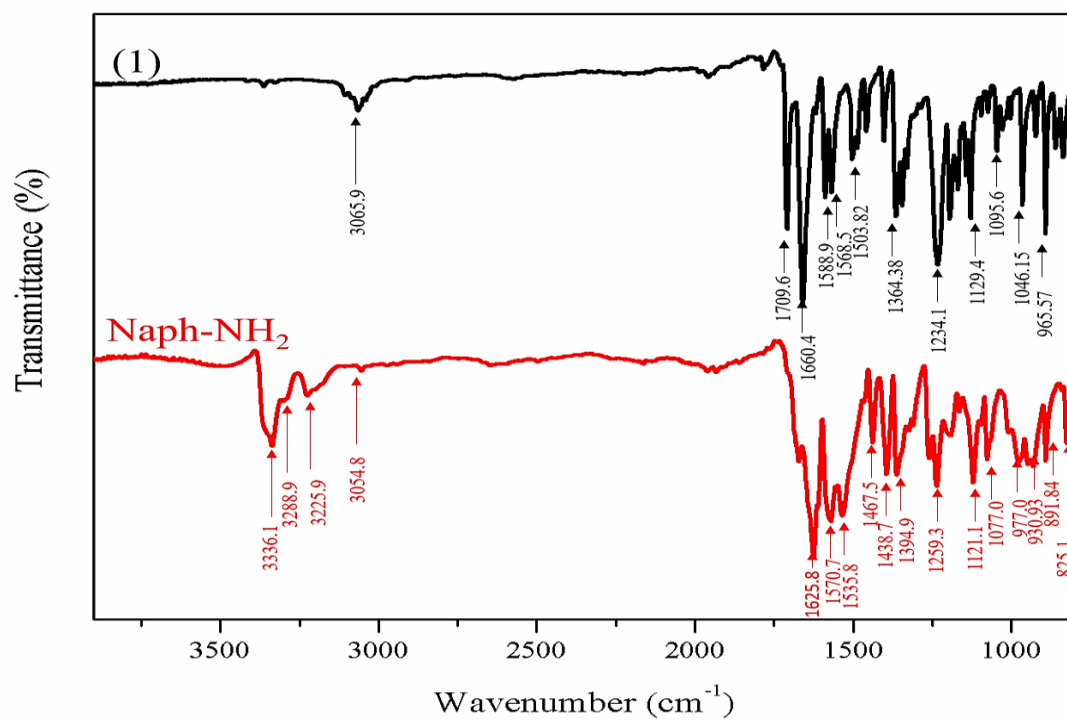


Figure A9 The FT-IR spectrum (ATR) of compound 1 and Naph-NH₂

Synthesis of sucrose laurate monoester (Gel 1)

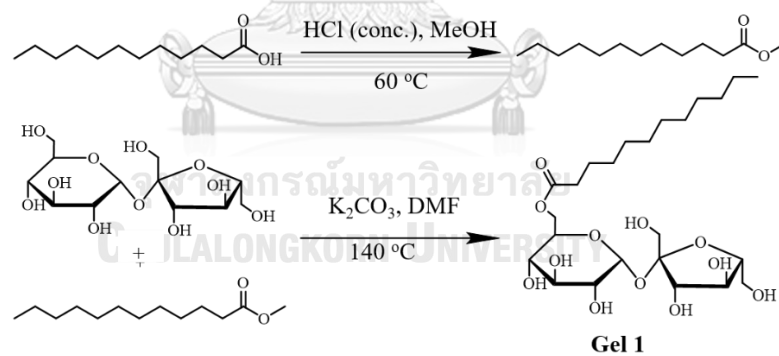
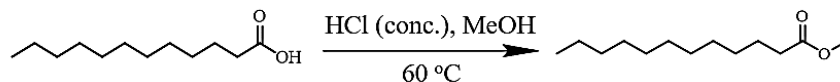


Figure 2.5

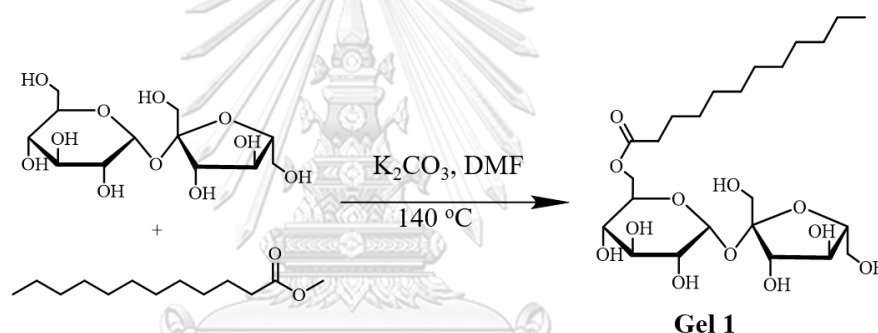
Figure A 10 Synthesis pathway of sucrose laurate monoester (Gel 1)

- Synthesis of methyl dodecanoate



Lauric acid (200 g, 1.0 mol) was dissolved in methanol (700 mL). The concentrated hydrochloric acid was added into the solution and the reaction was refluxed for 5 days under nitrogen atmosphere. The reaction mixture was concentrated on a rotatory evaporator. The two layers of crude product was separated and collected the colorless oil layer was collected methyl dodecanoate.

- Synthesis of sucrose laurate monoester (**Gel 1**)



The mixture of sucrose (100 g, 0.292 mol) and potassium carbonate (50 g, 0.36 mol) in DMF was stirred at 140 °C for 15 min. Consequently, laurate methyl ester (50 g, 0.23 mol) was added into and refluxed for 5 days under nitrogen atmosphere. After cooling to the room temperature, the resulting brown colored solution was filtered. The white sediment was obtained after adding the saturated NaCl solution into the filtrate. After that, sucrose laurate monoester was collected and dried with small amount of diethyl ether.

¹H-NMR (400 MHz, *d*₆-CDCl₃): δ (in ppm) = 7.88 (s, 1 H, CH), 3.34 (t, *J* = 6.1 Hz, 6 H, CH), 2.85 (s, 3 H, OH), 2.69 (s, 4 H, OH), 1.35 (m, 6 H, CH₂), 1.17 (m, 13 H, CH₂), 0.81 (dd, 10 H, *J* = 9.0, 3.0, CH₂, CH₃)

¹³C-NMR (100 MHz, *d*₆-DMSO): 104.74, 92.70, 83.14, 77.89, 75.01, 73.25, 72.23, 70.39, 62.98, 60.91, 32.23, 29.34, 25.85, 22.66, 14.54.

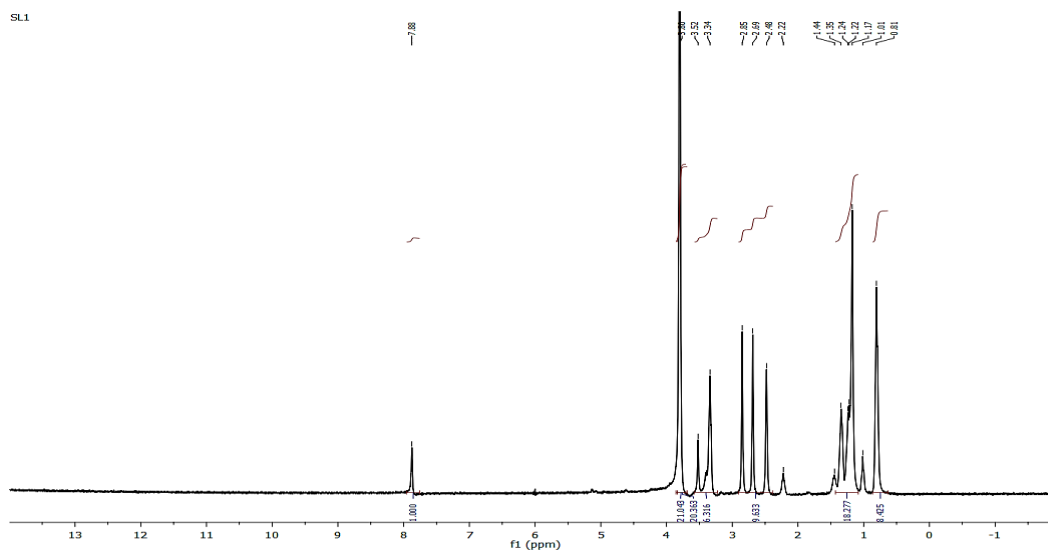


Figure A11 The $^1\text{H-NMR}$ spectrum of sucrose laurate monoester (**Gel 1**) in d_6 -DMSO at 400 MHz

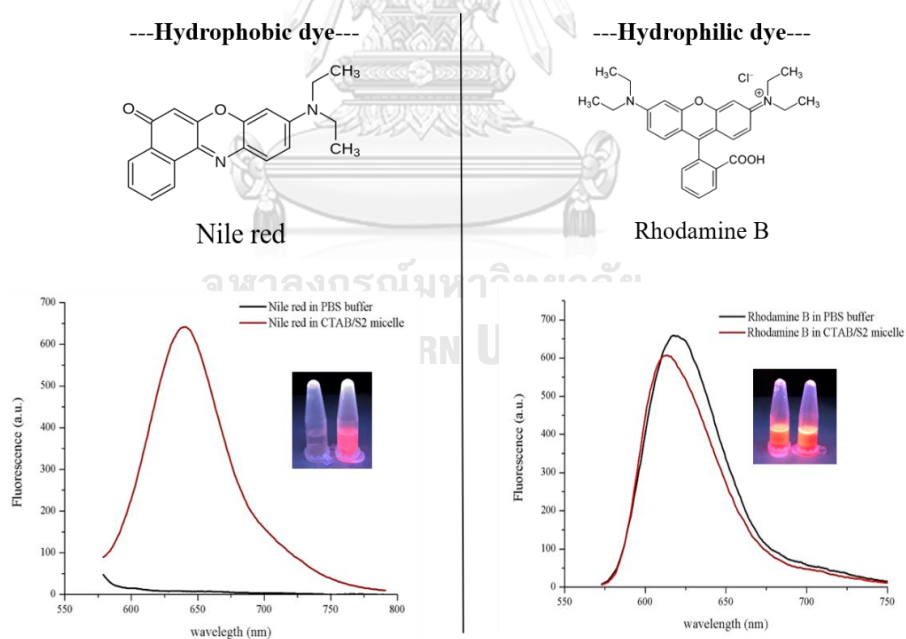


Figure A12 The studies of hydrophobic and hydrophilic properties of CTAB/S2 micellar system

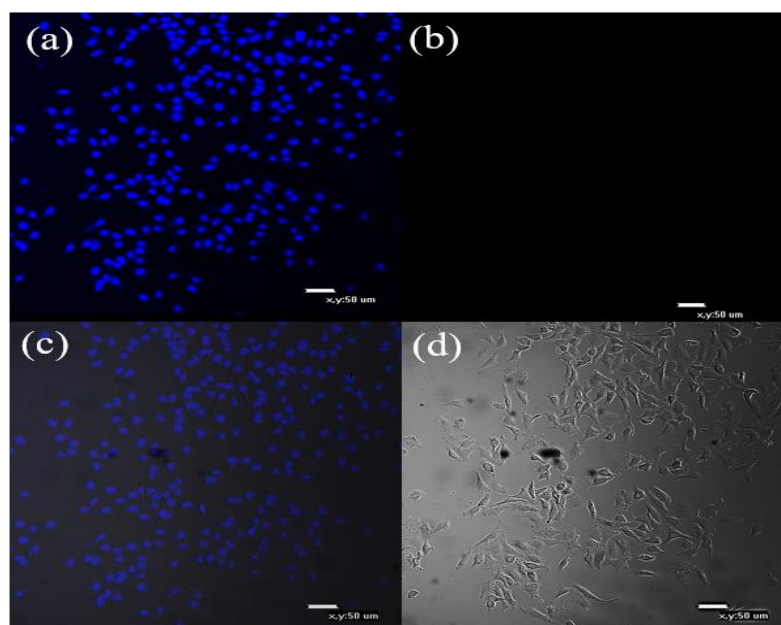


Figure A13 Confocal images of A549 cells (control) at magnification 10X; (a) the nuclear dye channel, (b) the **Naph-NH₂/CTAB/S2** micellar material channel, (c) the merge of three channels (d) the brightfield image

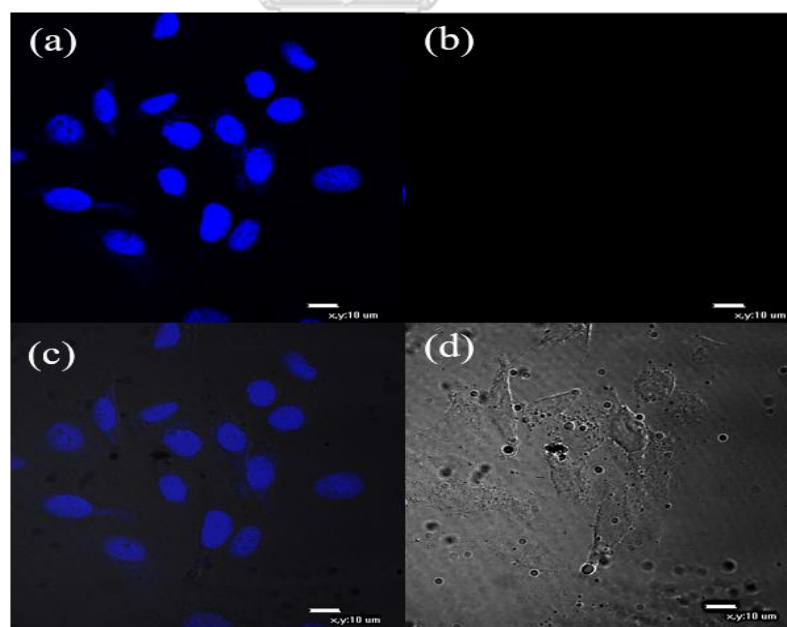


Figure A14 Confocal images of A549 cells (control) at magnification 100X; (a) the nuclear dye channel, (b) the **Naph-NH₂/CTAB/S2** micellar material channel, (c) the merge of three channels (d) the brightfield image

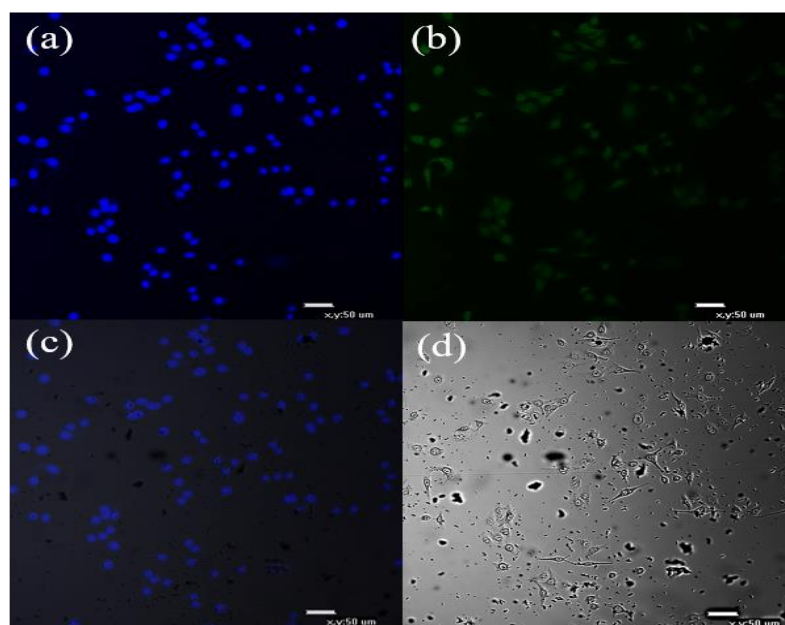


Figure A15 Confocal images of A549 cells incubated with **Naph-NH₂/CTAB/S2** for 4 hr at magnification 10X; (a) the nuclear dye channel, (b) the **Naph-NH₂/CTAB/S2** micellar material channel, (c) the merge of three channels (d) the brightfield image

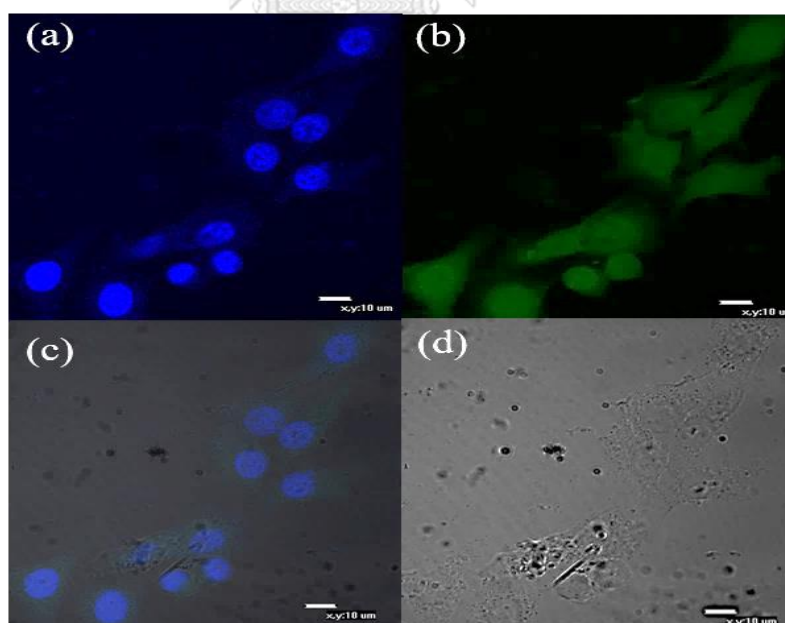


Figure A16 Confocal images of A549 cells incubated with **Naph-NH₂/CTAB/S2** for 4 hr at magnification 100X; (a) the nuclear dye channel, (b) the **Naph-NH₂/CTAB/S2** micellar material channel, (c) the merge of three channels (d) the brightfield image

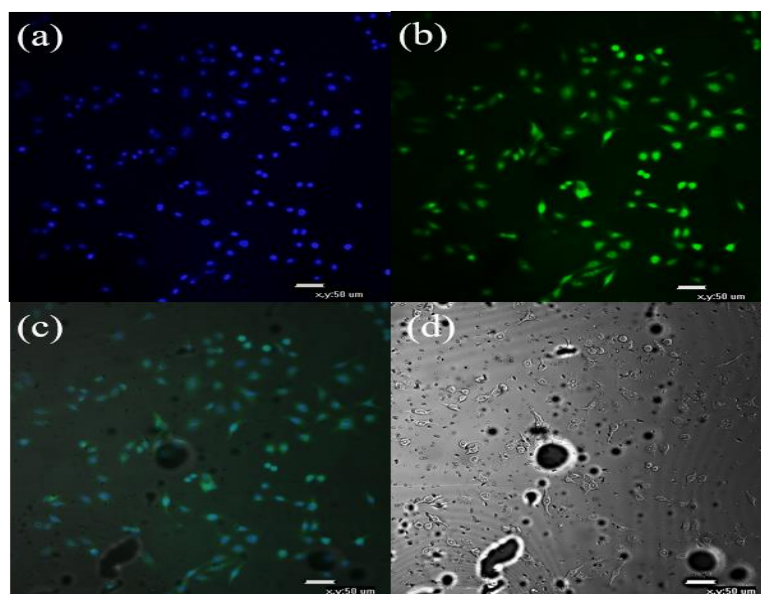


Figure A17 Confocal images of A549 cells incubated with **Naph-NH₂/CTAB/S₂** + heptanal for 4 hr at magnification 10X; (a) the nuclear dye channel, (b) the **Naph-NH₂/CTAB/S₂** micellar material channel, (c) the merge of three channels (d) the brightfield image

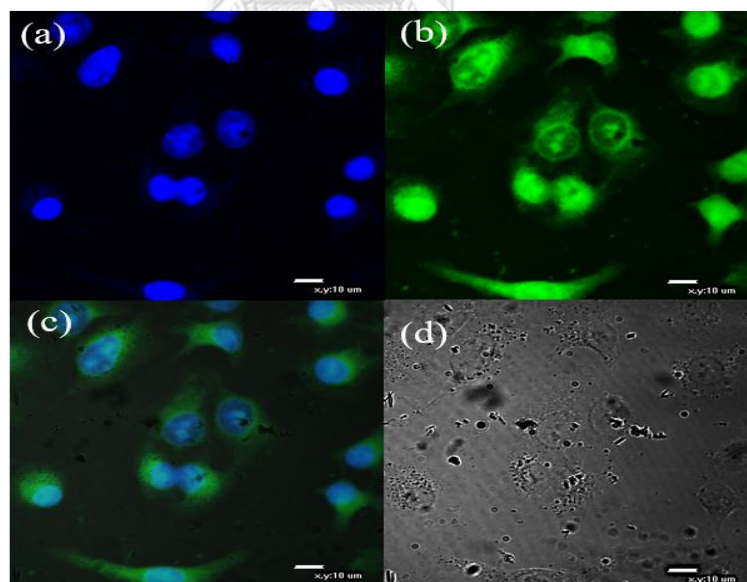


Figure A18 Confocal images of A549 cells incubated with **Naph-NH₂/CTAB/S₂** + heptanal for 4 hr at magnification 100X; (a) the nuclear dye channel, (b) the **Naph-NH₂/CTAB/S₂** micellar material channel, (c) the merge of three channels (d) the brightfield image

VITA

NAME	Miss Piyanan Pranee
DATE OF BIRTH	September 7, 1993
PLACE OF BIRTH	Chonburi, Thailand
INSTITUTIONS ATTENDED	<p>2016 – 2018 Master degree's degree in Chemistry, Faculty of Science, Chulalongkorn University, Bangkok, Thailand (GPA:3.89), Science Achievement Scholarship of Thailand (SAST)</p> <p>2012 – 2016 Bachelor's degree in Chemistry, Faculty of Science, Srinakharinwirot University, Bangkok, Thailand (GPA:3.83), Science Achievement Scholarship of Thailand (SAST)</p> <p>2009 – 2012 Triamudomsuksanomkiao school, Bangkok, Emphasis on Science and Mathematics, High School Certificate equivalent</p>
HOME ADDRESS	49/111 KC Village, Lampakchee, Suwintawong Road, Nongjok, Bangkok, 10530
PUBLICATION	<p>Journal publication "Fluorescent Micellar sensor for long-chain aldehydes detection" KKU Research Journal, ISSN 1906-201X, (accepted; September 18, 2018)</p> <p>Poster presentation "Effective fluorescence probes based on nanomicelles for specific determination of long-chain aldehydes" Advanced Functional Carbon-based Materials (1st AFCM) TRF symposium, Vidyasirimedhi Institute of Science and Technology (VISTEC), Rayong, Thailand (September 4, 2018)</p> <p>2018 Poster presentation "Hydrazine-functionalized fluorescent micellar sensor for detection of long-chain aldehydes" Composite Material congress 2018 (CMC 2018) Stockholm, Sweden (June 3-6, 2018)</p> <p>Poster presentation "Optimization of GFAAS method for determination of Zinc Oxide nanoparticles in products" The 11th Conference on Science and Technology for Youths 2016, BITEC, Bangna district, Bangkok, Thailand (June 10-11, 2018)</p>